Chapter 4A

A novel class of pivalamide based organogelators with potential applications in oil spill remediation and sequestration of dyes from water

Published in ***Colloids and Surfaces A: Physicochemical and Engineering Aspects*****, 632 (2022) 127813.**

4.1 INTRODUCTION

Marine oil spills occur as a result of accidental discharge of crude oil and petrochemicals in large water bodies. They pose a serious threat to the ecosystem and contribute to environmental pollution. They can have disastrous consequences like severely affected marine flora and fauna, spillage of non-renewable fossil fuels, impact on climate change, to name a few.[1] Conventional methods for containing oil spills include biochemical and chemical practices like burning[2], bioremediation[3], use of adsorbents[4], dispersants, etc. each of which has its own set of disadvantages and in turn, end up contributing to environmental pollution at large. While much research has been carried out to contain oil spills in large water bodies[5], cost-effective and efficient methods remain a challenge. However, these methods are not viable for large scale solution, as they can be economically exorbitant and can leave behind toxic residues, eventually causing bioaccumulation in the sensitive marine environment. In this regard, the efficiency of phase selective organogelation (PSOG) is unsurpassed, as it ensures safe and maximum recovery of oil from the water surface. PSOG allows *selective gelation of oil from the oil-water biphasic system*, making the technique a quick and efficient remedy for marine oil spills.[6–8] They offer various advantages like- (i) simple and low-cost synthesis, (ii) environmental compatibility, (iii) easy transportation and thermo-reversibility which can facilitate oil recovery and (iv) recyclability and reusability.[7]

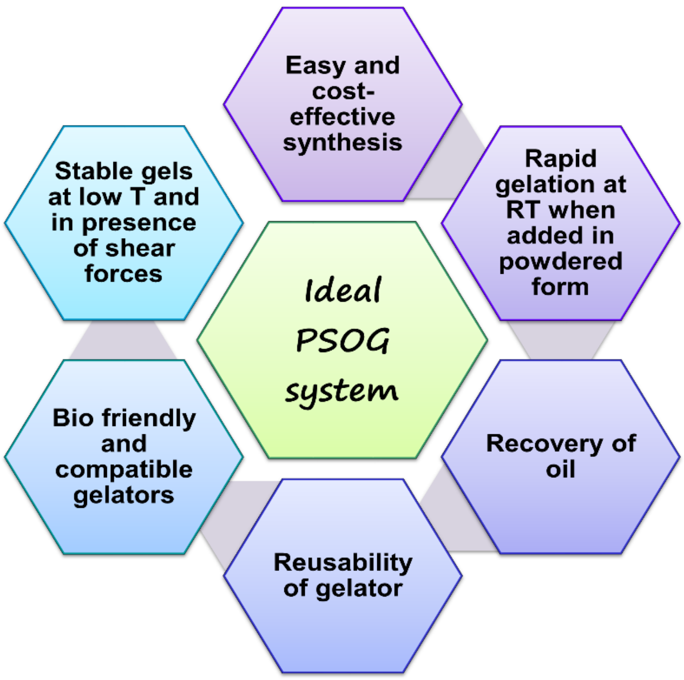

Figure 4.1 Desirable attributes of an ideal PSOG system

The initial reports of congealing oil in presence of sea water date back to early 1970s.[9] In 1985, dibenzylidene-D-sorbitol (DBS) and its derivatives were patented as potential phase selective organo-gelators.[10] In 2001, Bhattacharya and Krishnan-Ghosh reported amino acid based N-lauroyl-L-alanine for selectively congealing marine oil spills.[11] Since then, there have been various reports of selective gelation of oil in oil-water biphasic systems by use of phase selective organo-gelators (PSOGs).[12–20] These gelators are most commonly derived from polymeric/amino acid (dipeptides)/sugar-based moieties, cholesterol-based compounds, or long-chain fatty acids. One noteworthy aspect of this phenomenon is that PSOGs may involve addition of gelators in presence of secondary solvents, which tend to be miscible with the oil phase. Although this ensures efficient gelation and even distribution of gelator molecules in the oil layer, it can contaminate the oil and even the aqueous phase. Ideally, an efficient PSOG should involve the gelator to form a gel at room temperature when added in powdered form as well as in presence of secondary solvents (Figure 4.1).

Small molecules, derived from multi-component systems, amides, etc. form a very distinct class of organogelators as their supramolecular self-assembly leads to the formation of 1-D aggregates which, after effective crosslinking, cause immobilization of the solvent molecules. It is purely the role of highly efficient non-covalent interactions that is responsible for the gelation behavior of LMOGs.

4.2 PIVALIC ACID BASED COMPOUNDS – Importance of *tert*-butyl group

Even though significant progress in the discovery of new LMOGs has been made in the last decade or so; surprisingly, most of the discoveries are predominantly driven by serendipity rather than design. However, efforts have always been directed towards the design of new LMOGs by incorporating a structural moiety with known gelation behavior and well-directed hydrogen bonding groups. One of the well-known and extensively studied examples is **ALS**-type gelators (Anthryl-Linker-Steroid)[21,22] developed by Weiss and his group.

Inspired by those early efforts to design a new series of LMOGs, we synthesized a series of compounds having three parts –

1. **structural moiety** which can promote van der Waals/**π-π** interactions (e.g., long chain aliphatic/ aromatic compounds)
2. directional hydrogen bonding **linker** (amide) and
3. **bulky** end group, i.e., *tert*-butyl (Figure 4.2(c)).

Although the presence of 1-D hydrogen-bonded networks is believed to be a prerequisite for the formation of LMOGs, there are many examples where additional non-covalent interactions, such as Halogen…Halogen interactions proved to be deterrent to gel formation despite the presence of 1-D hydrogen-bonded networks in the crystal structure of gelling compounds[23,24] and thus, a detailed study on the effect of substituent along with directional hydrogen-bonded networks is very crucial.

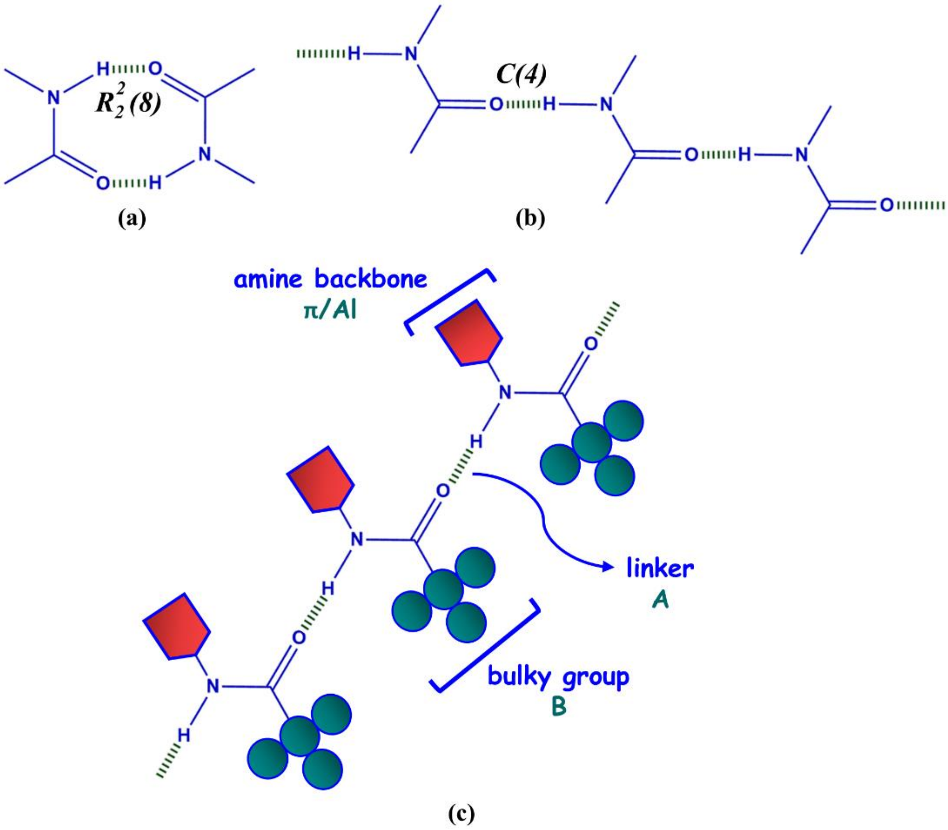

Figure 4.2 (a), (b) plausible hydrogen bonding models in straight chain amides; (c) designing strategy of the compounds based on *π/Al-A-B* approach

Additionally, this series of compounds synthesized is motivated by our success with pivalic acid salts-based gels.[25] In our designing strategy of new LMOGs, both aliphatic/aromatic structural units are incorporated along with the bulky functional group on one side of the molecules to induce the synergistic effect of long-chain interdigitation/ π-π interactions, which would bring stability to the overall supramolecular assemblies formed by 1-D hydrogen bonding of amide functionality. Moreover, the presence of sterically hindered *tert*-butyl group would avert very close packing among the neighboring molecules. The amide group incorporated in all newly synthesized molecules would act as a linker capable of forming 0-D or 1-D supramolecular synthon. We believe that the introduction of *tert*-butyl group could force the molecules to pack into 1-D hydrogen-bonded networks rather than closed packed 0-D assemblies (Figure 4.2(a), (b)) and the presence of bulky groups might not favor crystallization as (is commonly believed) physical gel formation occurs when crystallization goes erratic.[26]

Fortunately, our strategy worked successfully as most of the compounds synthesized in the present study primarily displayed a 1-D supramolecular synthon of amide groups rather than 0-D dimeric amide synthons. In the present study, 13 new compounds (**PIV1-PIV13**) were synthesized having *aromatic/aliphatic backbone–amide linker–bulky group* (**π/Al-A-B**), where aromatic/aliphatic substituents were systematically varied from long-chain aliphatic groups to aromatic groups, alicyclic group and moieties containing both alicyclic and aromatic backbones. This approach could not only bring us closer to the daunting task of designing LMOGs but also provide a better understanding about the driving forces which might be causing such an exceptional behavior in these small molecules.

Compounds **PIV1-PIV6** could instantly congeal alkane homologues (n>5 carbon atoms), diesel, engine oil, silicone oil, cooking oil, etc. under the effect of strong sunlight, UV light and ultrasonication. These compounds were tested for their ability to selectively congeal oil from oil-water systems at room temperature, in various forms (powder as well in solution form using various solvents). We also utilized these compounds for efficiently removing dyes present in aqueous solutions, which can contribute to tackle water pollution.

4.3 EXPERIMENTAL PROCEDURES

4.3.1 Synthesis

Oxalyl chloride (0.9 mL, 10 mmol) was slowly added to a solution of pivalic acid (0.25 mL, 2 mmol) in dry dichloromethane under nitrogen atmosphere and the solution was subjected to continuous stirring at RT (~25°C). After 12 hours, excess oxalyl chloride and the solvent were removed by distillation under reduced pressure. The pivaloyl chloride so formed was dissolved in dry dichloromethane (10 mL) and added to a solution of amine (1 mol equiv. for monoamines, 2 mol equiv. for diamines and so on; **1-13**) and triethylamine (0.25 mL, 2 mmol) mixture in a round-bottom flask. The mixture was stirred under N_2 atmosphere overnight. The reaction mixture was then added to dil. HCl (5%) and extracted with dichloromethane. The solvent was removed using rotary evaporator and the compounds (**PIV1-PIV13**, Scheme 4.1) were kept for recrystallization in various solvents (yield= 64-71%).

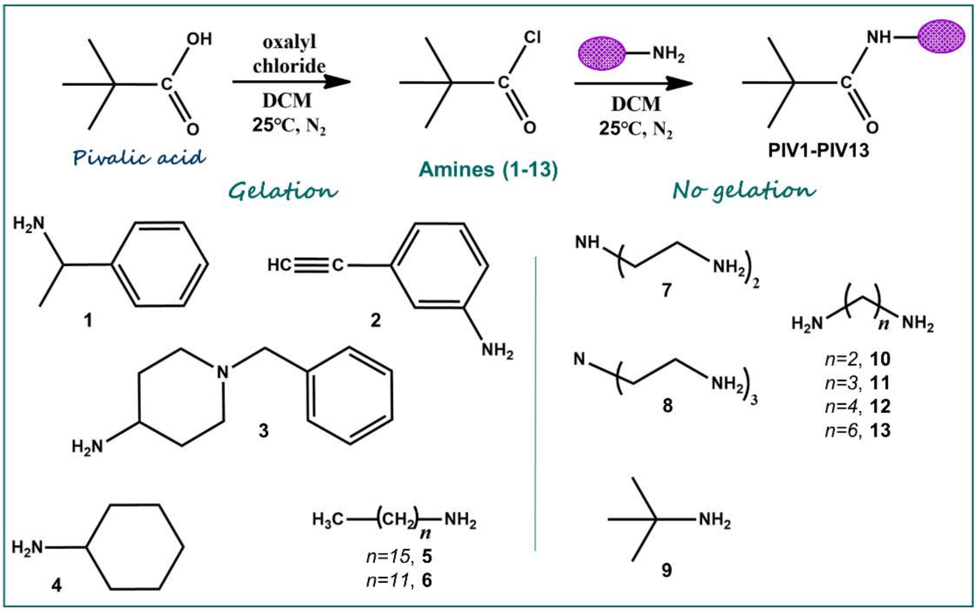

Scheme 4.1 Pivalamides PIV1-PIV13 synthesized in the study

4.3.2 Gelation trials

The mgc values of all gelators were determined using dilution method. To a glass vial containing 10 mg gelator, 0.2 mL of solvent was added, and a heat-cool cycle was employed to observe gel formation. To this system, gradual dilution was carried out till no gelation was observed. The last concentration at which gelation was observed was recorded as mgc value (%wt/v or mg/mL). The same process was repeated in triplicates for each system and average values were reported as mgc values.

T_{gel} (gel-to-sol conversion temperature) was also measured using the same inverted vial method. The vials containing the gels were heated in a temperature-controlled silicone oil bath at a steady rate of 0.5°C/min. The temperature at which first drop of gel melted was considered as T_{gel}.

4.3.3 Phase selective organo-gelation (PSOG)

A weighed amount of gelator was added to a biphasic mixture of water and organic solvent in dry or solution form. The system was subjected to heat, strong sunlight or UV irradiation after which selective gelation of solvent was observed and recorded.

4.3.4 Dye removal studies

The ability of gels to uptake dyes from aqueous phase was determined using UV-vis studies. The concentration of dyes in the aqueous phase was calculated by Beer-Lambert law (***A= αlc***, where *A*= absorbance of dye at a certain concentration, *α*= extinction coefficient ($Lmg^{-1}cm^{-1}$), *l*= path length of incident light (cm) and *c*= concentration of dye in solution). The maximum absorption wavelengths were monitored at 554 nm for Rhodamine B and 664 nm for Methylene Blue.

4.3.5 Materials and Methods

All the chemicals were obtained from Sigma Aldrich and TCI and the solvents were obtained from SD Fine Chemicals, India, and were used without any further purification.

4.3.5.1 NMR studies

NMR data was recorded on Bruker AVANCE, 400 MHz spectrometer in $CDCl_3$, with TMS as internal standard. The ^1H NMR spectra of all compounds can be found in Supplementary Data* at the end of the chapter.

4.3.5.2 FT-IR studies

FT-IR studies were performed on Bruker Alpha FT-IR spectrometer in a solid-state as KBr pellets. The FT-IR spectra of all compounds can be found in Supplementary Data* at the end of the chapter. FT-IR spectra of **PIV1** in gel and solution phase (with *n*-octane as solvent) were recorded using CaF_2 discs.

4.3.5.3 Crystallography

Single crystal diffraction data were collected on an Xcalibur, EOS, Gemini diffractometer with graphite monochromatic Mo Kα radiation (0.71073 Å). The data for **PIV1** was collected on a Bruker APEX-II CCD diffractometer with monochromatic Mo Kα radiation (0.71073 Å). All structures were solved and refined using the Olex2[27] software and ShelXL[28] refinement package. Graphics were generated using MERCURY, version 4.3.1. All structures were solved by direct methods and refined in a regular pattern. In all the cases, non-hydrogen atoms were treated anisotropically. Wherever required, the hydrogen atoms were refined by locating on a difference Fourier map. The crystallographic parameters and H-bond parameters are tabulated in Tables S4.1* and S4.2*. ORTEP images of all crystals are combined in Figure S4.1*.

4.3.5.4 Hirshfeld studies

The 3D Hirshfeld surfaces[29] and 2D fingerprint plots were obtained using Crystal Explorer 3.1.[30] 3D Hirshfeld surfaces of all crystals are combined in Figure S4.2*.

4.3.5.5 Rheology

Rheology studies were performed on an Anton Paar MCR 102 Modular Compact Rheometer at 25°C. The instrument has a parallel plate geometry with a plate diameter of 50 mm, maintained at a gap of 1 mm; the gel samples were subjected to frequency sweep range of 0 to 100 rad/s and values of G' (storage modulus) and G" (loss modulus) were evaluated with respect to oscillation strain (%).

4.3.5.6 Morphology

For SEM, the frozen gel samples (in various solvents) were used directly for viewing images using JEOL JSM-5610LV Scanning Electron Microscope instrument. POM analyses were performed using LEICADM2500P polarizing microscope. Images were captured using LEICADFC295 camera which is attached with the instrument. A thin layer of gel was formed on a glass slide and allowed to dry at RT, whose images were captured.

4.3.5.7 Powder XRD

Representative powder diffraction patterns of bulk (crystalline) gelator and xerogel samples (diesel, decane, and octane) of **PIV1** were recorded on an XPERT (Cu Kα radiation, $\lambda = 1.54056$ Å) diffractometer on a continuous scanning mode at 2θ value 5-50º.

4.3.5.8 UV-vis studies

Dye removal studies were performed using Perkin Elmer Lambda 35 dual beam UV-vis Spectrophotometer.

4.3.6 Analytical Data

All the amides were characterized using ^{1}H and ^{13}C NMR and FT-IR. All compounds showed characteristic IR bands for C=O stretching around 1690-1640 cm^{-1}, two N-H stretching bands around 3300 cm^{-1}, 2900 cm^{-1} and N-H bending around 1550-1640 cm^{-1}, indicating the formation of amides.

Compound PIV1 (N-(1-phenylethyl)-2,2-dimethylpropanamide). M.P.= 154°C, ^{1}H NMR (400 MHz, $CDCl_3$, TMS) = δ (ppm) 7.381-7.260 (*m*, 5H, 5(CH) ar), δ 5.833 (*s*, 1H, -CONH), δ 5.161-5.090 (*m*, 1H, (CH)), δ 1.508 (*s*, 3H, CH_3), δ 1.220 (*s*, 9H, 3(CH_3)). ^{13}C = δ (ppm) 177, 143, 128, 127, 126, 48, 38, 27, 21.

FT-IR, cm^{-1} (KBr) – 3340, 3029, 2974, 1638, 1529, 1452, 1365, 1308, 1220, 1131, 1095, 1011, 904, 809, 754, 697, 653, 543, 524.

Compound PIV2 (N-(3-ethynylphenyl)-2,2-dimethylpropanamide). M.P.= 98°C, ^{1}H NMR (400 MHz, $CDCl_3$, TMS) = δ (ppm) 7.673-7.605 (*m*, 1H, (CH) ar), δ 7.594-7.585 (*m*, 1H, (CH) ar), δ 7.315 (*m*, 2H, 2(CH) ar), δ 7.296-7.236 (*m*, 1H, (CH) ar), δ 3.075 (*s*, 1H, ≡CH), δ 1.331 (*s*, 9H, 3(CH_3)). ^{13}C = δ (ppm) 176, 138, 128, 127, 123, 122, 120, 83, 39, 27.

FT-IR, cm^{-1} (KBr) – 3303, 2968, 1656, 1580, 1526, 1473, 1417, 1368, 1293, 1276, 1247, 1186, 885, 789, 692, 652, 626.

Compound PIV3 (N-(1-benzylpiperidin-4-yl)-2,2-dimethylpropanamide). M.P.= 78°C, ^{1}H NMR (400 MHz, $CDCl_3$, TMS) = δ (ppm) 7.352-7.253 (*m*, 5H, 5(CH) ar), δ 5.495 (*s*, 1H, -CONH), δ 3.815-3.785 (*m*, 1H, (CH)), δ 3.777 (*s*, 2H, CH_2)),δ 2.830-

2.801 (*d*, 2H, 2(C$\underline{H}_2$)), δ 2.160-2.064 (*m*, 2H, 2(C$\underline{H}_2$)), δ 1.925-1.885 (*m*, 2H, 2(C$\underline{H}_2$)), δ 1.489-1.402 (*m*, 2H, 2(C$\underline{H}_2$)), δ 1.392-1.257 (*m*, 1H, CH), δ 1.161 (*s*, 9H, 3(CH_3)). ^{13}C = δ (ppm) 177, 138, 129, 128, 127, 63, 52, 46, 38, 32, 27.

FT-IR, cm^{-1} (KBr) – 3324, 2947, 1632, 1545, 1493, 1452, 1395, 1364, 1344, 1326, 1263, 1209, 1145, 1121, 1083, 1020, 982, 859, 786, 733, 697, 667, 530.

Compound PIV4 (N-cyclohexyl-2,2-dimethylpropanamide). M.P.= 104°C, ^{1}H NMR (400 MHz, $CDCl_3$, TMS) = δ (ppm) 5.472 (*s*, 1H, -CONH), δ 3.795-3.702 (*m*, 1H, (CH)), δ 1.918-1.880 (*m*, 3H, 3(C$\underline{H}_2$)), δ 1.729-1.678 (*m*, 2H, 2(C$\underline{H}_2$)), δ 1.644-1.604 (*m*, 1H, C$\underline{H}_2$), δ 1.428-1.327 (*m*, 2H, 2(C$\underline{H}_2$)), δ 1.210 (*s*, 9H, 3(CH_3)), δ 1.188-1.620 (*m*, 2H, 2(C$\underline{H}_2$)). ^{13}C = δ (ppm) 177, 47, 38, 33, 27, 25, 24.

FT-IR, cm^{-1} (KBr) – 3342, 2933, 2853, 1631, 1535, 1478, 1450, 1365, 1318, 1243, 1207, 1150, 1095, 971, 934, 891, 815, 783, 641, 572.

Compound PIV5 (N-hexadecyl-2,2-dimethylpropanamide). M.P.= 40°C, ^{1}H NMR (400 MHz, $CDCl_3$, TMS) = δ (ppm) 5.624 (*s*, 1H, -CONH), δ 3.263-3.213 (*m*, 2H, CH_2), δ 1.719-1.702 (*m*, 1H, C$\underline{H}_2$), δ 1.517-1.482 (*m*, 2H, CH_2), δ 1.306-1.265 (*m*, 25H, CH_2), δ 1.206 (*s*, 9H, 3(CH_3)), δ 0.910-0.876 (*m*, 3H, C$\underline{H}_3$). ^{13}C = δ (ppm) 178, 39, 38, 32, 29.6-29.3, 27.6, 26.9, 22, 14.

FT-IR, cm^{-1} (KBr) – 3358, 2954, 2850, 1632, 1529, 1472, 1432, 1362, 1305, 1227, 1157, 1065, 1019, 913, 883, 853, 826, 722, 654.

Compound PIV6 (N-dodecyl-2,2-dimethylpropanamide). M.P.= 42°C, ^{1}H NMR (400 MHz, $CDCl_3$, TMS) = δ (ppm) 5.642 (*s*, 1H, -CONH), δ 3.258-3.207 (*m*, 2H, CH_2), δ 1.512-1.478 (*m*, 2H, CH_2), δ 1.301-1.262 (*m*, 18H, 9(CH_2)), δ 1.201 (*s*, 9H, 3(CH_3)), δ 0.905-0.870 (*m*, 3H, C$\underline{H}_3$). ^{13}C = δ (ppm) 178, 39, 38, 32, 29.6-29.3, 27.6, 26.9, 22, 14.

FT-IR, cm^{-1} (KBr) – 3355, 2924, 2853, 1631, 1531, 1465, 1432, 1396, 1363, 1306, 1259, 1229, 1210, 1158, 1033, 948, 906, 869, 836, 721, 657, 544.

Compound PIV7 (N,N-bis(2-pivalamidoethyl)-2,2-dimethylpropanamide). M.P.= 138°C, ^{1}H NMR (400 MHz, $CDCl_3$, TMS) = δ (ppm) 6.479 (*s*, 2H, -CONH), δ 3.599-3.567 (*m*, 4H, 2(CH_2)), δ 3.483-3.437 (*m*, 4H, 2(CH_2)), δ 1.305 (*s*, 9H, 3(CH_3)), 1.198 (*s*, 18H, 6(CH_3)). ^{13}C = δ (ppm) 179, 39, 38, 28, 27.

FT-IR, cm^{-1} (KBr) – 3348, 3045, 2972, 2873, 1659, 1640, 1608, 1527, 1482, 1443, 1420, 1366, 1305, 1208, 1107, 1072, 1018, 927, 759, 723, 657, 529.

Compound PIV8 (N,N',N''-(nitrilotris(ethane-2,1-diyl)) tris (2,2-dimethylpropanamide)). M.P.= 48°C, ^{1}H NMR (400 MHz, $CDCl_3$, TMS) = δ (ppm) 6.240 (*s*, 3H, -CONH), δ 3.319-3.274 (*m*, 6H, 3(CH_2)), δ 2.627-2.596 (*m*, 6H, 3(CH_2)), 1.202 (*s*, 27H, 9(CH_3)). ^{13}C = δ (ppm) 178, 54, 38, 37, 27.

FT-IR, cm^{-1} (KBr) – 3328, 3075, 2962, 2870, 2827, 1647, 1550, 1479, 1427, 1361, 1300, 1222, 1168, 1088, 1066, 952, 854, 822, 780, 745, 668, 553, 496.

Compound PIV9 (N-(*tert*-butyl)-2,2-dimethylpropanamide). M.P.= 46°C, ^{1}H NMR (400 MHz, $CDCl_3$, TMS) = δ (ppm) 5.411 (*s*, 1H, -CONH), 1.352 (*s*, 9H, $3(CH_3)$), 1.175 (*s*, 9H, $3(CH_3)$). ^{13}C = δ (ppm) 178, 50, 39, 28, 27.

FT-IR, cm^{-1} (KBr) – 3377, 2977, 1643, 1525, 1477, 1450, 1394, 1361, 1296, 1238, 1028, 927, 905, 814, 766, 595, 510.

Compound PIV10 (N,N'-(ethane-1,2-diyl)bis(2,2-dimethylpropanamide)). M.P.= 40°C, ^{1}H NMR (400 MHz, $CDCl_3$, TMS) = δ (ppm) 6.527 (*s*, 2H, -CONH), 3.415-3.403 (*m*, 4H, $2(CH_2)$), 1.200 (*s*, 9H, $3(CH_3)$). ^{13}C = δ (ppm) 180, 40, 38, 27.

FT-IR, cm^{-1} (KBr) – 3304, 3066, 2957, 1634, 1547, 1479, 1442, 1363, 1297, 1243, 1214, 1059, 1017, 915, 818, 788, 691, 494.

Compound PIV11 (N,N'-(propan-1,3-diyl)bis(2,2-dimethylpropanamide)). M.P.= 96°C, ^{1}H NMR (400 MHz, $CDCl_3$, TMS) = δ (ppm) 6.388 (*s*, 2H, -CONH), 3.297-3.251 (*m*, 4H, $2(CH_2)$), 1.240 (*s*, 9H, $3(CH_3)$). ^{13}C = δ (ppm) 179, 38, 35, 29, 27.

FT-IR, cm^{-1} (KBr) – 3323, 2962, 1624, 1526, 1480, 1434, 1399, 1361, 1332, 1292, 1260, 1213, 1119, 897, 688, 646.

Compound PIV12 (N,N'-(butan-1,4-diyl)bis(2,2-dimethylpropanamide)). M.P.= 110°C, ^{1}H NMR (400 MHz, $CDCl_3$, TMS) = δ (ppm) 5.931 (*s*, 2H, -CONH), 3.292-3.244 (*m*, 4H, $2(CH_2)$), 1.541-1.508 (*m*, 4H, $2(CH_2)$), 1.198 (*s*, 9H, $3(CH_3)$). ^{13}C = δ (ppm) 178, 38.9, 38.6, 27, 26.

FT-IR, cm^{-1} (KBr) – 3346, 2963, 1640, 1536, 1478, 1452, 1431, 1398, 1366, 1296, 1195, 957, 797, 773, 694, 664.

Compound PIV13 (N,N'-(hexan-1,6-diyl)bis(2,2-dimethylpropanamide)). M.P.= 50°C, ^{1}H NMR (400 MHz, $CDCl_3$, TMS) = δ (ppm) 5.850 (*s*, 2H, -CONH), 3.241-3.192 (*m*, 4H, $2(CH_2)$), 1.506-1.473 (*m*, 4H, $2(CH_2)$), 1.357-1.286 (*m*, 4H, $2(CH_2)$), 1.188 (*s*, 9H, $3(CH_3)$).^{13}C = δ (ppm) 178, 38.9, 38.6, 29, 27, 25.

FT-IR, cm^{-1} (KBr) – 3331, 3075, 2956, 1635, 1542, 1477, 1428, 1365, 1296, 1225, 1177, 1068, 1011, 993, 970, 942, 882, 815, 674, 538.

4.4 RESULTS AND DISCUSSION

All the synthesized compounds were tested for their gelation performance. **PIV1-PIV6** showed gelation in various aliphatic solvents. Compounds **PIV1** and **PIV4** displayed exceptional gelation behavior in diesel, engine oil, silicone oil, kerosene, cooking oil, and crude oil fractions (n>5 carbon atoms) (Table 4.1). A conventional heat-cool cycle was employed to check the gelation behavior in a variety of solvents (Table 4.2). The gels could be formed in presence of strong sunlight (temperature ≈ 45°C), UV light as well as under the effect of ultrasonication. Interestingly, no gelation was observed in petrol, and we suspect that the presence of lower hydrocarbons in petrol might be hindering its immobilization among the gelator fibers (Figure 4.3).

Table 4.1 Gelation behavior of compounds PIV1-PIV6 in various solvents; mgc values are enclosed in parentheses

	PIV1	PIV2	PIV3	PIV4	PIV5	PIV6
n-hexane	G (7.5)	ppt	S	G (9.5)	S	S
n-heptane	G (6.0)	ppt	S	G (9.1)	S	S
n-octane	G (2.5)	S	S	G (6.2)	S	S
n-decane	G (3.12)	G (5.0)	S	G (4.1)	G (8.5)	G (9.5)
Dodecane	G (2.2)	G (4.0)	S	G (3.5)	G (6.5)	G (7.0)
Hexadecane	G (1.9)	G (3.1)	S	G (2.5)	G (4.0)	G (4.5)
Cyclohexane	G (3.3)	S	S	G (10.0)	S	S
Diesel	G (2.2)	G (3.3)	S	G (5.0)	G (10.0)	WG(10.0)
Kerosene	G (3.0)	ppt	S	S	S	S
Engine oil	G (3.5)	G (3.5)	G (2.8)	G (3.6)	G (2.8)	G (3.0)
Cooking oil	G (4.5)	S	G (3.1)	G (4.5)	G (3.2)	G (3.5)
Silicone oil	G (1.8)	G (2.1)	G (2.5)	G (2.5)	G (1.8)	G (2.0)
Polyethylene glycol	S	S	G (3.4)	G (3.5)	G (2.8)	G (3.1)
Propan-1,2-diol	S	S	G (3.8)	G (3.3)	S	S
DMSO	S	S	G (4.0)	G (3.5)	S	S

G - gel, WG - weak gel, S - solution, I – insoluble, ppt – precipitate.

4.4.1 Gelation studies and effect of solvents on gelation

We also observed that the minimum concentration of gelator (mgc) required by the alkane homologs in all the compounds reduced with an increase in hydrophobicity of the solvent (Figure 4.4). Furthermore, better gelation performance was observed in the case of higher alkanes like n-decane, dodecane, and hexadecane as these gels required lesser temperature to trigger gelation and formed stronger (more durable) gels, instantly. This could be a result of increased van der Waals interactions between the gelator fibrils and the solvent molecules.

Table 4.2 List of solvents utilized in gelation trials

Sr.	Solvent type	Nature	Solvents
1.	Polar	Protic	Water Methanol Ethanol Isopropanol n-butanol tert-butanol **propan-1,2-diol** hexan-1-ol octan-2-ol decan-1-ol **polyethylene glycol**
2.	Polar	Aprotic	Acetone Ethyl acetate **Dimethyl Sulfoxide** Dimethyl Formamide Acetonitrile Tetrahydrofuran Diethyl ether Dibenzyl ether Diisopropyl ether
2.	Halogenated	Aprotic	Chloroform Dichloromethane Carbon tetrachloride
3.	Hydrocarbon	Aliphatic	**Petroleum ether** **n-Hexane** **n-Heptane** **n-Octane** **n-Decane** **n-Dodecane** **n-Hexadecane** **Cyclohexane** Petrol **Diesel** **Kerosene** **Engine oil** **Cooking oil** **Silicone oil**
4.	Aromatic		Benzene Toluene Chlorobenzene Bromobenzene Nitrobenzene Xylenes (o-,m-,p-)

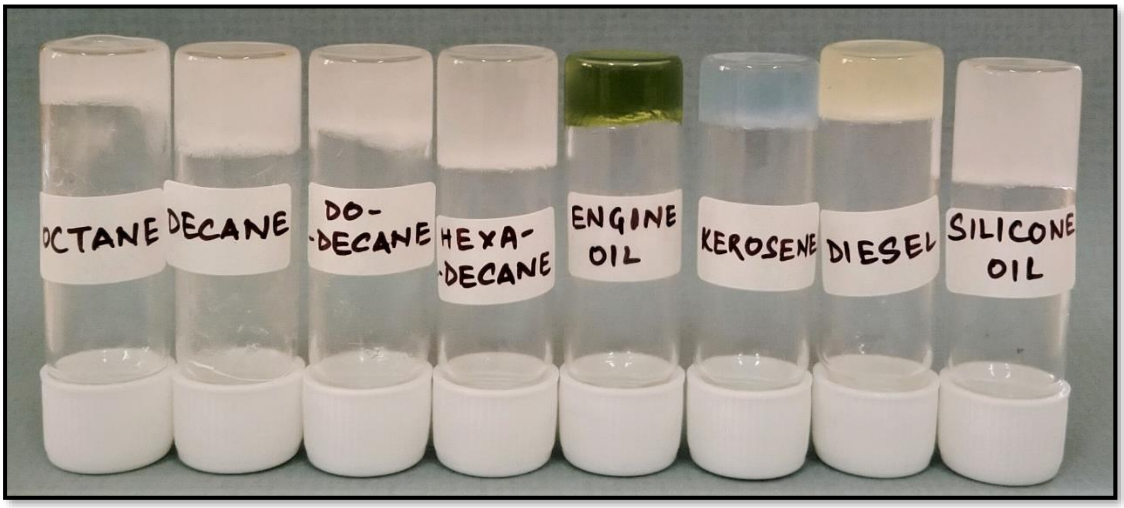

Figure 4.3 Gels obtained from PIV1

The gels remained stable for more than a month, at RT (~25°C) as well as at low temperatures (4-10°C), which suggests the formation of efficient and stable self-assembly leading to gelation of solvents.

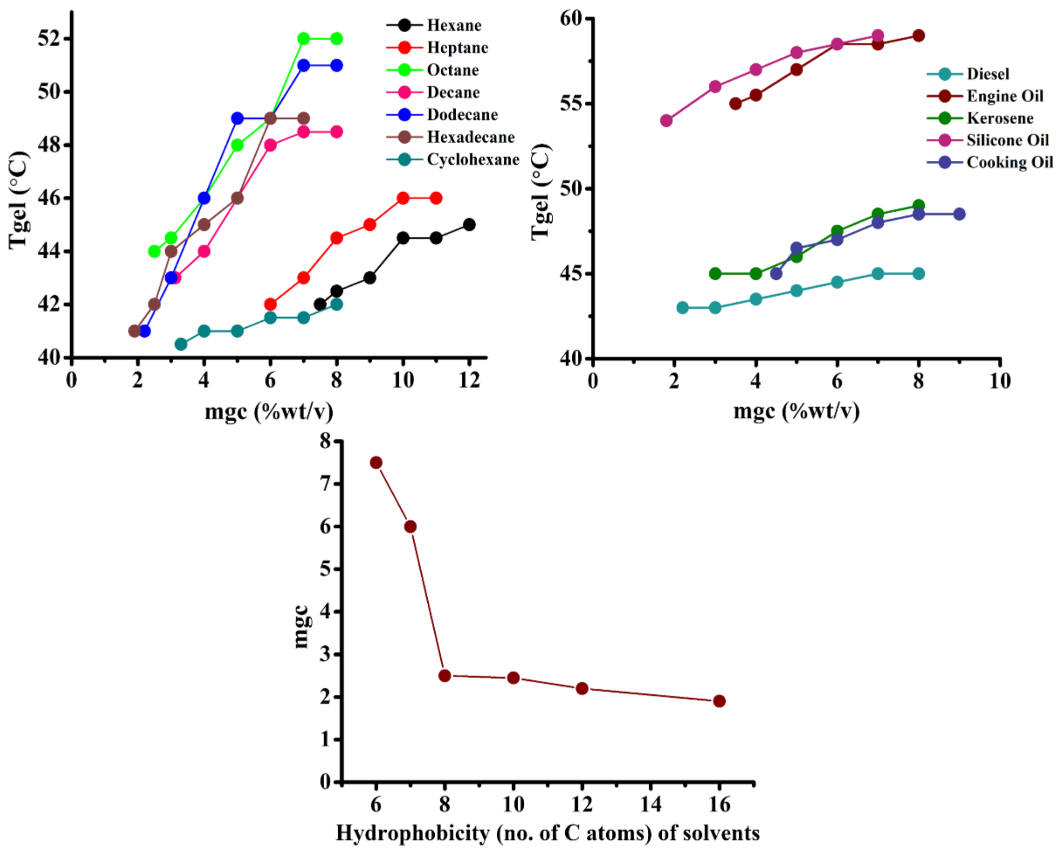

Figure 4.4 T_{gel} vs. concentration plots for PIV1 and variation of mgc values with hydrophobicity of solvents

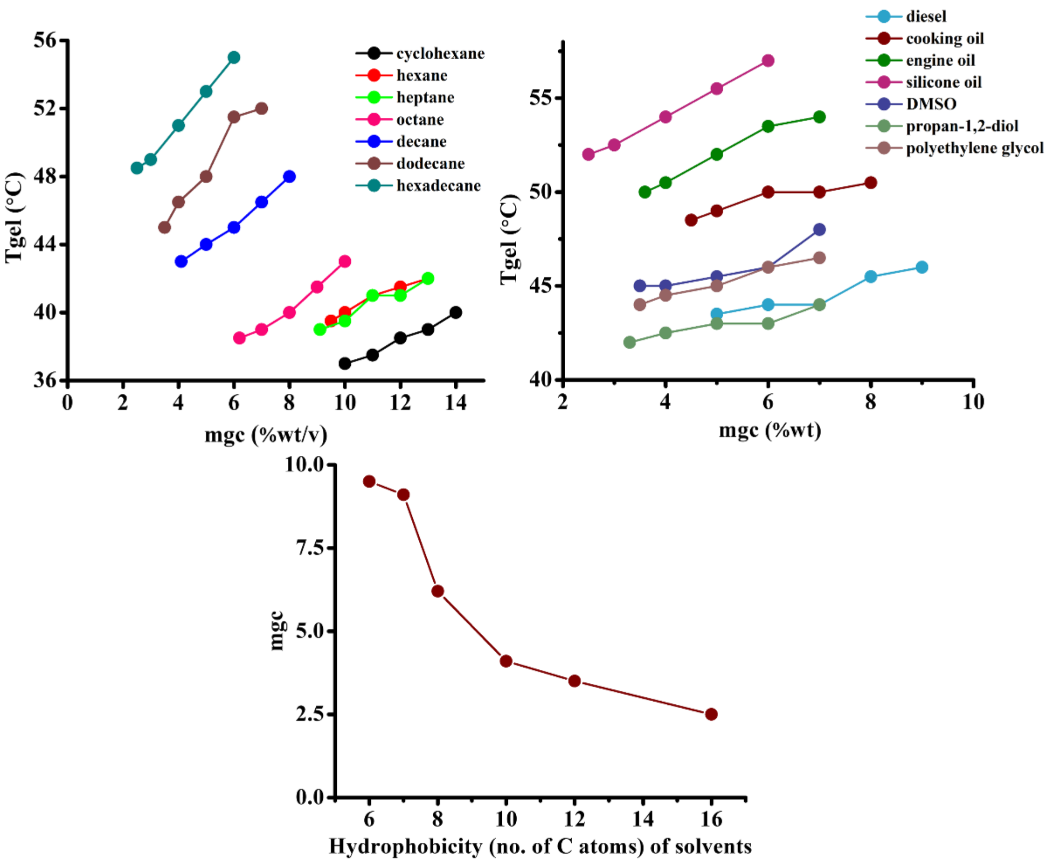

Figure 4.5 T_{gel} vs. concentration plots for PIV4 and variation of mgc values with hydrophobicity of solvents

The compounds **PIV1** and **PIV4** remained soluble in all the solvents tested for gelation (Table 4.2) except water. Besides, all synthesized compounds displayed a lack of gelation property towards aromatic (protic as well as aprotic) solvents like benzene, toluene, nitrobenzene, halobenzenes, xylenes, benzyl alcohol, aniline, etc.

Compounds **PIV3** and **PIV4** formed gels in polar solvents such as DMSO and propan-1,2-diol along with aliphatic solvents and fuels which makes them versatile gelators. **PIV4** turned out to be the most versatile in terms of the number and types of solvents congealed. **PIV5** and **PIV6** are amides of long-chain fatty acids and could congeal higher alkane homologs, engine oil, silicone oil, etc. fairly well (Figures 4.5, 4.6). The gelation ability of **PIV5** was found to be better than **PIV6** because of the presence of longer terminal aliphatic chain which may increase van der Waals interactions and lipophilicity of the molecules to achieve the delicate hydrophilic-hydrophobic balance required for gelation of organic solvents.

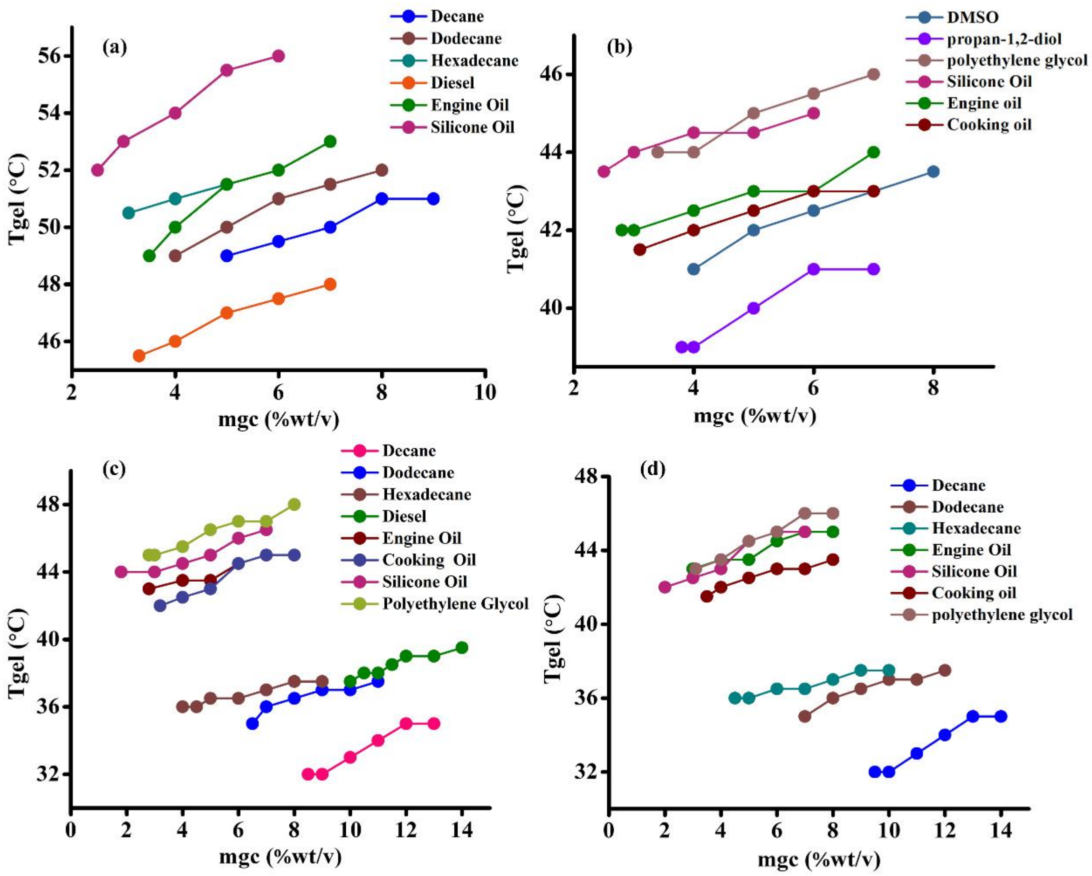

Figure 4.6 T_{gel} vs. concentration plots for (a) PIV2, (b) PIV3, (c) PIV5, (d) PIV6

A semilog graph of mole fraction of gelator concentration plotted against 1/1000 T_{gel} (K^{-1}) for gels in alkane homologs and DMSO, propan-1,2-diol, etc. gave a nearly linear relationship according to the Schroeder-van Laar equation- (equation 4.1)

$$\textbf{ln[gelator]} = - \left(\frac{\Delta \mathbf{Hm}}{RT_{gel}}\right) + \textbf{constant} \qquad - (4.1)$$

ΔH_m values calculated from the plots fell within a range of 77-320 kJ/mol (Figure 4.7). This further confirmed that the gel-to-sol transition can be considered a first-order transition as the gel melts into a solution and a known amount of gelator is involved in the transition.

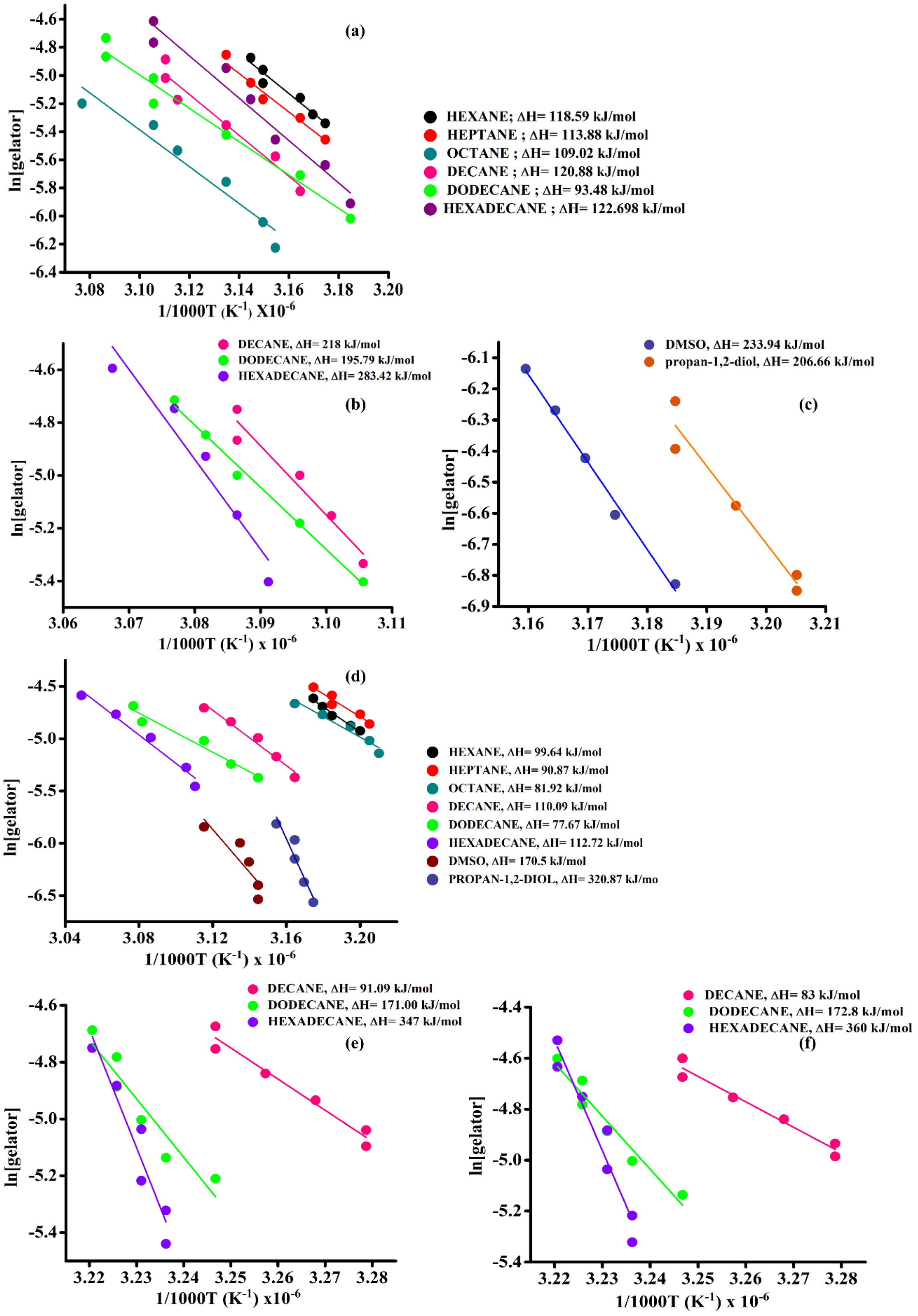

Figure 4.7 ΔH values for (a)-(f) PIV1-PIV6 according to the Schroeder-van Laar equation

4.4.2 Phase selective organo-gelation in oil-water systems

In the light of the above results, we extended our efforts to optimize these gelation systems in presence of water, for possible remediation of marine oil spills. We carried out phase selective organogelation of **PIV1**, **PIV2**, **PIV4** and **PIV5** in diesel and similar aliphatic solvents (decane, dodecane, hexadecane, kerosene, silicone oil, engine oil) in presence of water. Gelation could also be achieved in presence of water containing salts like NaCl, Na_2SO_4, $MgCl_2$, and impurities like $KMnO_4$, which could be useful in tackling oil spill issues in an environmental setting.

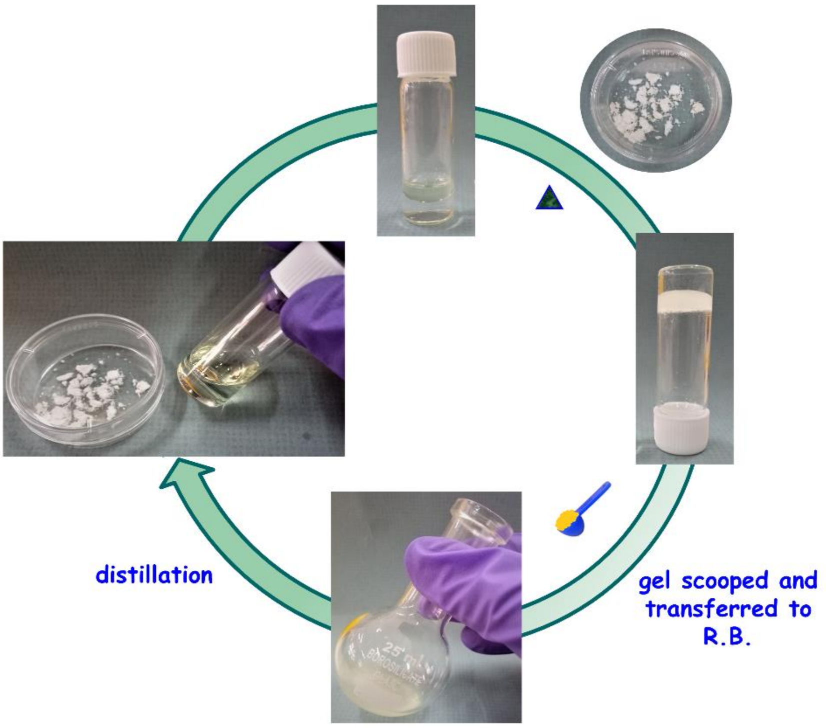

Figure 4.8 Demonstration of Phase Selective Organo-Gelation (PSOG)

All the compounds could gel diesel on water surface efficiently when added in powder form, as well as in presence of carrier solvents. However, in powder form, it required a minimum temperature of 44°C (or very strong sunlight) to instigate gelation (Figure 4.8). The idea of employing a powder-based gelator came from the fact that carrier solvents often ended up dispersing in water, thus polluting it and doing more harm than good.[7,14] But attaining a temperature of 44°C in a large water body could be tough and we decided to improvise the gelation trials in presence of secondary solvents.

Solution-based PSOGs have so far displayed better performance than powder gelators as they enhance the gelling ability and increase the solubility of gelator molecules in the gelling solvent.[13] Also, we minimize the issue of poor diffusion of gelator which can cause uneven gelation in the case of powder gelators. To our satisfaction, methanolic and ethanolic solutions of compound **PIV1** (6-8%) showed efficient gelation of diesel from the diesel-water mixture at 32-36℃. But in order to avoid dispersion of water-soluble carrier solvents, we decided to employ non-polar solvents, which exhibited good gelation behavior in their own right. A solution of diesel (6-8%) was prepared and added to the diesel-water mixture in warm condition. This led to the gelation of all the diesel present in the system over the water surface, without contaminating either solvent.

4.4.3 Toxic dye removal

Dyes are widely used in paints, plastics, textiles, drugs, food products, rubbers, printing, cosmetics, etc. Most of the dyes which are commercially employed are non-biodegradable, highly persistent in environment and can have hazardous toxic effects (even at low concentrations) on aquatic life when discharged in the water bodies. In this regard, supramolecular gels have a great potential for effective adsorption of dyes into the gel network, thereby reducing the concentration of pollutants in aqueous medium. They have a high nano-scale surface area which can directly interact with the solvated dyes. They allow reversible binding, and their responsiveness has a great potential for recyclability and reusability.

Figure 4.9 Inverted glass vials in dye removal experiments

Dyes have hydrophobic conjugated π-systems which are responsible for their color, and hydrophilic groups which allow them to be water soluble. This provides a structural similarity with LMOGs which make them compatible for a reversible binding *via* efficient hydrophobic interactions between the gel networks with the dye molecules, as, gels are often amphiphilic in nature which can assist them in forming interactions with the dye molecules.

This inspired us to explore the synthesized organogelators for removal of toxic dyes from water. The dyes dissolved in aqueous medium can be absorbed by the organogel on the water surface *via* aforementioned mechanism. Thus, employing PSOG for removal of pollutants from effluent wastewater can be one of the most exotic applications of low molecular weight gelators.

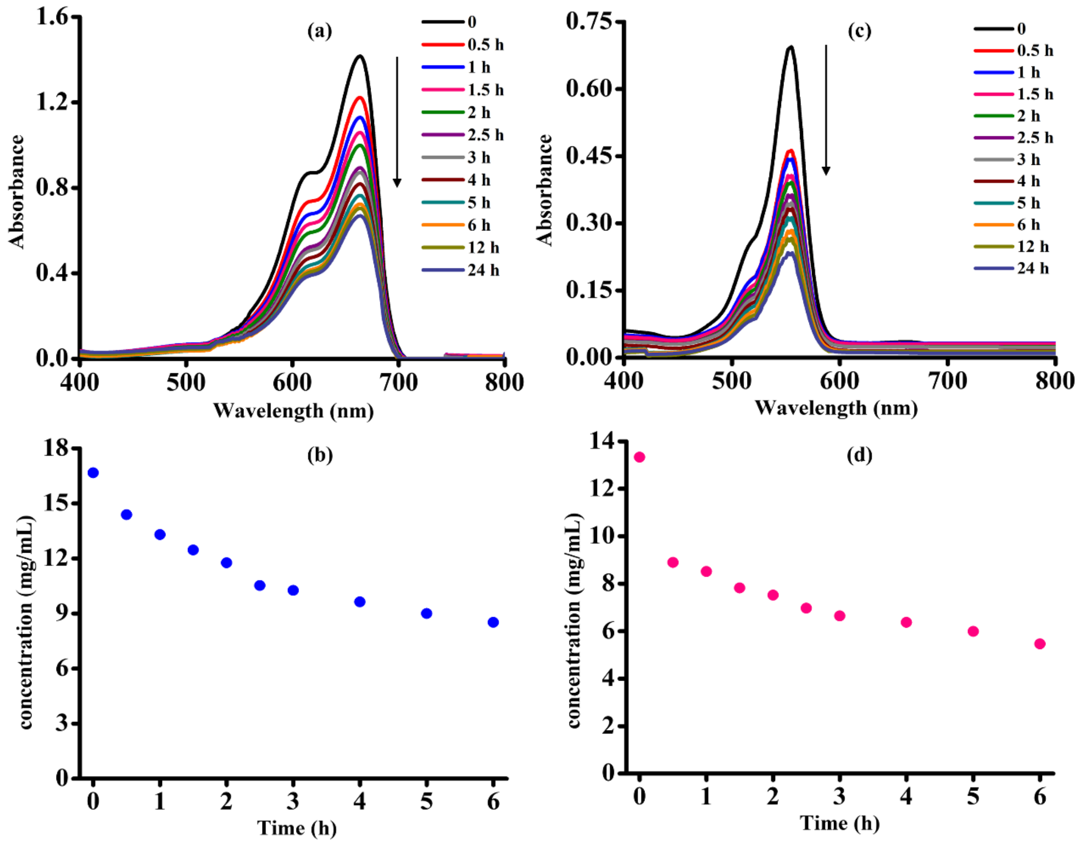

Figure 4.10 Time dependent absorption studies for PIV1 in an aqueous solution of 1.5 mL which contains (a) methylene blue dye at an initial concentration of 25mg/1.5 mL and (b) concentration-time correlation at 664 nm, (c) Rhodamine B dye at an initial concentration of 20mg/1.5mL, in presence of 1mL of diesel congealed on the water surface using 8% of PIV1 and (d) its concentration-time correlation at 554 nm.

Compounds **PIV1**, **PIV4** and **PIV5** were employed for this purpose for removal of Rhodamine B and Methylene Blue dyes. Since we have primarily focused on phase selective gelation of fuels in this study, we chose diesel as the gelation solvent. In a typical experiment, a biphasic mixture containing 1 mL diesel and 1.5 mL aqueous solution of dye (20 mg/1.5 mL Rhodamine B or 25 mg/1.5 mL Methylene Blue) was formed, the gelator was added in powder form from the top, and the solution was gently heated to approx. 40℃ to form a strong gel over the aqueous layer (Figure 4.9).

The ability of gelator to adsorb these dyes was monitored at 554 nm (for Rhodamine B) and 664 nm (for Methylene Blue) by UV-vis spectroscopy.

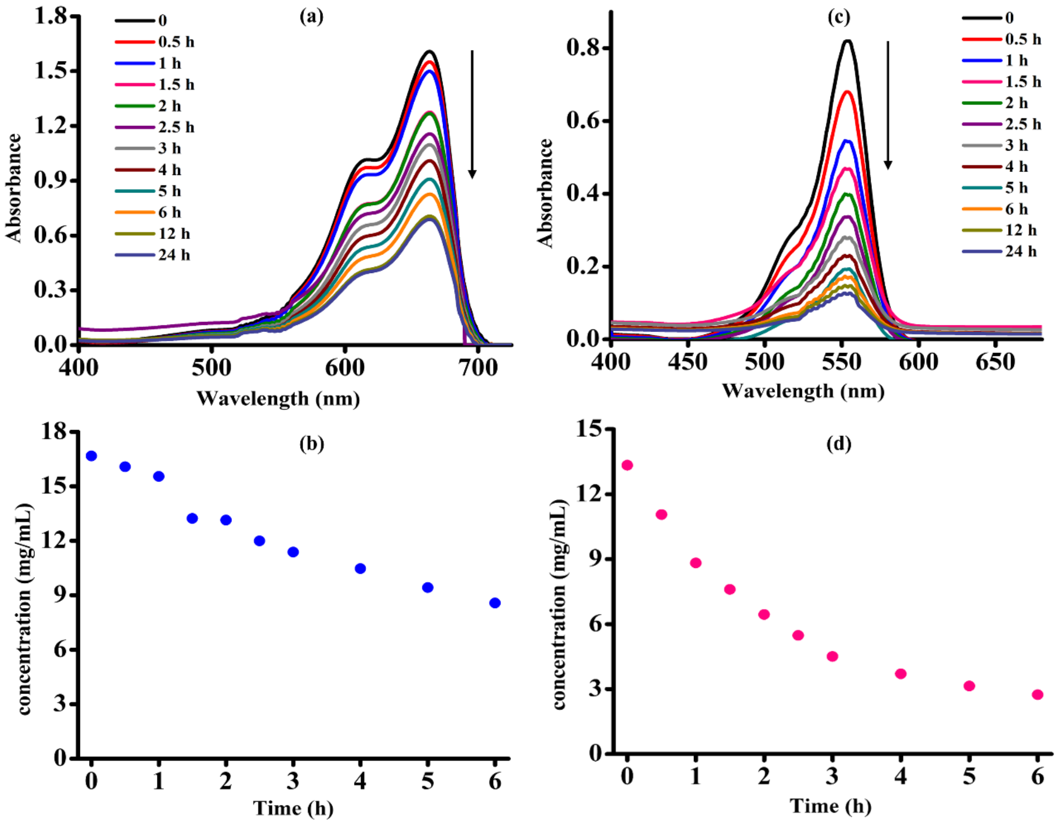

Figure 4.11 Time dependent absorption studies for PIV4 in an aqueous solution of 1.5 mL which contains (a) methylene blue dye at an initial concentration of 25mg/1.5 mL and (b) concentration-time correlation at 664 nm, (c) Rhodamine B dye at an initial concentration of 20mg/1.5mL, in presence of 1mL of diesel congealed on the water surface using 8% of PIV4 and (d) its concentration-time correlation at 554 nm.

The dye removal efficiencies were calculated from equation 4.2)

$$\boldsymbol{Removal\ efficiency} = \frac{C_0 - C_t}{C_0} * \mathbf{100}\% \qquad - (4.2)$$

where C_0= initial dye concentration, C_t= dye concentration at time t (mg/mL)

Table 4.3 Removal efficiencies

	PIV1		PIV4		PIV5	
	After 12h	After 24h	After 12h	After 24h	After 12h	After 24h
Rhodamine B	78.59	81.9	61.59	82.45	66.4	84.8
Methylene Blue	51.96	54.8	50.27	56.08	52.7	57.2

Compound **PIV4** showed maximum removal efficiency for both the dyes, 84.8% for Rhodamine B and 57.2% for Methylene Blue after 24 hours. All the compounds showed better removal efficiencies in Rhodamine B (Table 4.3), where maximum absorption could be achieved only after 12 hours, which proves that dye absorption is a time-consuming process and can take up to 24 hours for maximum absorption (Figures 4.10-4.12).

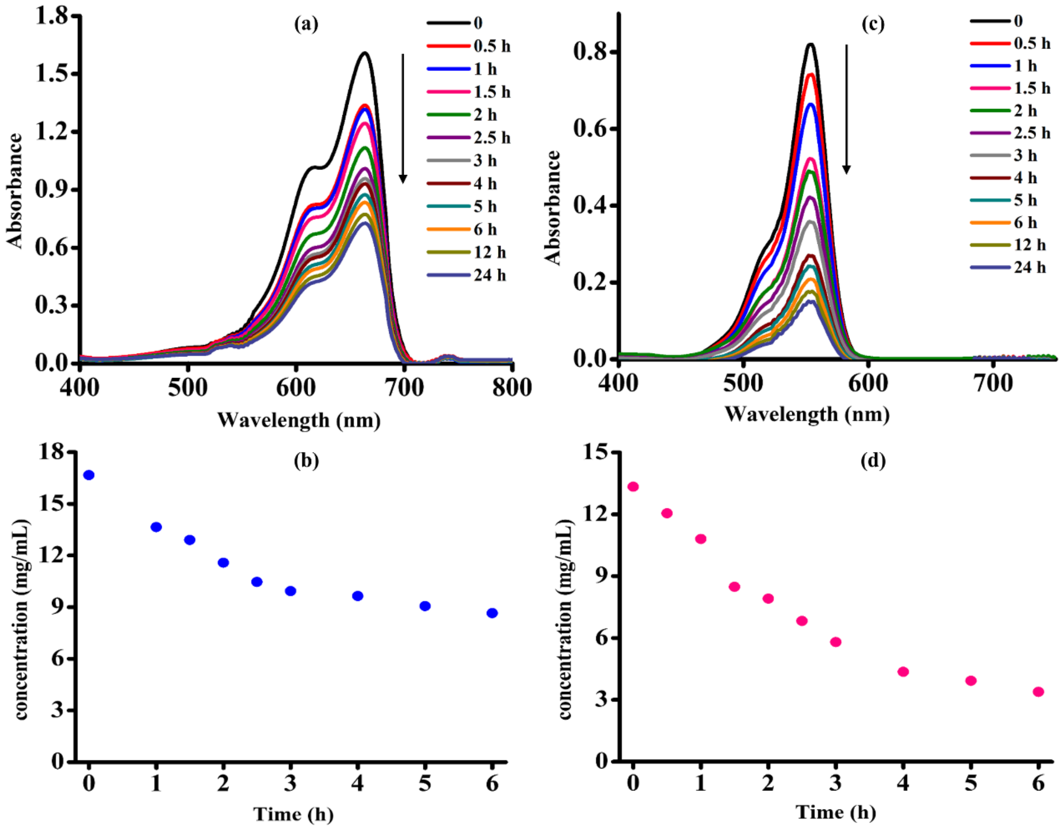

Figure 4.12 Time dependent absorption studies for PIV5 in an aqueous solution of 1.5 mL which contains (a) methylene blue dye at an initial concentration of 25mg/1.5 mL and (b) concentration-time correlation at 664 nm, (c) Rhodamine B dye at an initial concentration of 20mg/1.5mL, in presence of 1mL of diesel congealed on the water surface using 8% of PIV5 and (d) its concentration-time correlation at 554 nm.

4.4.4 Rheology

The mechanical strength of the gels was evaluated using rheology. Representative studies of compounds **PIV1**, **PIV2** and **PIV4** were performed in silicone oil gels (Figure 4.13). As depicted, the plots of storage modulus, G' and loss modulus, G" remain nearly parallel throughout and the value of G' is almost an order greater than that of G" across the frequency sweep range. This suggests that the gels have high degree of elasticity. Also, the value of tan δ, which corresponds to the loss angle was less than 1, which indicates that the gel-like elastic property was the predominant form and the compounds tend to remain in gel phase. Typically, the value of G' in all gels remained of the order of 10^5-10^4 Pa and shear thinning behavior was observed for all the three gels. The gels remained stable for several months and did not exhibit thixotropic behavior at room temperature, making them a good candidate to be employed for PSOG.

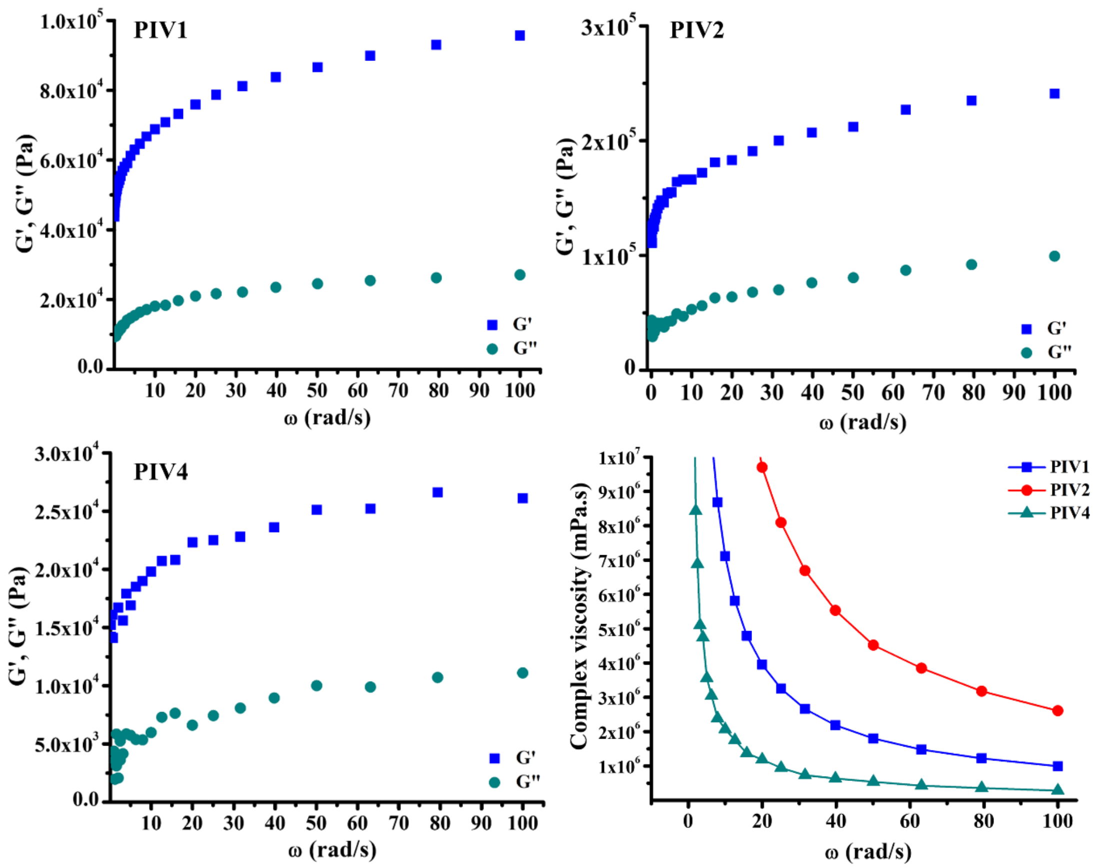

Figure 4.13 Rheological behavior of compounds and complex viscosity trends

4.4.5 Morphology

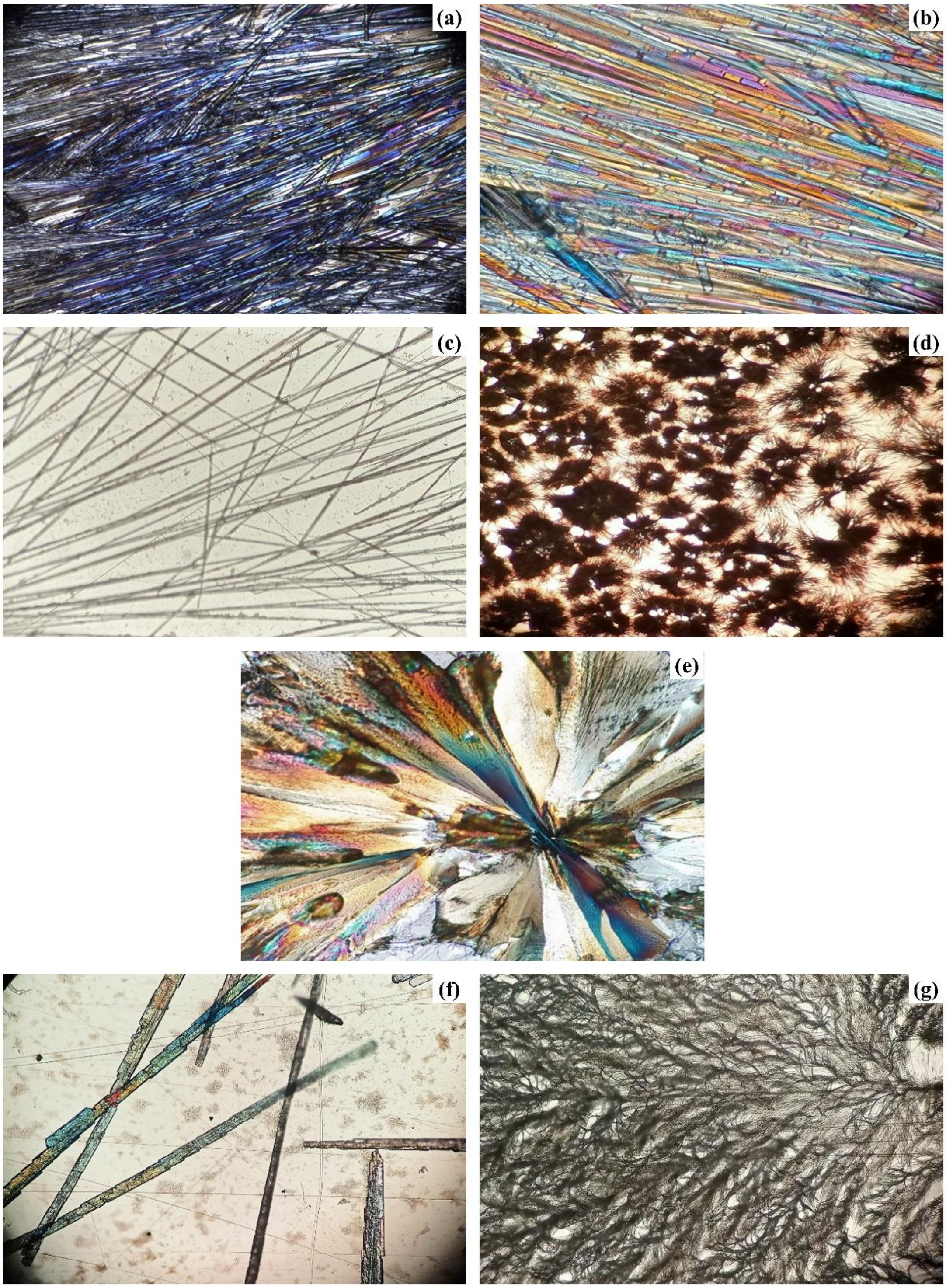

Figure 4.14 Polarized optical micrographs of PIV1 (a) 4x 0deg, (b) 10x 45 deg, in hexadecane gel (c) 10x 0 deg in decane gel; PIV2 (d) 4x 0 deg; PIV3 (e) 4x 45 deg; PIV4 (f) 10x 0 deg; PIV5 (g) 10x 90 deg in decane gels

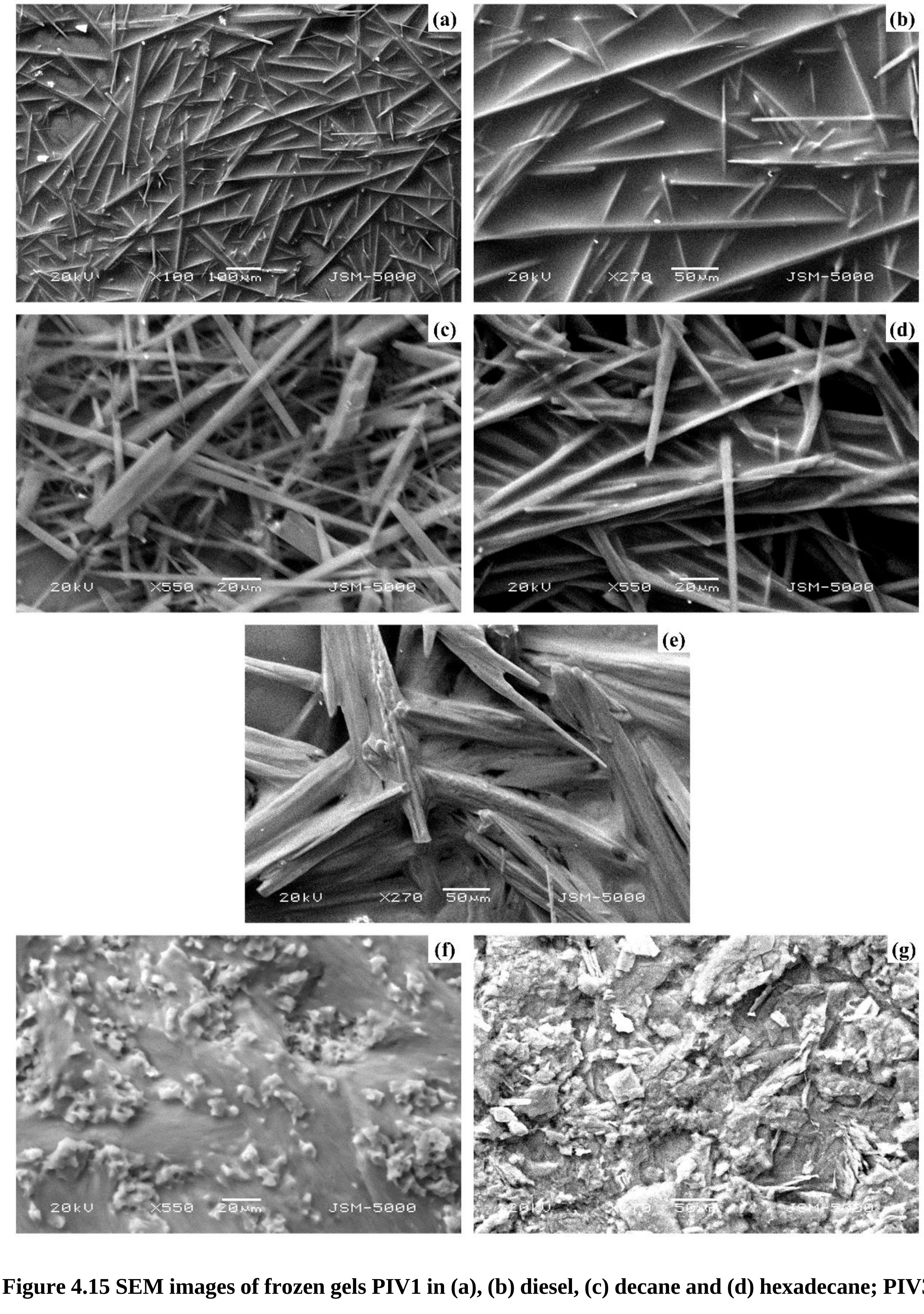

Figure 4.15 SEM images of frozen gels PIV1 in (a), (b) diesel, (c) decane and (d) hexadecane; PIV3 in (e) DMSO; PIV5 in (f) octane, (h) decane

Representative SEM of the gels in various solvents was carried out by freezing the gel layer on the SEM stubs with Liq. N_2. This was done to minimize the possibility of any morphological changes, thereby preserving and capturing the primary self-assembly of the gelator molecules. All the images are evident of long crystalline fibrils in the system, which accounts for the high opacity of the gels.

Optical micrographs of the various gel samples were captured in hexadecane solvent (Figure 4.14 (a), (b)) and n-decane solvent (Figure 4.14 (c)-(i)). Images of **PIV1** clearly show a needle-like morphology in both the solvents. Birefringence was observed in the images of **PIV1** and **PIV4**, which indicate highly ordered three-dimensional assemblies. These 3-D assemblies are generally responsible for optical anisotropy, which is an important feature of liquid crystals. It also appears that the size of the fibers increases with an increase in the carbon chain length of the solvent, which could be a result of stronger interactions among the gelator and solvent molecules, thus forming stronger self-assemblies.

The SEM images (Figure 4.15) of gels **PIV1** and **PIV3** in different solvents clearly showed a well-defined needle-shaped crystalline arrangement, (also evident in the polarizing optical microscopy images) which may be governed by corresponding 1-D hydrogen-bonded networks as observed in the single-crystal structures. However, the gels formed by **PIV4** and **PIV5**, displaying bundles of crystals and irregularly shaped crystals respectively, suggested a different type of supramolecular packing in gel/xerogel state as compared to its single-crystal X-ray structures.

4.4.6 Structure – Property correlation (Single crystal X-ray studies)

To understand the probable non-covalent interactions supporting gelation/non-gelation performance of the newly synthesized series of compounds, efforts were directed to grow crystals suitable for single-crystal X-ray diffraction studies as, obtaining single crystals suitable for the X-ray diffraction studies of gelator molecules is still considered to be a challenging task. Fortunately, in this study, we could obtain single crystals for both gelling and non-gelling compounds.

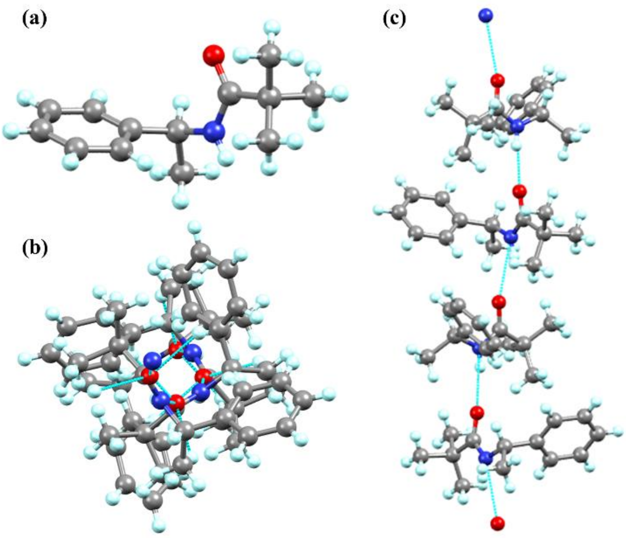

Figure 4.16 (a) asymmetric unit of PIV1 as obtained from single crystal studies, (b) 1-D pattern of PIV1 as viewed from *a* axis, (c) H-bonded assembly as viewed from *c* axis

PIV1 ***[(N-(1-phenylethyl)-2,2-dimethylpropanamide]*** The crystals of compound **PIV1** were obtained from nitrobenzene, the molecule crystallizes in a unique tetragonal crystal system with a chiral $P4_32_12$ space group. The structure contains a distinct 1-D H-bonded pattern commonly observed in amide…amide supramolecular synthons (Figure 4.16). Other interactions such as C-H…O are also prevalent in the structure which further enhances the stability of 1-D H-bond and overall packing. The presence of chiral center (promoted the crystallization of **PIV1** in higher symmetry space group) and the bulky group (hindered the proximity of two molecules) at the end of the **PIV1** appeared to favor the formation of 1-D hydrogen-bonded network.

PIV2 ***[N-(3-ethynylphenyl)-2,2-dimethylpropanamide]*** The crystals of **PIV2** were obtained from methanol and the structure belongs to the orthorhombic, $Pca2_1$ space group. This structure too, exhibits a 1-D arrangement of molecules (Figure 4.17) formed as a result of N-H…O bonds (bond length= 2.050 Å, *C(4)* graph set). The 1-D hydrogen-bonded network extends to the 2-D assembly through multiple weak interactions, i.e. (acetylenic) C-H…π(benzene) [(Bond distance C-H…centroid(benzene)=3.055Å)]

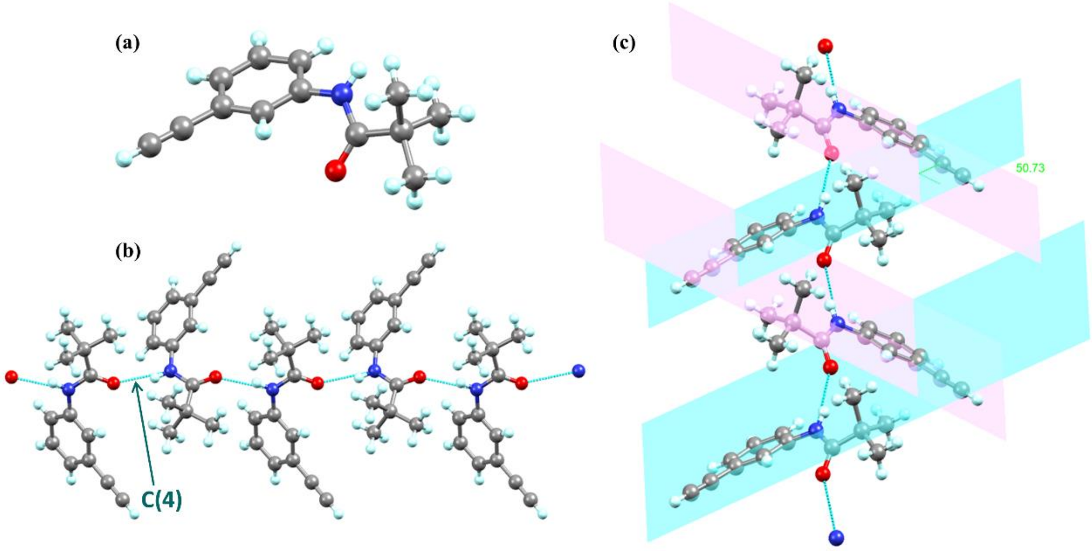

Figure 4.17 (a) 1-D systematic arrangement formed in PIV2 as viewed from *b* axis, (b), (c) angles formed between adjacent benzene rings in PIV2 forming an alternative arrangement

PIV5 ***[N-hexadecyl-2,2-dimethylpropanamide]*** Crystals of **PIV5** were obtained in a mixture of ethanol and acetonitrile at a low temperature. The structure belongs to the monoclinic, *Pc* space group and contains 2 molecules in the asymmetric unit. The structure showcases an ordered one-dimensional array of **PIV5** molecules extended as a result of N-H…O bonding (bond length= 2.189 Å, Figure 4.18 (a)). Surprisingly, no interdigitation or van der Waals interactions between the neighboring aliphatic chains were observed. The 1-D hydrogen-bonded network supports the formation of a fibrillar network and a highly hydrophobic environment promoted the immobilization of hydrocarbon solvents leading to the formation of a gel. Although, an alternate arrangement of aliphatic chains between consecutive molecules was observed which ensures minimal repulsive interactions between them, providing extra stability to the so-formed assembly.

PIV7 ***[N,N-bis(2-pivalamidoethyl)-2,2-dimethylpropanamide]*** **PIV7** is a pivalamide of diethylene triamine where all the three nitrogen atoms form amide with pivalic acid. Single crystals of **PIV7** were obtained from ethanol. The compound crystallizes out in $P2_1/n$ space group and the asymmetric unit contains one molecule. The close proximity of amide groups leads to intramolecular hydrogen bond formation (N-H…O) among the neighboring amide groups which restricted the movement of aliphatic chains leading to the formation of a zero-dimensional (0-D) hydrogen-bonded network. The 0-D network extends to 3-D through multiple C-H…O interactions. The H-bonding contacts extend in a dense 3-D pattern as a result of various N-H…O bonds (bond length= 2.053 Å), forming a *C(4)* type graph set. The structure also forms an intramolecular N-H…O bond (bond length= 2.067 Å) bearing *S(7)* type graph set. (Figure 4.18 (b))

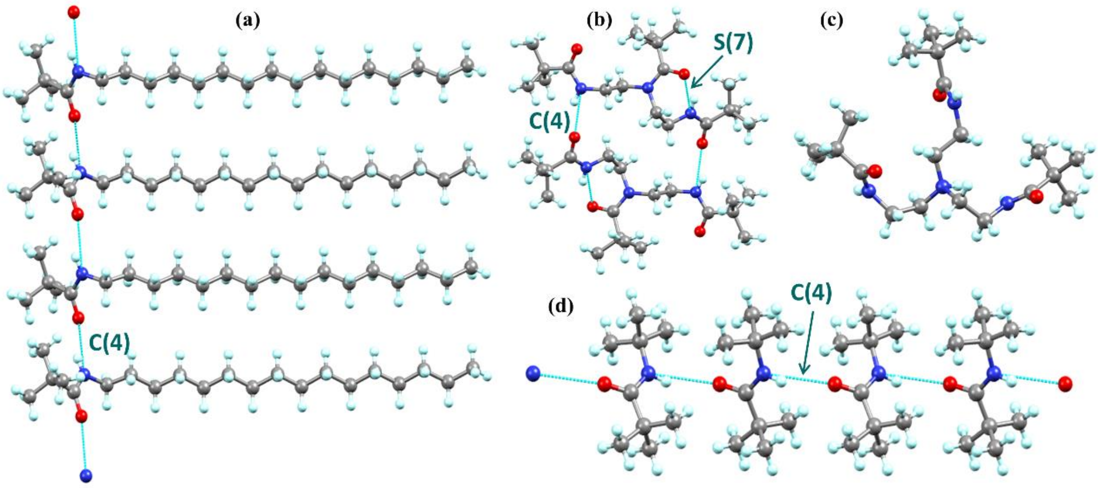

Figure 4.18 (a) molecules of PIV5 forming a 1D H-bonded network, (b) closed assembly formed in PIV7 *via C(4)* and *S(7)* type graph sets; (c) asymmetric unit of PIV8; (d) 1D pattern of PIV9 as observed from *b* axis

PIV8 ***[N, N', N"- (nitrilotris(ethane-2,1-diyl))tris(2,2-dimethylpropanamide)]*** **PIV8** is a pivalamide of tris(2-aminoethyl)amine. The crystals were obtained by slow evaporation from acetonitrile and methanol at 20℃ and the structure belongs to monoclinic, *P2₁/c* space group. All the amide groups in the structure were found to involve in 1-D hydrogen bonding interactions (bond length= 2.062 Å), commonly known as amide…amide synthons. Interestingly, the increase in the chain length of each branch of molecules deterred the formation of intramolecular hydrogen bonds and promoted the formation of a 1-D hydrogen-bonded network in the three directions leading to the formation of 3-D hydrogen-bonded assembly. Multiple C-H…O interactions further stabilized the 3-D network of compound **PIV8**. (Figure 4.18 (c)).

PIV9 ***[N-(tert-butyl)-2,2-dimethylpropanamide]*** Single crystals of **PIV9** were obtained from a mixture of methanol and ethanol. The structure crystallizes out in $P2_1/c$ space group of the monoclinic crystal system. The molecules of **PIV9** displayed unusual non-covalent interactions between (amide) N-H…O (carbonyl) and (methyl) C-H…O (carbonyl) with a very long bond distance between the N…O and C…O, i.e. 3.218 Å and 3.505 Å, respectively. Understandably, the absence of a commonly occurring 1-D chain or 0-D hydrogen-bonded network in amide-based synthons may be attributed to the proximity of two bulky tert-butyl groups. Moreover, such a long distance between the donor (N, C) and acceptor (O) atoms qualify them as very weak H-bond or van der Waals interactions (Figure 4.18 (d)). Overall, the assembly is a 1-D network without any additional short contacts.

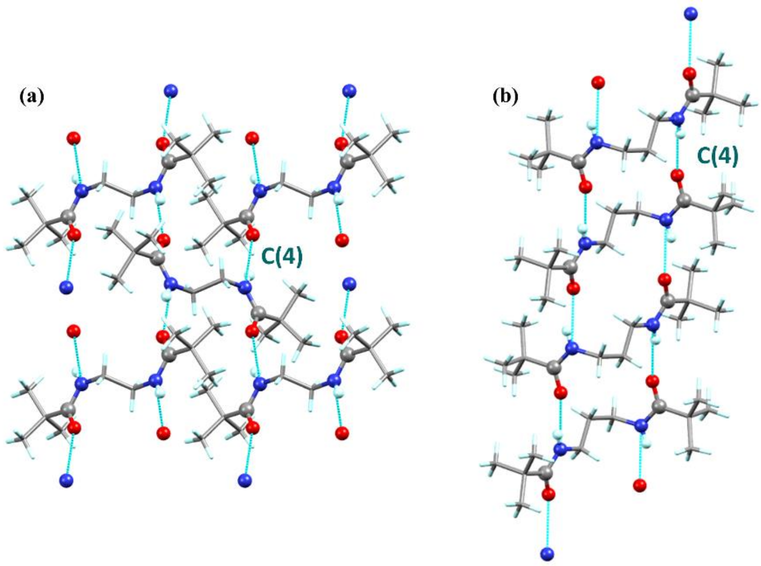

Figure 4.19 (a) overall 3D assembly formed in PIV10, as viewed from b axis; (b) 1D assembly of PIV11 as viewed from *b* axis

PIV10 ***[N,N'-(ethane-1,2-diyl)bis(2,2-dimethylpropanamide)]*** Single crystals of **PIV10** were obtained from a mixture of methanol and ethanol. The structure belongs to the monoclinic $P2_1/c$ space group. The presence of two amide functionalities along with tert-butyl groups at the end of the molecule leads to the formation of a 2-D hydrogen-bonded network. Interestingly, the 1-D supramolecular synthon commonly observed in the amide…amide hydrogen-bonded network is also present in the structure. Multiple C-H…O interactions between neighboring molecules further stabilizes the 2-D sheet type network. (Figure 4.19 (a)).

PIV11 ***[N,N'-(propan-1,3-diyl)bis(2,2-dimethylpropanamide)]*** Good diffraction quality single crystals were obtained from methanol. The asymmetric unit contains two molecules of **PIV11** and the crystal structure belongs to *P-1* space group of the triclinic crystal system. 1-D hydrogen-bonded ribbon structure is observed, driven by amide…amide 1-D hydrogen-bonded synthon. The 1-D ribbon structure further extends to a 3-D network through multiple van der Waals interactions between neighboring methyl groups. (Figure 4.19 (b)).

The single-crystal structures of mono-amide gelators (**PIV1**, **PIV2**, and **PIV5**) and non-gelators (**PIV9**) displayed 1-D hydrogen-bonded networks along with weak non-bonded interactions such as C-H…O, C-H…π, which further stabilized the 1-D networks. The presence of long-chain and more than one amide functionality in the structures promoted 2-D and 3-D hydrogen-bonded networks, thereby supporting the working hypothesis that 1-D hydrogen-bonded networks support organogelation.

4.4.7 Hirshfeld analyses

Hirshfeld studies performed on the crystal structures of gelators and non-gelators molecules showed the presence of a very high percentage of van der Waals interactions in the structures (ranging from 62.2-94.6 % H…H). Other significant contributions to Hirshfeld interactions viz. O…H (2.2-9.3%) and C…H/H…C (0.1-13.1%) were observed in all the structures. Understandably, the presence of *tert*-butyl groups in the gelling and non-gelling molecules promoted a very high % of van der Waals interactions. Interestingly, the amount of C…H/H…C interactions were found to be higher in the structures of gelling molecules as compared with non-gelling compounds, which is desirable, since it is ideal for a gelator structure to show some elevated amount of non-covalent interactions, e.g. H-bonding, π-π interactions, etc. which might be participating in the formation of 1-D networks which can immobilize solvent molecules, thus causing gelation (with an exception of non-gelator **10A**, which contains a long chain and multiple amide groups). (Figures 4.20, 4.21).

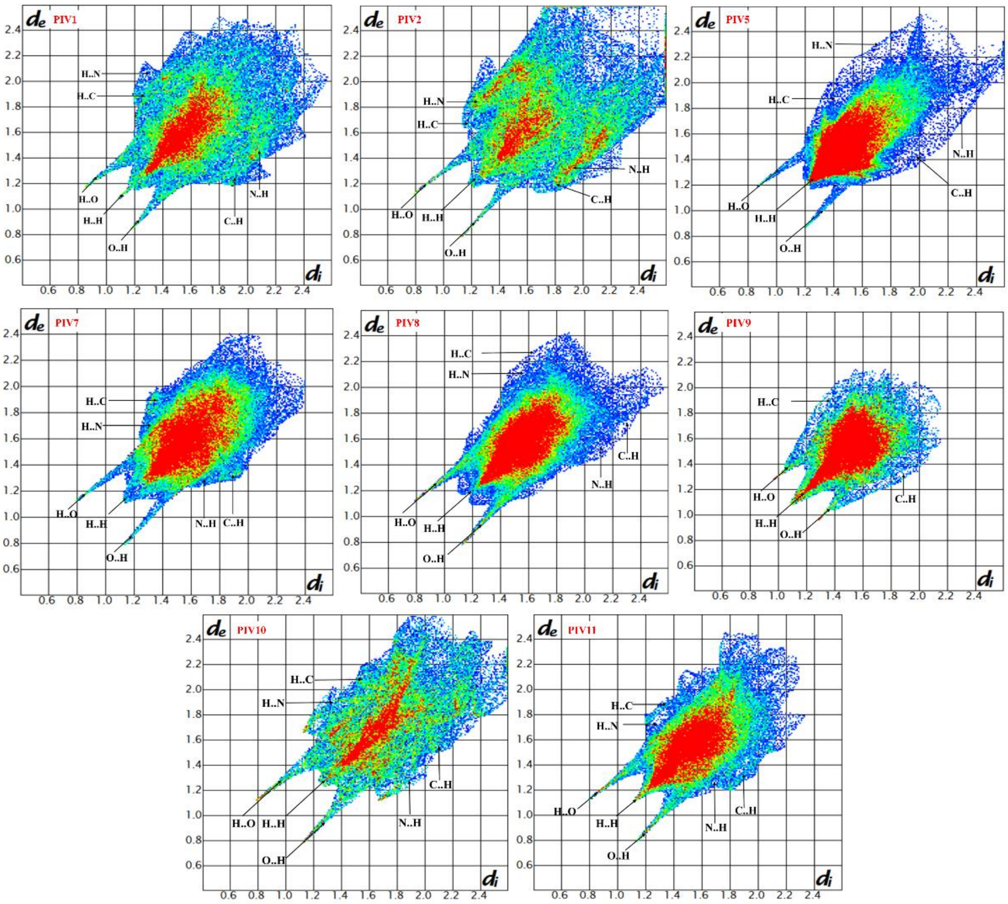

Figure 4.20 Two-Dimensional fingerprint plots of the compounds. Color in the sequence white-blue-green-red is a summary of the frequencies of each combination of distances d_e and d_i across the Hirshfeld surfaces of a molecule (in increasing order), where d_i is internal distance and d_e, external distance from the Hirshfeld surface to the nearest molecule

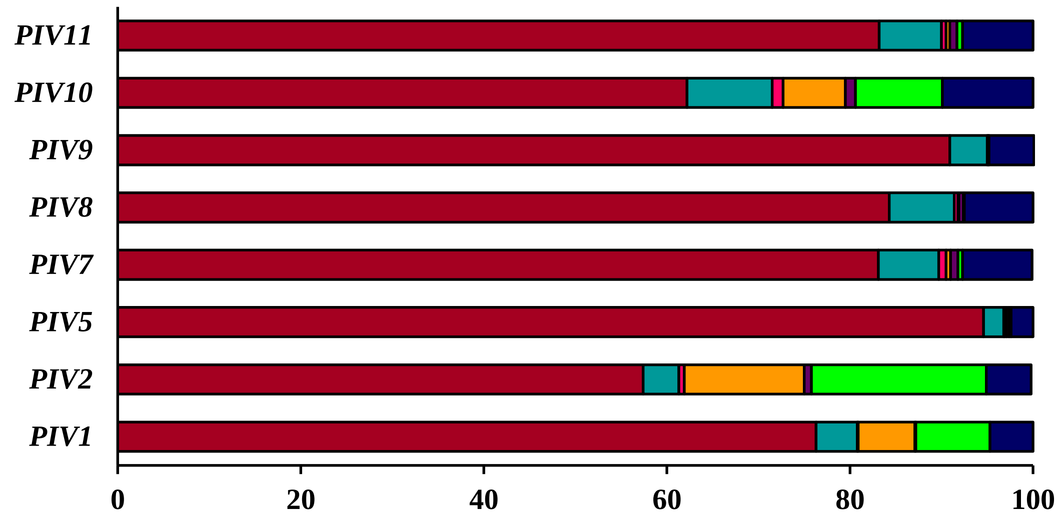

	PIV1	PIV2	PIV5	PIV7	PIV8	PIV9	PIV10	PIV11
H…H	76.3	57.4	94.6	83.1	84.3	90.9	62.2	83.2
H…O	4.5	3.9	2.2	6.6	7.1	4.1	9.3	6.8
H…N	0.1	0.6	0.1	0.8	0.4	0	1.2	0.5
H…C	6.2	13.1	0.2	0.5	0.1	0.1	6.8	0.4
N…H	0.1	0.8	0.3	0.8	0.5	0	1.1	0.8
C…H	8.1	19.1	0.2	0.5	0.1	0.1	9.5	0.6
O…H	4.7	4.9	2.4	7.6	7.5	4.9	9.9	7.7

Figure 4.21 Hirshfeld interactions for all crystals obtained in the series

4.4.8 PXRD studies

To confirm whether the packing observed in the single-crystal structure of the gelator is retained in the xerogel or not, we carried out PXRD studies of bulk compound **PIV1**, and its xerogel samples obtained from various solvents. Comparative spectra of PXRD were plotted for **PIV1** (bulk), simulated (obtained from X-ray structure) and xerogel (obtained from different solvents) to get an insight into the packing of **PIV1** in various states. (Figure 4.22).

The plot showed that all the major peaks remained intact, which confirms that the molecular packing in crystalline and bulk solid is similar. Also, all the major peaks of xerogels resembled those in the bulk system/simulated indicates that no significant change in hydrogen bonding pattern and packing of **PIV1** even after drying of solvents (xerogel).

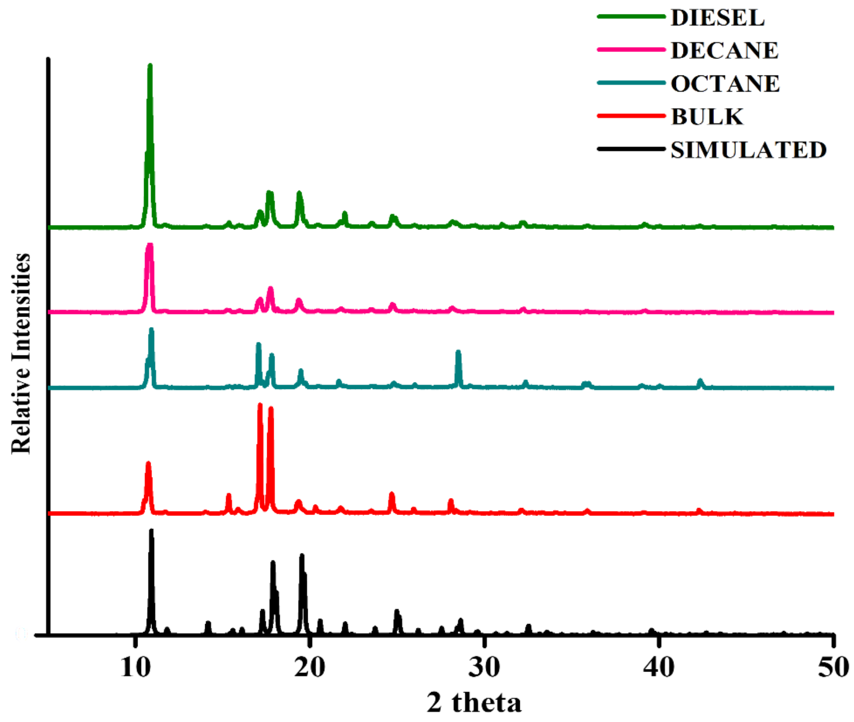

Figure 4.22 Stacked PXRD patterns in simulated, bulk and xerogel forms for PIV1

4.4.9 Comparative FT-IR studies

Comparative FT-IR studies were carried out where the spectra were recorded for **PIV1** in various states, namely, bulk, xerogel, gel form, and in solution phase (solvent- n-octane).

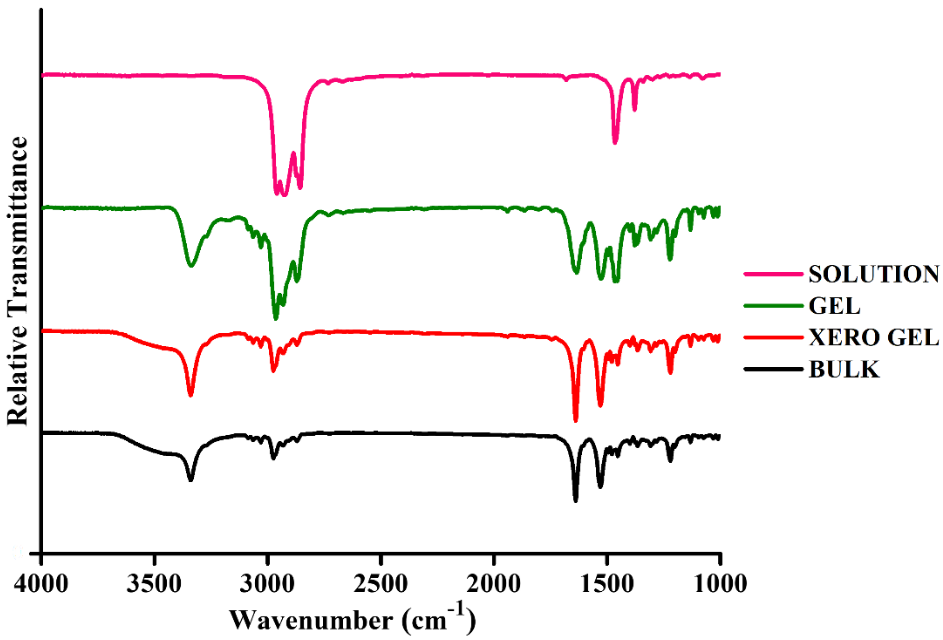

Figure 4.23 Stacked FT-IR spectra of PIV1 in bulk, xerogel, gel and solution forms

A strong band corresponding to C=O stretching vibration was observed at 1639 cm^{-1} in bulk, 1638.7 cm^{-1} in xerogel, 1634 cm^{-1} in the gel phase, and a weak band around 1680 cm^{-1} were observed in solution (Figure 4.23). Similar was the trend in N-H bending vibration band around 1530 cm^{-1} and N-H stretching band around 3339 cm^{-1}, both of which were retained in the gel phase and found to be absent in the solution phase.

4.5 CONCLUSIONS

We have demonstrated organogelation in a library of newly designed and synthesized *tert*-butyl functionalized small molecules. The designing strategy for a new gelator based on **π/Al-A-B** (aromatic/aliphatic-amide linker-bulky group) type design turned out to be quite successful, leading to the discovery of six new gelators. However, the role of the aliphatic backbone, number of amide functionalities, and structure of terminal groups attached to the molecules, by and large govern the gelling and non-gelling property of the molecules in this series. These compounds were extensively exploited to showcase an exceptional gelation behavior towards aliphatic long-chain solvents in various conditions (viz. external heat, strong sunlight, UV light, and ultrasonication). By far, these compounds are some of the smallest molecules (prepared by easy one-step synthesis) employed for successful phase selective organogelation in water-oil type mixtures, with an extraordinary gelation performance in both powder form and presence of secondary solvents, offering a viable method for easy recovery and good recyclability, also applicable in a typical environmental setting.

The single-crystal structures show prominent 1-D columnar networks in all the gelling compounds whereas non-gelators mostly displayed 2-D and 3-D hydrogen-bonded networks. Non-gelator **PIV9** displayed a 1-D hydrogen-bonded network but a short carbon chain in **PIV9** appears to be insufficient to reach the delicate hydrophilic-hydrophobic balance required for gelling organic solvents.

Additionally, these compounds were successfully tested for their ability to uptake dyes present in an aqueous medium, with satisfactory removal efficiencies. We believe such a simple strategy of designing new molecules may open a door of opportunities for the synthesis of new organogelators with potential applications.

REFERENCES

1. Schrope, M. Oil spill: Deep wounds. *Nature* **472**, 152–154 (2011).
2. Buist, L., McCourt, J., Potter, S., Ross, S. & Trudel, K. In situ burning. *Pure Appl. Chem.* **71**, 43–65 (1999).
3. Kumar, V., Kumar, M. & Prasad, R. *Microbial action on hydrocarbons*. *Microbial Action on Hydrocarbons* (Springer, 2019).
4. Adebajo, M. O., Frost, R. L., Kloprogge, J. T., Carmody, O. & Kokot, S. Porous Materials for Oil Spill Cleanup: A Review of Synthesis and Absorbing Properties. *J. Porous Mater.* **10**, 159–170 (2003).
5. Wang, S., Liu, K., Yao, X. & Jiang, L. Bioinspired surfaces with superwettability: New insight on theory, design, and applications. *Chem. Rev.* **115**, 8230–8293 (2015).
6. Ohsedo, Y. Low-molecular-weight organogelators as functional materials for oil spill remediation. *Polym. Adv. Technol.* **27**, 704–711 (2016).
7. Okesola, B. O. & Smith, D. K. Applying low-molecular weight supramolecular gelators in an environmental setting – self-assembled gels as smart materials for pollutant removal. *Chem. Soc. Rev.* **45**, 4226–4251 (2016).
8. Vibhute, A. M. & Sureshan, K. M. How Far Are We in Combating Marine Oil Spills by Using Phase-Selective Organogelators? *ChemSusChem* **13**, 5343–5360 (2020).
9. Saito, T., Matsuzawa, Y., Ninagawa, S., Honna, M., Takesada, M. & Takehara, M. Gels of nonpolar liquids with N-acyl amino acids and derivatives thereof as gelling agents. US Patent 3969087 A (1976).
10. Kobayashi, T., Kawashima, Y., Yoshimura, M., Sugiura, M., Nobe, T. & Fujimoto, S. Compositions for recovering an organic material from an oily layer on a body of water. US Patent US4502975A (1982).
11. Bhattacharya, S. & Krishnan-Ghosh, Y. First report of phase selective gelation of oil from oil/water mixtures. Possible implications toward containing oil spills. *Chem. Commun.* 185–186 (2001).
12. Ballabh, A., Trivedi, D. R. & Dastidar, P. New series of organogelators derived from a combinatorial library of primary ammonium monocarboxylate salts. *Chem. Mater.* **18**, 3795–3800 (2006).
13. Li, J., Huo, Y. & Zeng, H. Combinatorial identification of a highly soluble phase-selective organogelator with high gelling capacity for crude oil gelation. *J. Mater. Chem. A* **6**, 10196–10200 (2018).
14. Vibhute, A. M., Muvvala, V. & Sureshan, K. M. A Sugar-Based Gelator for Marine Oil-Spill Recovery. *Angew. Chemie - Int. Ed.* **55**, 7782–7785 (2016).
15. Ren, C., Ng, G. H. B., Wu, H., Chan, K. H., Shen, J., Teh, C., Ying, J. Y. & Zeng, H. Instant Room-Temperature Gelation of Crude Oil by Chiral Organogelators. *Chem. Mater.* **28**, 4001–4008 (2016).
16. Ren, C., Shen, J., Chen, F. & Zeng, H. Rapid Room-Temperature Gelation of Crude Oils by a Wetted Powder Gelator. *Angew. Chemie - Int. Ed.* **56**, 3847–3851 (2017).
17. Raju, C. S. K., Pramanik, B., Kar, T., Rao, P. V. C., Choudary, N. V. & Ravishankar, R. Low molecular weight gels: Potential in remediation of crude oil spillage and recovery. *RSC Adv.* **6**, 53415–53420 (2016).
18. Zhang, Y., Luan, T., Cheng, Q., An, W., Tang, R., Xing, P. & Hao, A. Highly Efficient Recovery of Oils in Water via Serine-Based Organogelators. *Langmuir* **35**, 4133–4139 (2019).
19. Lamont, K., Pensini, E. & Marangoni, A. Gelation on demand using switchable double

emulsions: A potential strategy for the in situ immobilization of organic contaminants. *J. Colloid Interface Sci.* **562**, 470–482 (2020).

20. Santschi, P. H., Chin, W. C., Quigg, A., Xu, C., Kamalanathan, M., Lin, P. & Shiu, R. F. Marine gel interactions with hydrophilic and hydrophobic pollutants. *Gels* **7**, 1–14 (2021).
21. Lin, Y.-C., Kachar, B. & Weiss, R. G. Novel Family of Gelators of Organic Fluids and the Structure of Their Gels. *J. Am. Chem. Soc.* **111**, 5542–5551 (1989).
22. Lu, L., Cocker, T. M., Bachman, R. E. & Weiss, R. G. Gelation of Organic Liquids by Some 5α-Cholestan-3β-yl N-(2-Aryl)carbamates and 3β-Cholesteryl 4-(2-Anthrylamino)butanoates. How Important Are H-Bonding Interactions in the Gel and Neat Assemblies of Aza Aromatic-Linker-Steroid Gelators? *Langmuir* **16**, 20–34 (2000).
23. Trivedi, D. R., Ballabh, A. & Dastidar, P. An Easy To Prepare Organic Salt as a Low Molecular Mass Organic Gelator Capable of Selective Gelation of Oil from Oil / Water Mixtures. *Chem. Mater.* **15**, 3971–3973 (2003).
24. Trivedi, D. R., Ballabh, A., Dastidar, P. & Ganguly, B. Structure-property correlation of a new family of organogelators based on organic salts and their selective gelation of oil from oil/water mixtures. *Chem. - A Eur. J.* **10**, 5311–5322 (2004).
25. Bhardwaj, V. & Ballabh, A. Design, synthesis, and application of a new series of organogelator using crystal engineering approach and solvent parameter study: A synergetic approach. *J. Mol. Liq.* **322**, 114520 (2021).
26. Dastidar, P. Supramolecular gelling agents : can they be designed ? *Chem. Soc. Rev.* **37**, 2699–2715 (2008).
27. Dolomanov, O. V., Bourhis, L. J., Gildea, R. J., Howard, J. A. K. & Puschmann, H. OLEX2: A complete structure solution, refinement and analysis program. *J. Appl. Crystallogr.* **42**, 339–341 (2009).
28. Sheldrick, G. M. A short history of SHELX. *Acta Crystallogr. Sect. A Found. Crystallogr.* **64**, 112–122 (2008).
29. Spackman, M. A. & Mckinnon, J. J. Fingerprinting intermolecular interactions in molecular crystals. *CrystEngComm* **4**, 378–392 (2002).
30. Spackman, M. A. & Jayatilaka, D. Hirshfeld surface analysis. *CrystEngComm* **11**, 19–32 (2009).

*SUPPLEMENTARY DATA

Crystallographic Parameters

Table S4.1 Crystallographic parameters of all single crystals solved in the study

Code	PIV1	PIV2	PIV5	PIV7
Empirical formula	$C_{13}H_{19}NO$	$C_{13}H_{15}NO$	$C_{42}H_{86}N_2O_2$	$C_{19}H_{37}N_3O_3$
Formula weight	205.29	201.26	651.12	355.51
Temperature/K	225.0	293	293	293
Crystal system	tetragonal	orthorhombic	monoclinic	monoclinic
Space group	$P4_32_12$	$Pca2_1$	Pc	$P2_1/n$
a/Å	11.4561(9)	11.198(3)	30.756(5)	14.7225(14)
b/Å	11.4561(9)	10.850(2)	7.5817(13)	10.7872(7)
c/Å	19.610(2)	10.027(2)	9.5349(15)	15.5370(14)
α/°	90	90	90	90
β/°	90	90	94.138(15)	117.949(12)
γ/°	90	90	90	90
Volume/Å^3	2573.7(5)	1218.4(5)	2217.6(6)	2179.7(4)
Z	8	4	2	4
ρ_{calc}g/cm^3	1.060	1.097	0.975	1.083
μ/mm^{-1}	0.066	0.069	0.058	0.073
F(000)	896.0	432.0	736.0	784.0
Crystal size/mm^3	0.3 × 0.1 × 0.1	0.1 × 0.1 × 0.05	0.3 × 0.2 × 0.1	0.6 × 0.5 × 0.3
Radiation	MoKα (λ = 0.71073)	MoKα (λ = 0.71073)	MoKα (λ = 0.71073)	MoKα (λ = 0.71073)
2Θ range for data collection/°	4.118 to 49.988	6.622 to 52.7	5.994 to 55.754	6.702 to 52.744
Index ranges	$-13 \leq h \leq 13$, $-13 \leq k \leq 13$, $-23 \leq l \leq 23$	$-13 \leq h \leq 13$, $-13 \leq k \leq 12$, $-12 \leq l \leq 12$	$-40 \leq h \leq 40$, $-9 \leq k \leq 9$, $-12 \leq l \leq 12$	$-18 \leq h \leq 12$, $-13 \leq k \leq 13$, $-11 \leq l \leq 19$
Reflections collected	78338	6953	45445	7084
Independent reflections	2268 [R_{int} = 0.1865, R_{sigma} = 0.0444]	2428 [R_{int} = 0.1012, R_{sigma} = 0.1445]	10293 [R_{int} = 0.1114, R_{sigma} = 0.1138]	3911 [R_{int} = 0.0141, R_{sigma} = 0.0256]
Data/restraints/parameters	2268/0/141	2428/1/139	10293/2/423	3911/0/243
Goodness-of-fit on F^2	1.035	0.872	1.059	1.475
Final R indexes [I>=2σ (I)]	R_1 = 0.0542, wR_2 = 0.1273	R_1 = 0.0679, wR_2 = 0.1517	R_1 = 0.0984, wR_2 = 0.2337	R_1 = 0.0666, wR_2 = 0.2044
Final R indexes [all data]	R_1 = 0.0951, wR_2 = 0.1552	R_1 = 0.1959, wR_2 = 0.2353	R_1 = 0.2479, wR_2 = 0.3180	R_1 = 0.0896, wR_2 = 0.2216
Largest diff. peak/hole / e Å^{-3}	0.15/-0.12	0.13/-0.19	0.30/-0.23	0.40/-0.29
Flack parameter	0.2(10)	-2.2(10)	-9.9(10)	-
CCDC No.	2051504	1993453	1993491	1861607

Code	PIV8	PIV9	PIV10	PIV11
Empirical formula	$C_{21}H_{43}N_4O_3$	$C_9H_{19}NO$	$C_{12}H_{24}N_2O_2$	$C_{26}H_{52}N_4O_4$
Formula weight	399.59	157.26	228.33	484.71
Temperature/K	293	277 K	293	293
Crystal system	monoclinic	monoclinic	monoclinic	triclinic
Space group	***P2₁/c*** → $P2_1/c$	$P2_1/c$	$P2_1/c$	***P-1***
a/Å	11.0099(10)	16.523(3)	10.207(6)	10.1712(9)
b/Å	11.6575(16)	5.9174(11)	8.167(2)	12.6952(11)
c/Å	18.9550(18)	10.2000(14)	10.051(5)	13.5196(13)
α/°	90	90	90	63.283(9)
β/°	92.455(9)	93.086(17)	118.48(7)	88.110(8)
γ/°	90	90	90	72.526(8)
Volume/Å^3	2430.6(5)	995.8(3)	736.5(7)	1476.7(3)
Z	4	4	2	2
ρ_{calc}g/cm^3	1.092	1.0488	1.030	1.090
μ/mm^{-1}	0.073	0.067	0.070	0.073
F(000)	884.0	352.1	252.0	536.0
Crystal size/mm^3	0.09 × 0.06 × 0.05	0.4 × 0.4 × 0.1	0.4 × 0.2 × 0.1	0.4 × 0.2 × 0.1
Radiation	MoKα (λ = 0.71073)	Mo Kα (λ = 0.71073)	MoKα (λ = 0.71073)	Mo Kα (λ = 0.71073)
2Θ range for data collection/°	7.41 to 51.362	7.96 to 52.74	6.746 to 52.714	6.482 to 52.744
Index ranges	$-13 \leq h \leq 13$, $-14 \leq k \leq 3$, $-13 \leq l \leq 22$	$-21 \leq h \leq 21$, $-7 \leq k \leq 6$, $-13 \leq l \leq 6$	$-12 \leq h \leq 12$, $-10 \leq k \leq 10$, $-12 \leq l \leq 12$	$-12 \leq h \leq 12$, $-15 \leq k \leq 15$, $-16 \leq l \leq 16$
Reflections collected	5510	4210	7679	24469
Independent reflections	4310 [R_{int} = 0.0298, R_{sigma} = 0.0834]	1959 [R_{int} = 0.0487, R_{sigma} = 0.0930]	1501 [R_{int} = 0.0687, R_{sigma} = 0.0582]	6028 [R_{int} = 0.0979, R_{sigma} = 0.0916]
Data/restraints/parameters	4310/0/263	1959/0/107	1501/0/76	6028/0/319
Goodness-of-fit on F^2	1.021	1.044	1.033	0.972
Final R indexes [I>=2σ (I)]	R_1 = 0.0672, wR_2 = 0.1589	R_1 = 0.0750, wR_2 = 0.1719	R_1 = 0.0664, wR_2 = 0.1640	R_1 = 0.0871, wR_2 = 0.2289
Final R indexes [all data]	R_1 = 0.1353, wR_2 = 0.1982	R_1 = 0.1237, wR_2 = 0.2129	R_1 = 0.1279, wR_2 = 0.2004	R_1 = 0.1683, wR_2 = 0.2944
Largest diff. peak/hole / e Å^{-3}	0.22/-0.46	0.53/-0.35	0.24/-0.15	0.48/-0.21
Flack parameter	-	-	-	-
CCDC No.	1858951	1858952	1861606	1993490

H-bond parameters

Table S4.2 H-bond parameters

D	H	A	d(D-H) /Å	d(H-A) /Å	d(D-A) /Å	D-H-A/°	Symmetry Op. for A
1A							
N1	H1	O1	0.87	2.14	2.938(4)	151.8	1/2+Y, -1/2-X, 1/4+Z
C8	H8A	O1	0.97	2.56	3.313(5)	134.2	1/2+Y, -1/2-X, 1/4+Z
2A							
N1	H1	O1	0.86	2.05	2.885	163.5	1/2-X,+Y,-1/2+Z
5A							
N1	H1	O1	0.86	2.19	2.961	149.3	+X,-Y,1/2+Z
N2	H2	O2	0.86	2.21	2.976	149.2	+X,1-Y,-1/2+Z
7A							
N1	H1	O2	0.86	2.07	2.812	144.6	+X, +Y, +Z
N3	H3	O1	0.86	2.05	2.846	152.8	2-X,1-Y,-Z
8A							
N3	H3	O3	0.86	2.07	2.905	164.5	-X,1-Y,-Z
N1	H1	O2	0.86	2.06	2.894	162.4	1-X,1-Y,-Z
N2	H2	N1	0.98	2.44	2.996	115.6	+X, +Y, +Z
N4	H4	O1	0.86	2.20	2.910	140.3	+X,1/2-Y,-1/2+Z
9A							
N1	H1	O1	0.86	2.39	3.218	160.7	+X,1/2-Y,1/2+Z
C9	H9A	O1	0.96	2.37	2.979	121.0	+X, +Y, +Z
C7	H7C	O1	0.96	2.59	3.163	118.6	+X, +Y, +Z
10A							
N1	H1	O1	0.86	2.05	2.852	155.2	+X,3/2-Y,1/2+Z
11A							
N1	H1	O2	0.86	2.10	2.900	154.6	1-X,2-Y,1-Z
N2	H2	O1	0.86	2.17	2.993	161.6	2-X,2-Y,1-Z
N3	H3	O4	0.86	2.18	3.019	165.4	-X,1-Y,-Z
N4	H4	O3	0.86	2.06	2.851	153.4	1-X,1-Y,-Z

ORTEP images

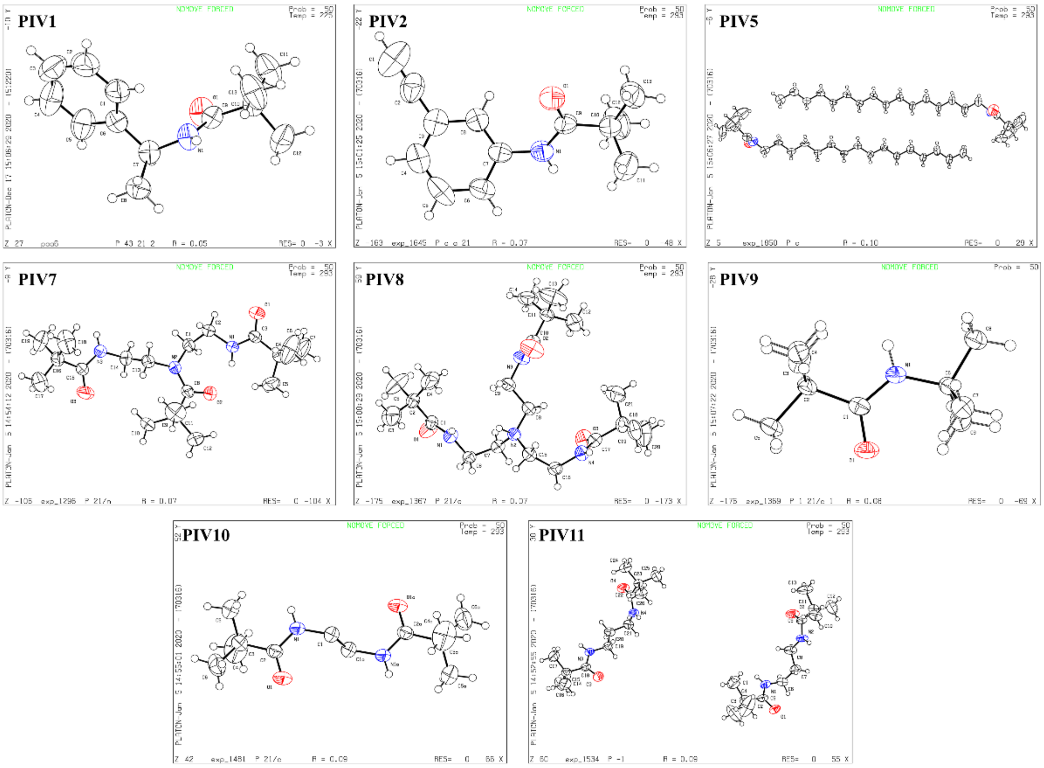

Figure S4.1 ORTEP images of all single crystals

3D Hirshfeld surfaces

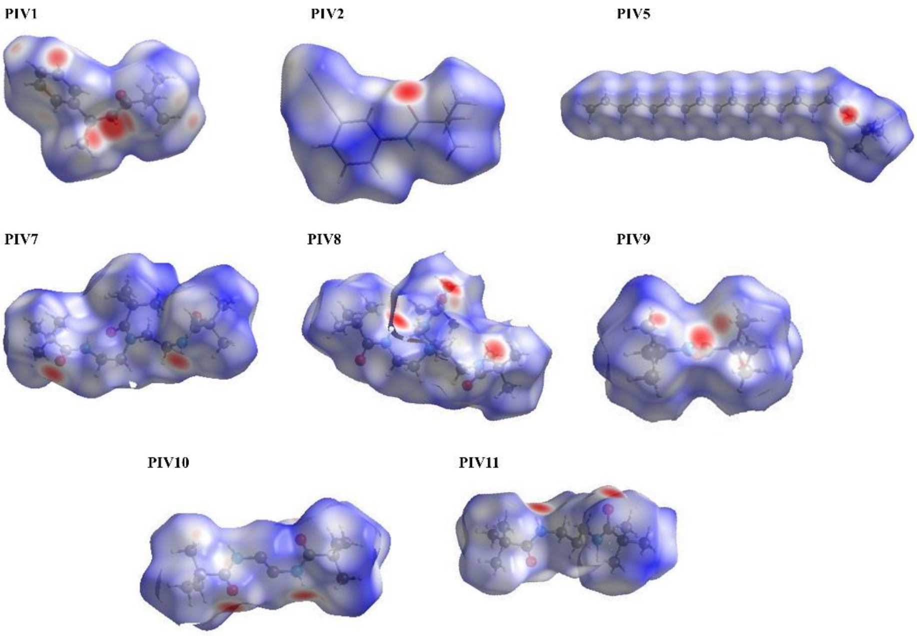

Figure S4.2 3D Hirshfeld surfaces of all single crystals

Spectral Data

^{1}H, ^{13}C and FT-IR

PIV1

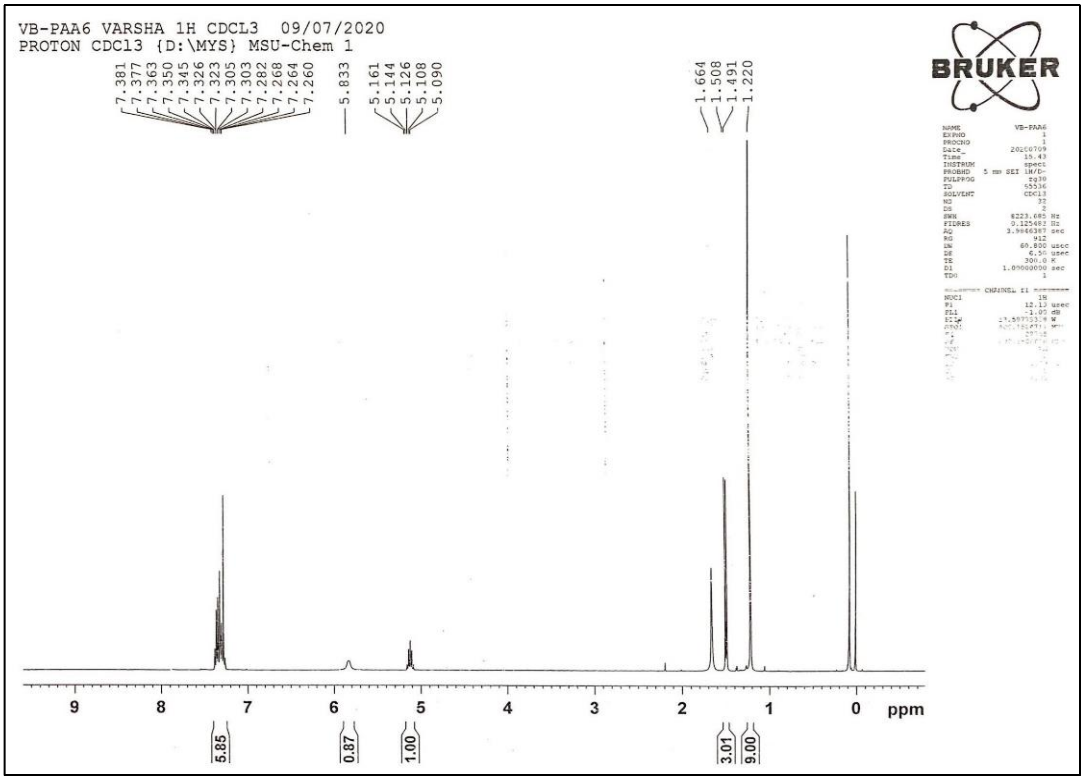

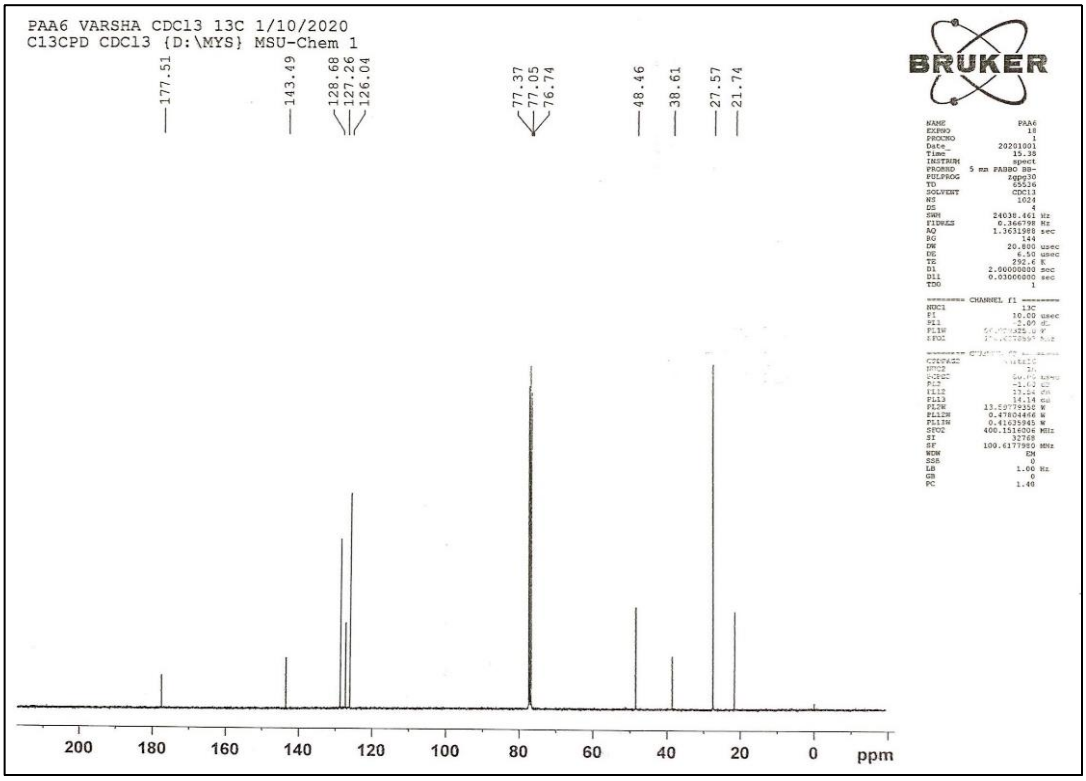

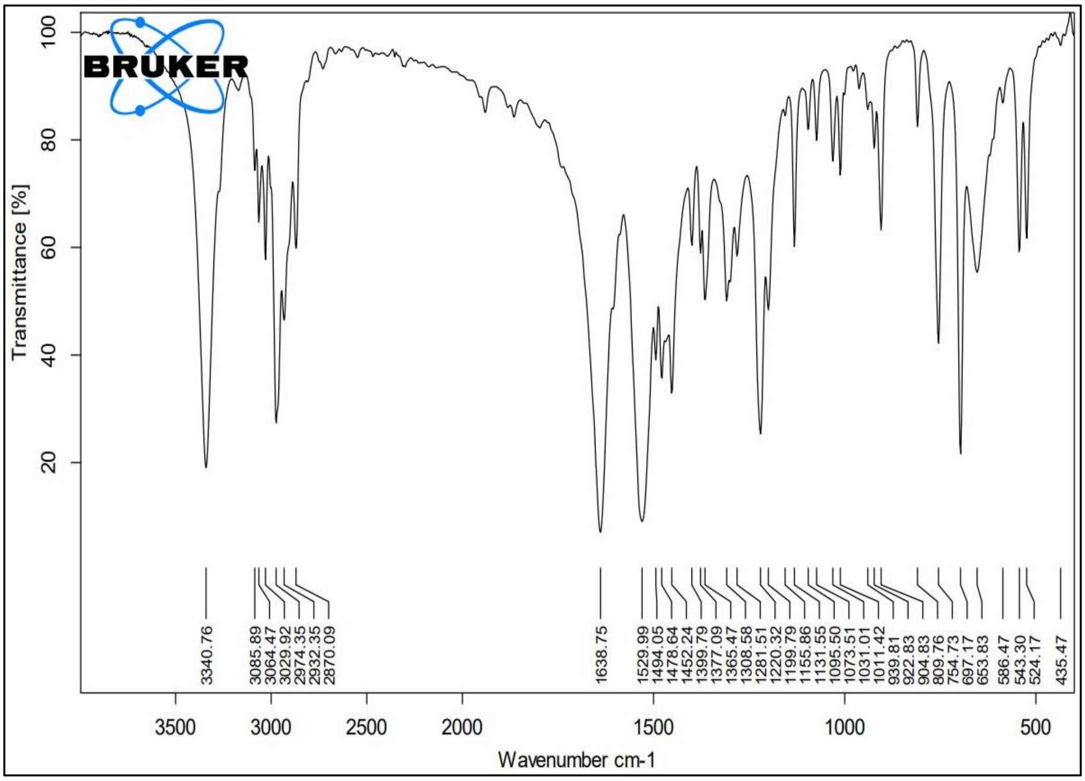
BRUKER
Transmittance [%]
Wavenumber cm-1
3340.76
3085.89
3064.47
3029.92
2974.35
2932.35
2870.09
1638.75
1529.99
1494.05
1478.64
1452.24
1399.79
1377.09
1365.47
1308.58
1281.51
1220.32
1199.79
1155.86
1131.55
1095.50
1073.51
1031.01
1011.42
939.81
922.83
904.83
809.76
754.73
697.17
653.83
586.47
543.30
524.17
435.47

PIV2

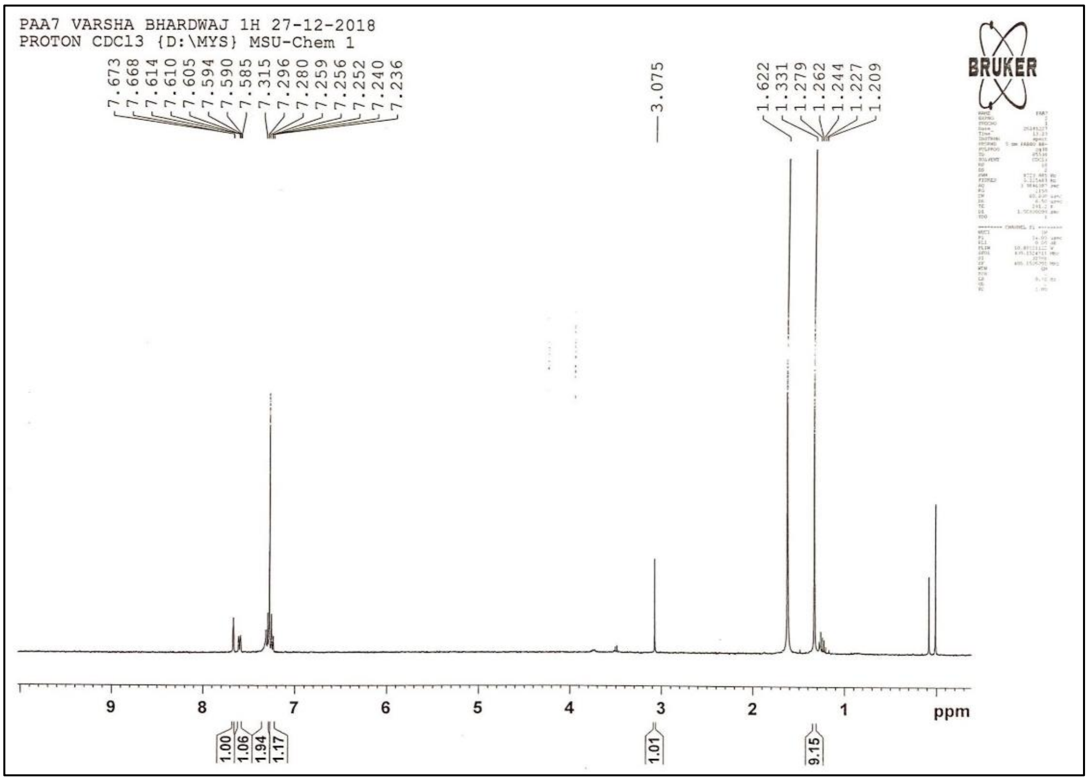
PAA7 VARSHA BHARDWAJ 1H 27-12-2018
PROTON CDCl3 {D:\MYS} MSU-Chem 1
7.673
7.668
7.614
7.610
7.605
7.594
7.590
7.585
7.315
7.296
7.280
7.259
7.256
7.252
7.240
7.236
3.075
1.622
1.331
1.279
1.262
1.244
1.227
1.209
BRUKER
ppm
1.00
1.06
1.94
1.17
1.01
9.15

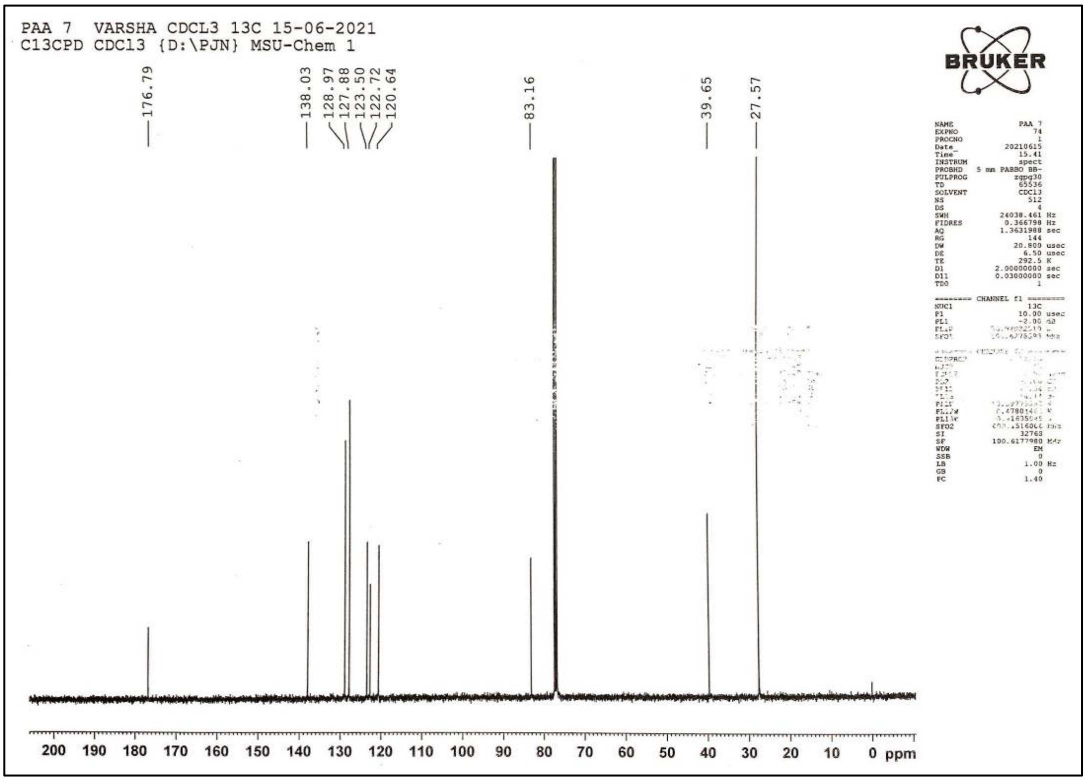
PAA 7 VARSHA CDCL3 13C 15-06-2021
C13CPD CDCl3 {D:\PJN} MSU-Chem 1
176.79
138.03
128.97
127.88
123.50
122.72
120.64
83.16
39.65
27.57
BRUKER
ppm

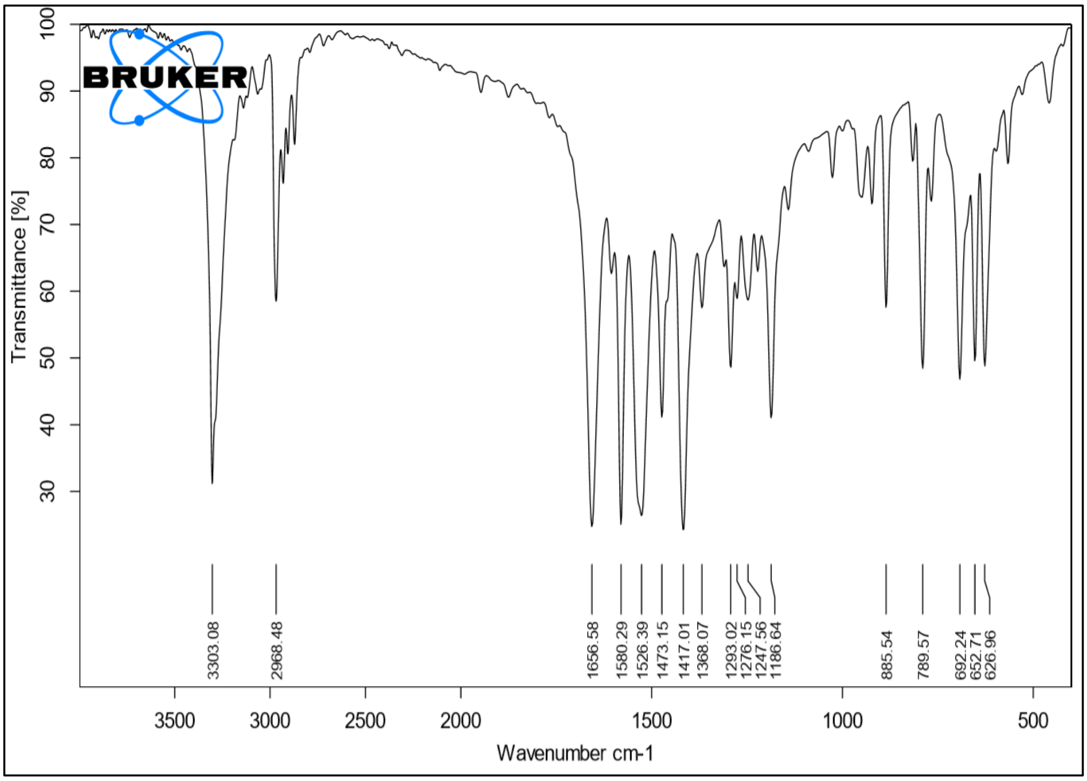
BRUKER
Transmittance [%]
Wavenumber cm-1
3303.08
2968.48
1656.58
1580.29
1526.39
1473.15
1417.01
1368.07
1293.02
1276.15
1247.56
1186.64
885.54
789.57
692.24
652.71
626.96

PIV3

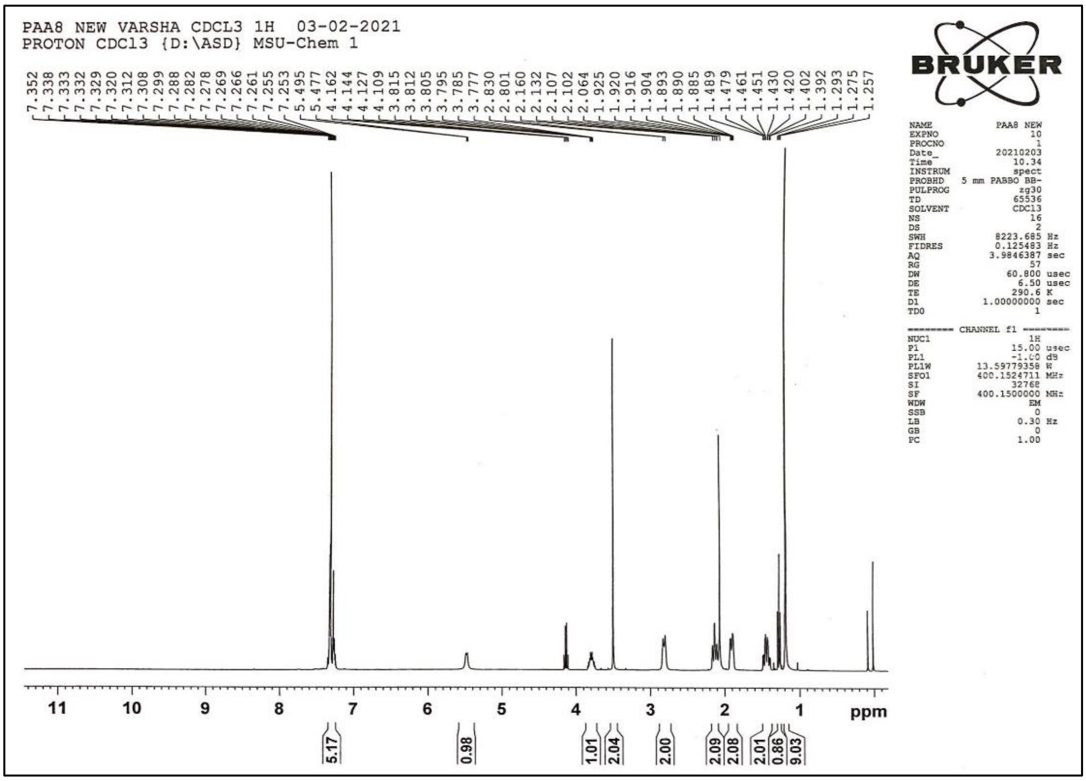

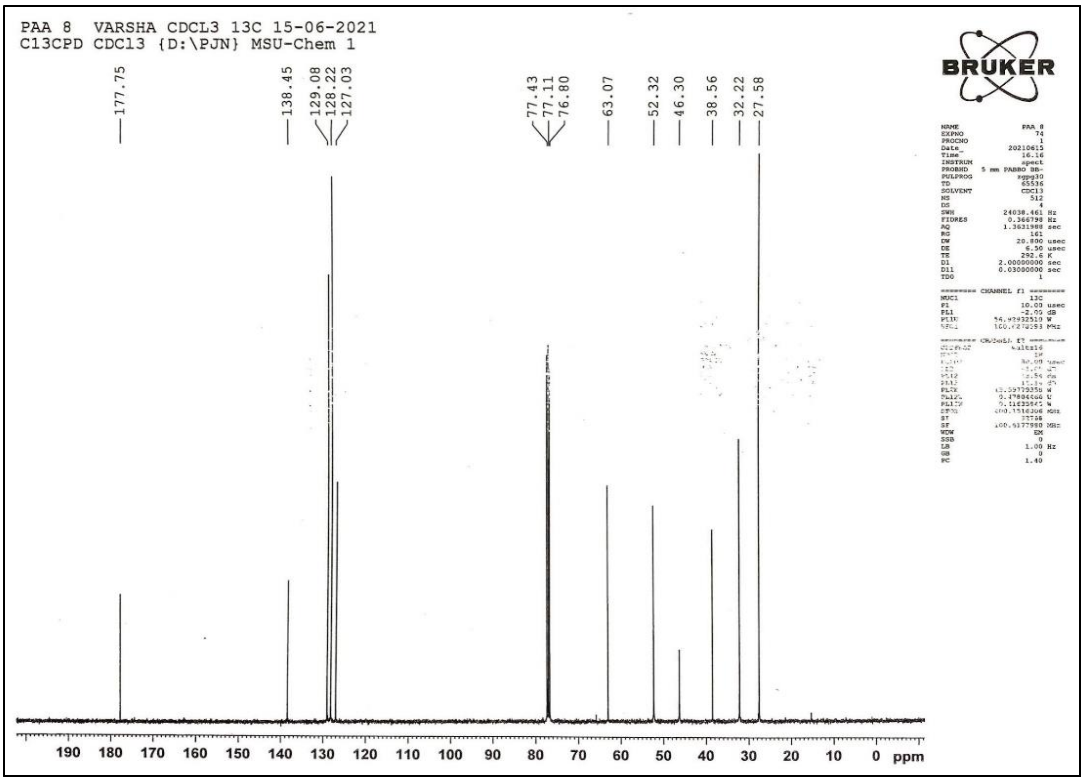

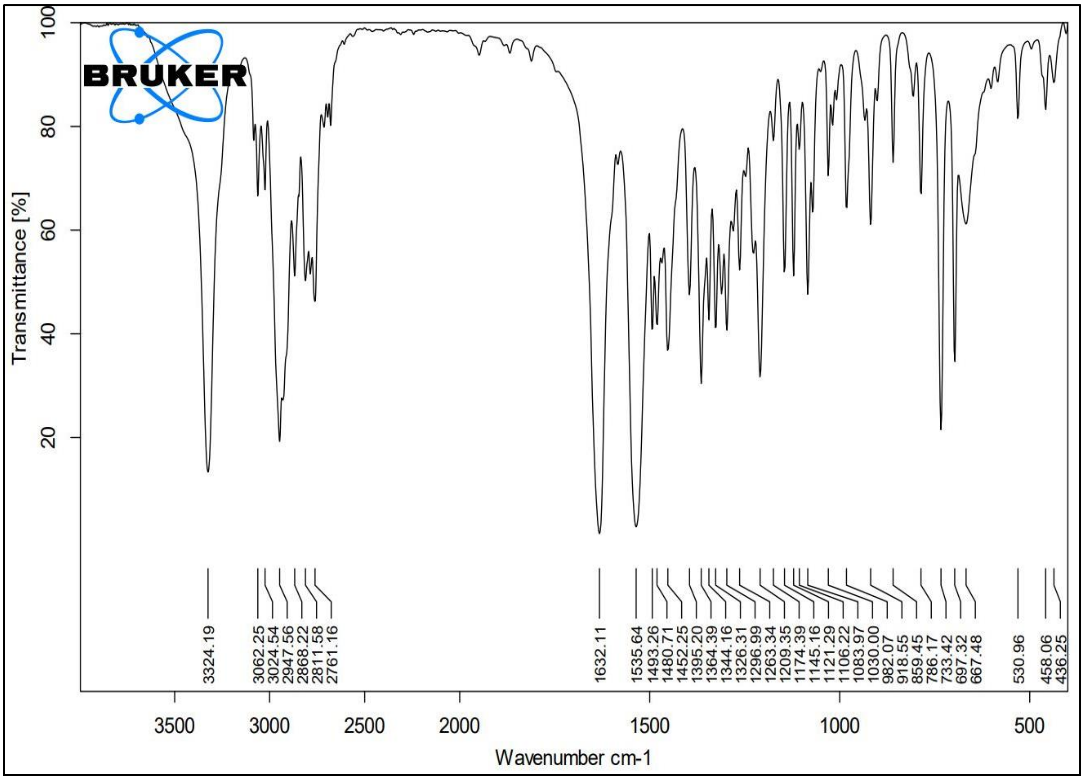
Transmittance [%]
Wavenumber cm-1
3324.19
3062.25
3024.54
2947.56
2868.22
2811.58
2761.16
1632.11
1535.64
1493.26
1480.71
1452.25
1395.20
1364.39
1344.16
1326.31
1296.99
1263.34
1209.35
1174.39
1145.16
1121.29
1106.22
1083.97
1030.00
982.07
918.55
859.45
786.17
733.42
697.32
667.48
530.96
458.06
436.25

PIV4

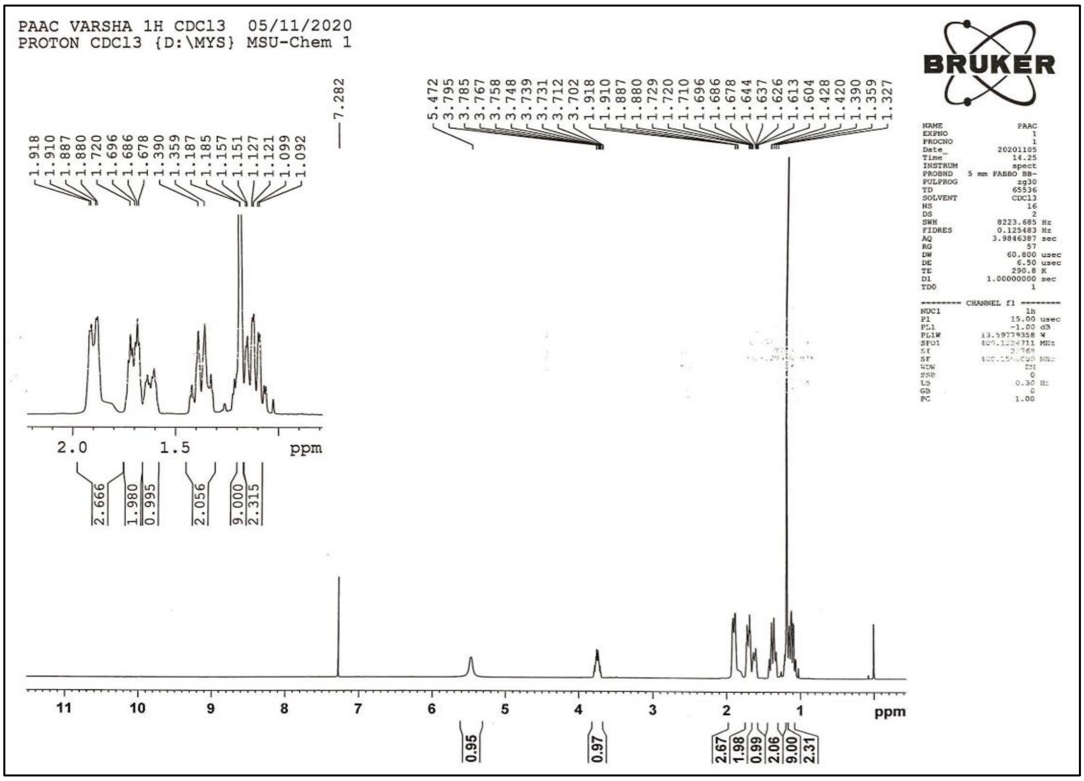
PAAC VARSHA 1H CDCl3 05/11/2020
PROTON CDCl3 {D:\MYS} MSU-Chem 1
ppm

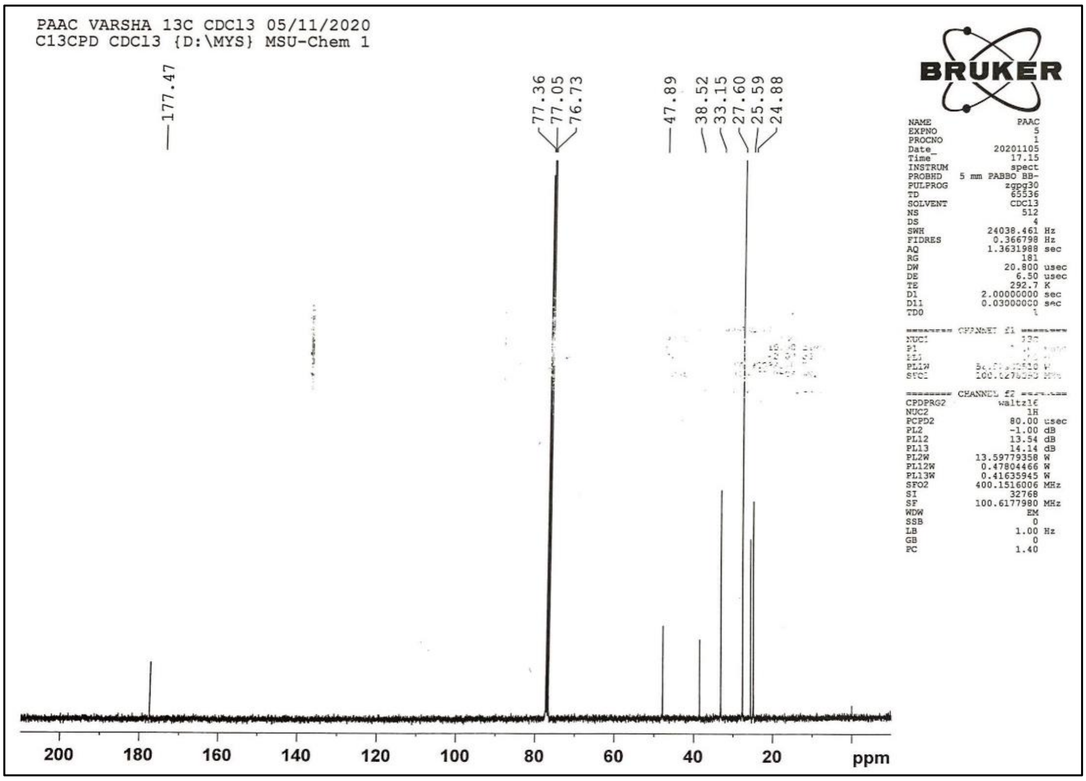
PAAC VARSHA 13C CDCl3 05/11/2020
C13CPD CDCl3 {D:\MYS} MSU-Chem 1
177.47
77.36
77.05
76.73
47.89
38.52
33.15
27.60
25.59
24.88
BRUKER
ppm

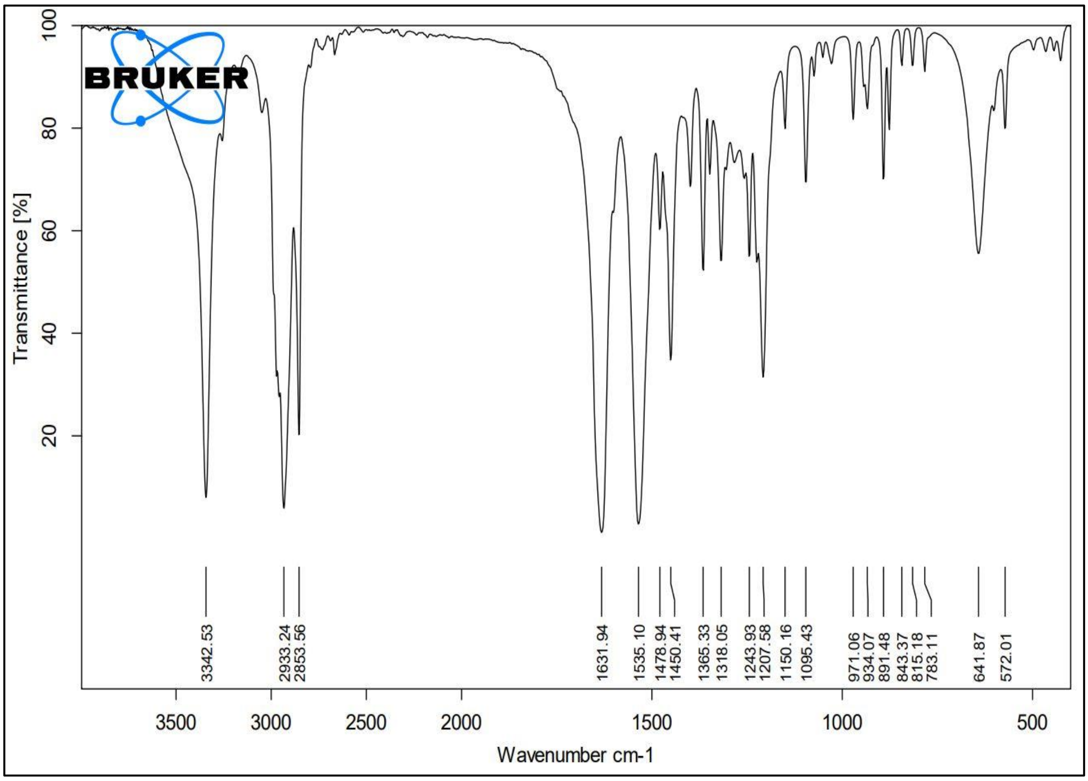
BRUKER
Transmittance [%]
Wavenumber cm-1
3342.53
2933.24
2853.56
1631.94
1535.10
1478.94
1450.41
1365.33
1318.05
1243.93
1207.58
1150.16
1095.43
971.06
934.07
891.48
843.37
815.18
783.11
641.87
572.01

PIV5

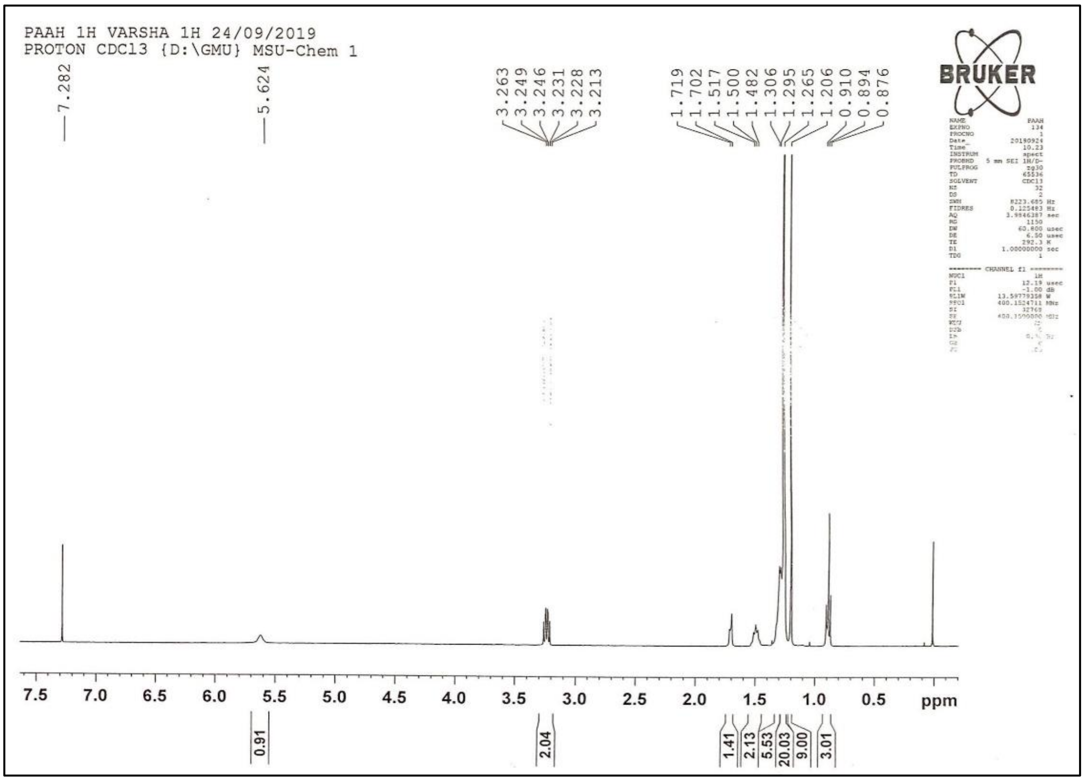
PAAH 1H VARSHA 1H 24/09/2019
PROTON CDCl3 {D:\GMU} MSU-Chem 1
7.282
5.624
3.263
3.249
3.246
3.231
3.228
3.213
1.719
1.702
1.517
1.500
1.482
1.306
1.295
1.265
1.206
0.910
0.894
0.876
BRUKER
ppm
0.91
2.04
1.41
2.13
5.53
20.03
9.00
3.01

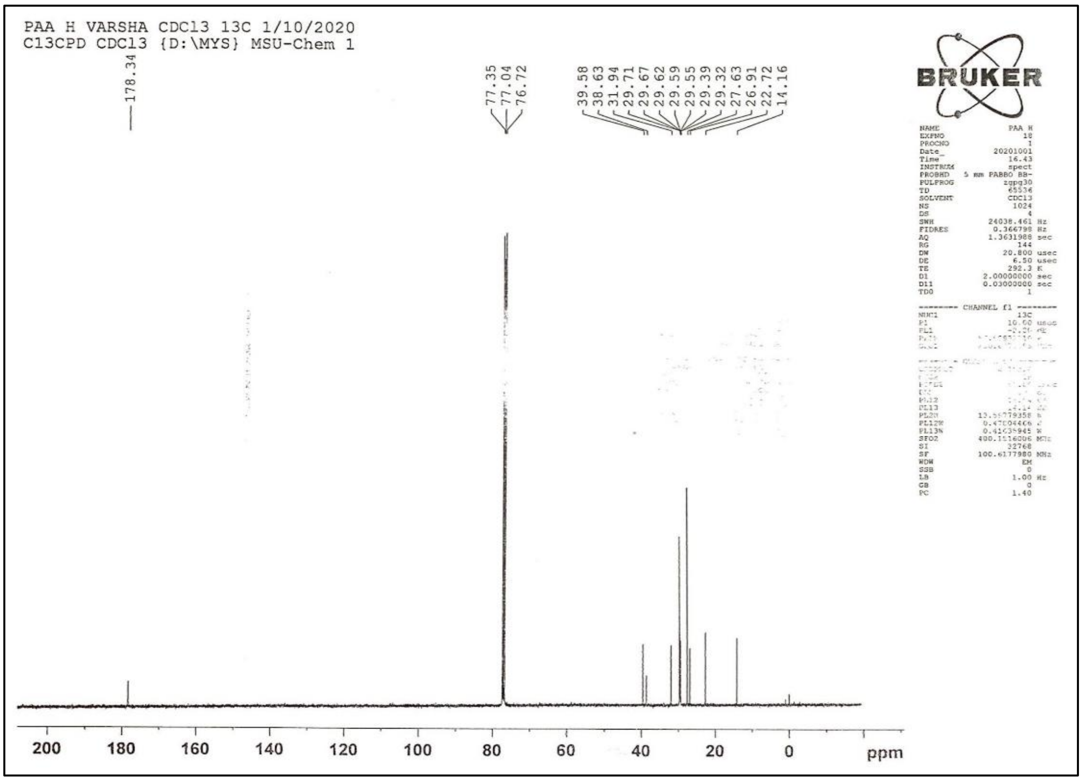
PAA H VARSHA CDCl3 13C 1/10/2020
C13CPD CDCl3 {D:\MYS} MSU-Chem 1
178.34
77.35
77.04
76.72
39.58
38.63
31.94
29.71
29.67
29.62
29.59
29.55
29.39
29.32
27.63
26.91
22.72
14.16
BRUKER
ppm

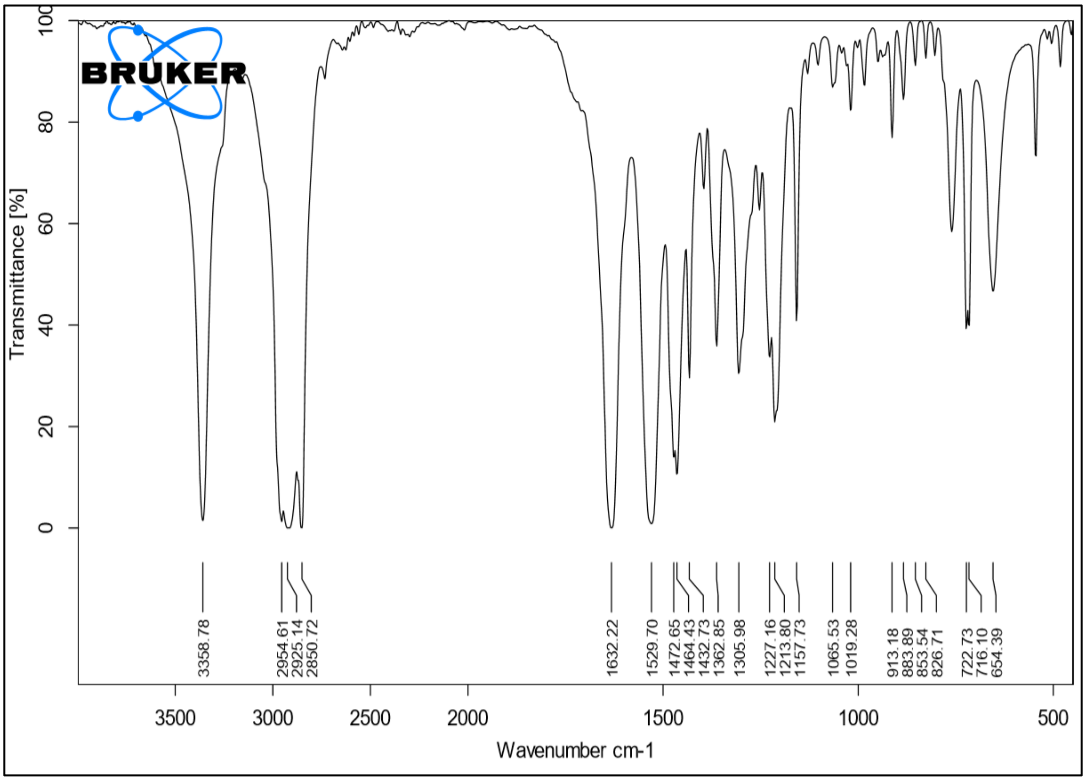

Transmittance [%]
100
80
60
40
20
0
3358.78
2954.61
2925.14
2850.72
1632.22
1529.70
1472.65
1464.43
1432.73
1362.85
1305.98
1227.16
1213.80
1157.73
1065.53
1019.28
913.18
883.89
853.54
826.71
722.73
716.10
654.39
3500
3000
2500
2000
1500
1000
500
Wavenumber cm-1

PIV6

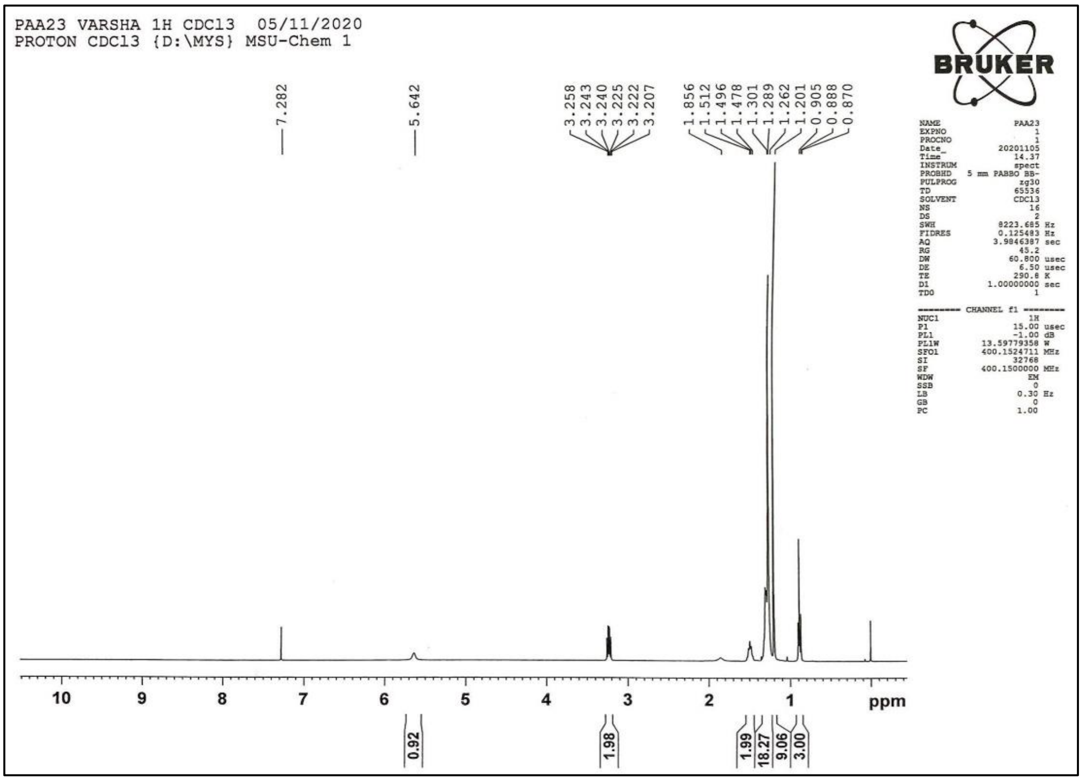

PAA23 VARSHA 1H CDCl3 05/11/2020
PROTON CDCl3 {D:\MYS} MSU-Chem 1
7.282
5.642
3.258
3.243
3.240
3.225
3.222
3.207
1.856
1.512
1.496
1.478
1.301
1.289
1.262
1.201
0.905
0.888
0.870
NAME PAA23
EXPNO 1
PROCNO 1
Date_ 20201105
Time 14.37
INSTRUM spect
PROBHD 5 mm PABBO BB-
PULPROG zg30
TD 65536
SOLVENT CDCl3
NS 16
DS 2
SWH 8223.685 Hz
FIDRES 0.125483 Hz
AQ 3.9846387 sec
RG 45.2
DW 60.800 usec
DE 6.50 usec
TE 290.8 K
D1 1.00000000 sec
TD0 1
======== CHANNEL f1 ========
NUC1 1H
P1 15.00 usec
PL1 -1.00 dB
PL1W 13.59779358 W
SFO1 400.1524711 MHz
SI 32768
SF 400.1500000 MHz
WDW EM
SSB 0
LB 0.30 Hz
GB 0
PC 1.00
10
9
8
7
6
5
4
3
2
1
ppm
0.92
1.98
1.99
18.27
9.06
3.00

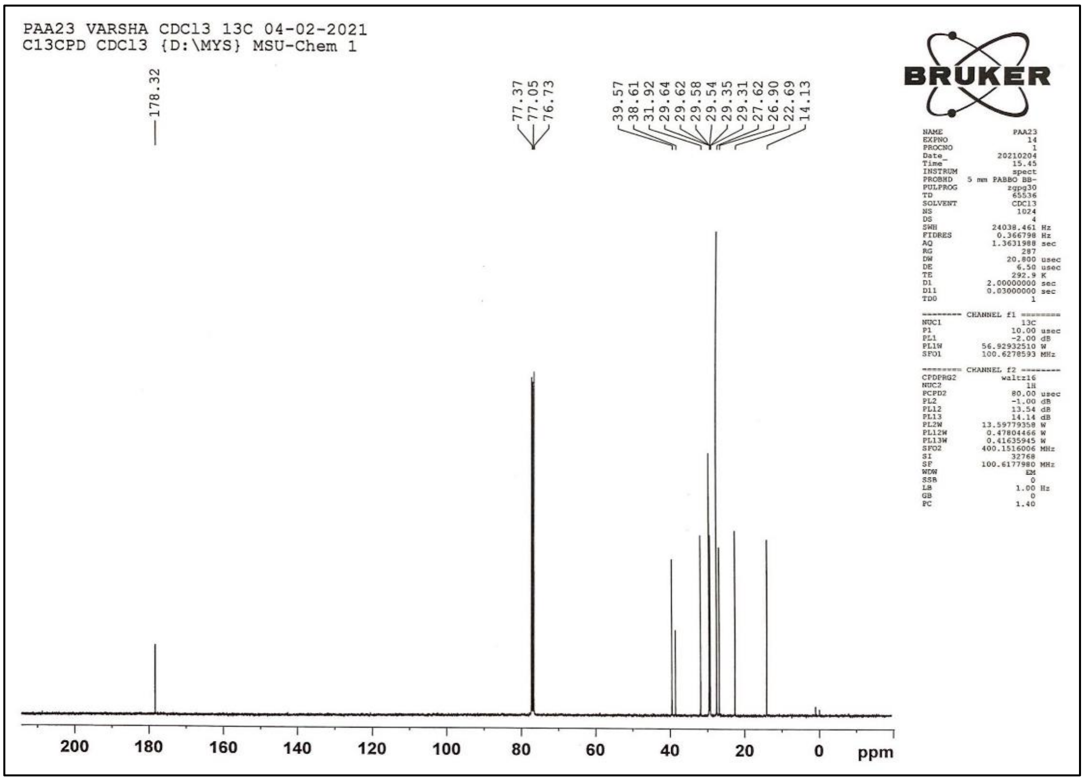
PAA23 VARSHA CDCl3 13C 04-02-2021
C13CPD CDCl3 {D:\MYS} MSU-Chem 1
178.32
77.37
77.05
76.73
39.57
38.61
31.92
29.64
29.62
29.58
29.54
29.35
29.31
27.62
26.90
22.69
14.13
BRUKER
200
180
160
140
120
100
80
60
40
20
0
ppm

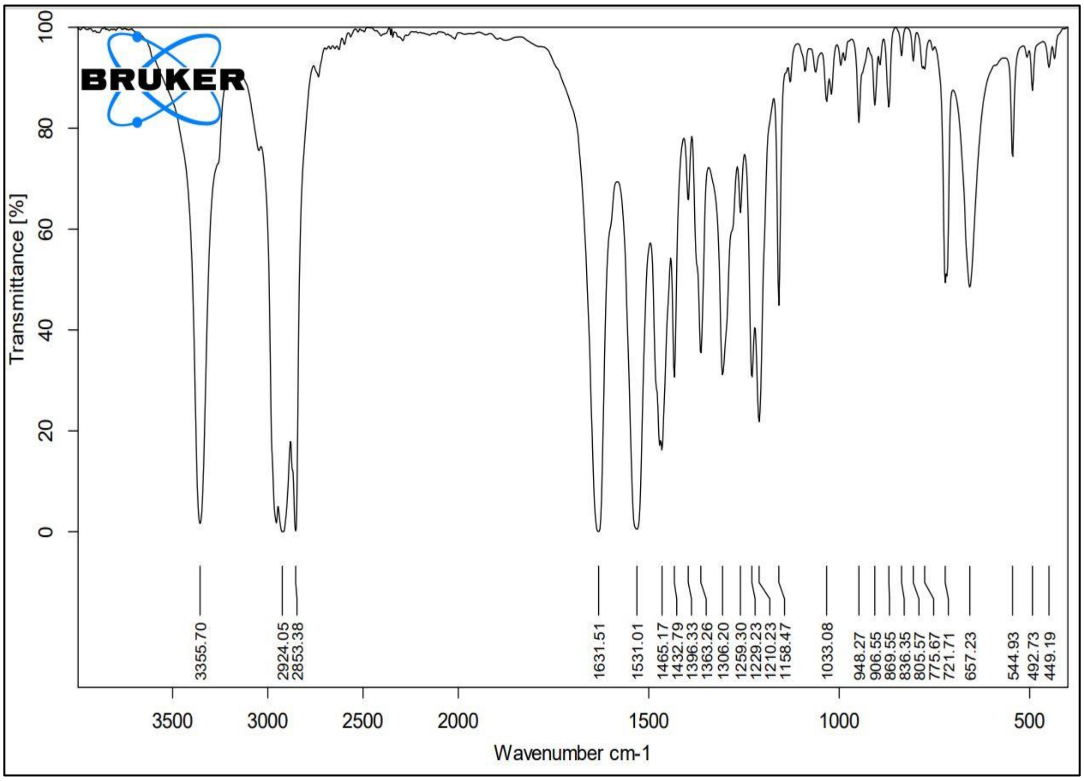
BRUKER
Transmittance [%]
100
80
60
40
20
0
3355.70
2924.05
2853.38
1631.51
1531.01
1465.17
1432.79
1396.33
1363.26
1306.20
1259.30
1229.23
1210.23
1158.47
1033.08
948.27
906.55
869.55
836.35
805.57
775.67
721.71
657.23
544.93
492.73
449.19
3500
3000
2500
2000
1500
1000
500
Wavenumber cm-1

PIV7

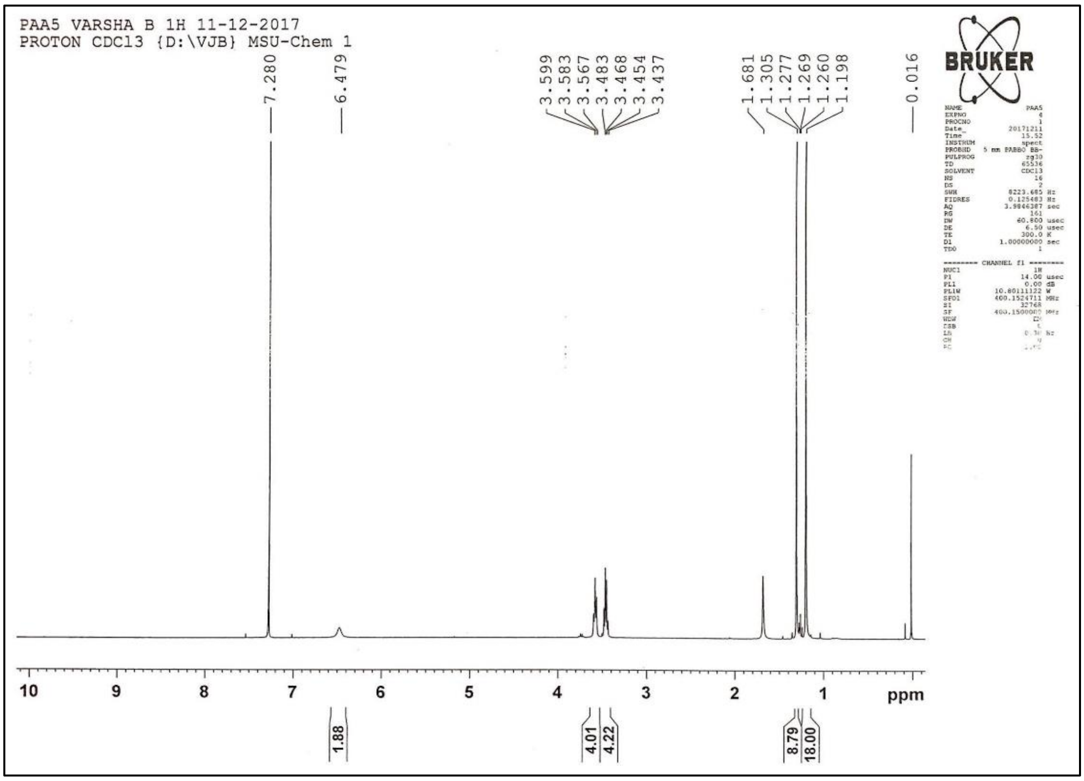
PAA5 VARSHA B 1H 11-12-2017
PROTON CDCl3 {D:\VJB} MSU-Chem 1
7.280
6.479
3.599
3.583
3.567
3.483
3.468
3.454
3.437
1.681
1.305
1.277
1.269
1.260
1.198
0.016
BRUKER
1.88
4.01
4.22
8.79
18.00
ppm

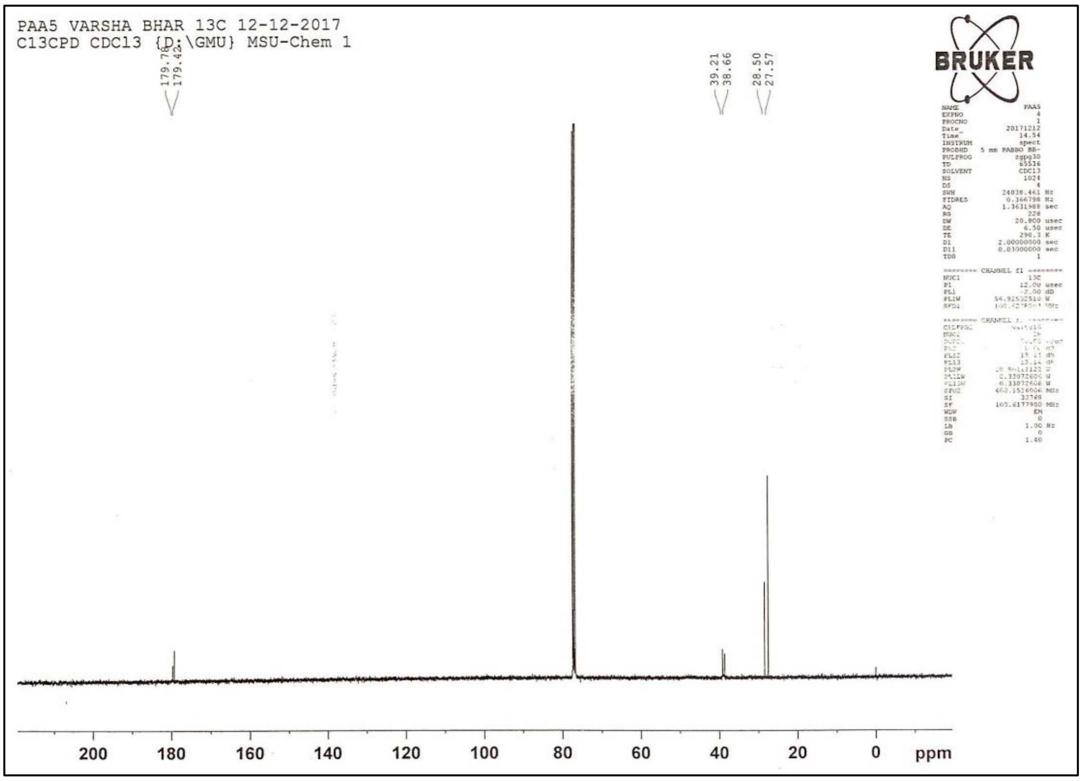
PAA5 VARSHA BHAR 13C 12-12-2017
C13CPD CDCl3 {D:\GMU} MSU-Chem 1
39.21
38.66
28.50
27.57
BRUKER
ppm

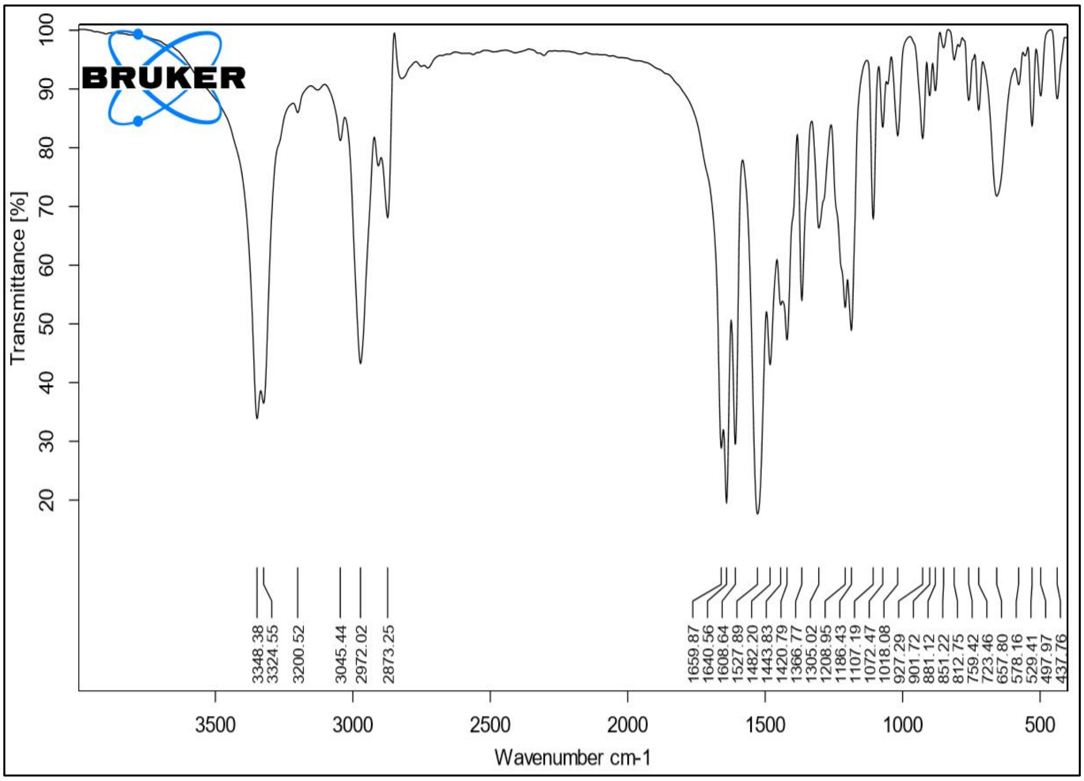

BRUKER
Transmittance [%]
Wavenumber cm-1
3348.38
3324.55
3200.52
3045.44
2972.02
2873.25
1659.87
1640.56
1608.64
1527.89
1482.20
1443.83
1420.79
1366.77
1305.02
1208.95
1186.43
1107.19
1072.47
1018.08
927.29
901.72
881.12
851.22
812.75
759.42
723.46
657.80
578.16
529.41
497.97
437.76

PIV8

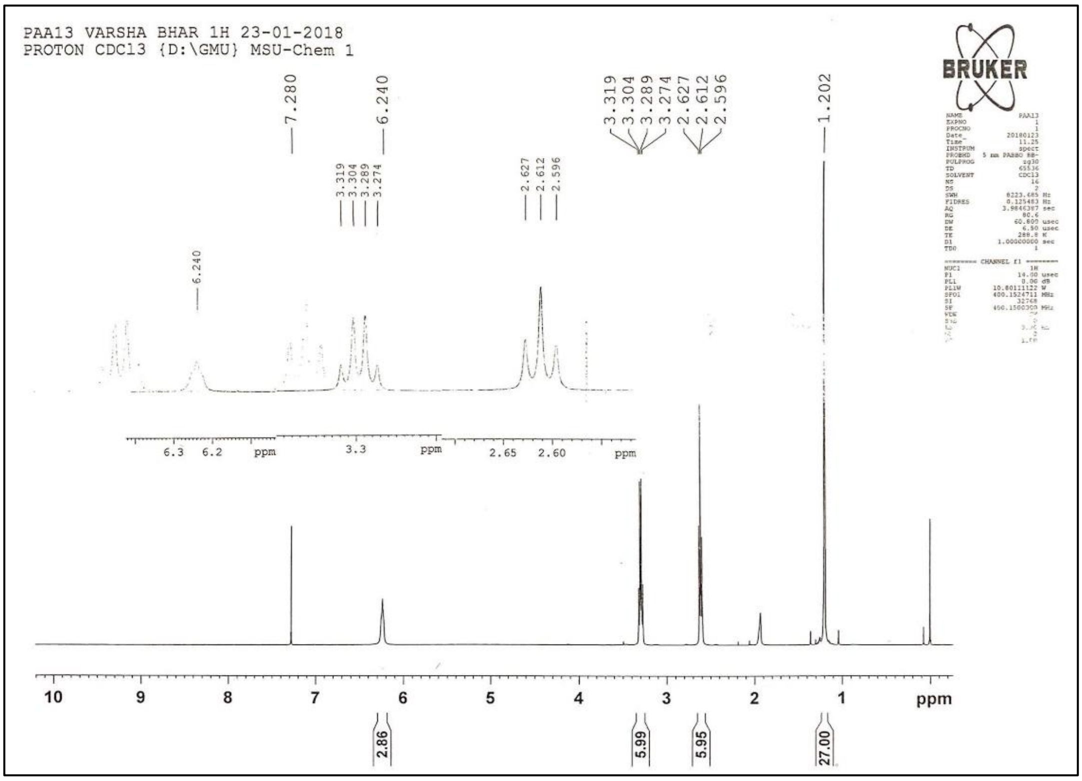

PAA13 VARSHA BHAR 1H 23-01-2018
PROTON CDCl3 {D:\GMU} MSU-Chem 1
BRUKER
7.280
6.240
3.319
3.304
3.289
3.274
2.627
2.612
2.596
1.202
ppm
2.86
5.99
5.95
27.00

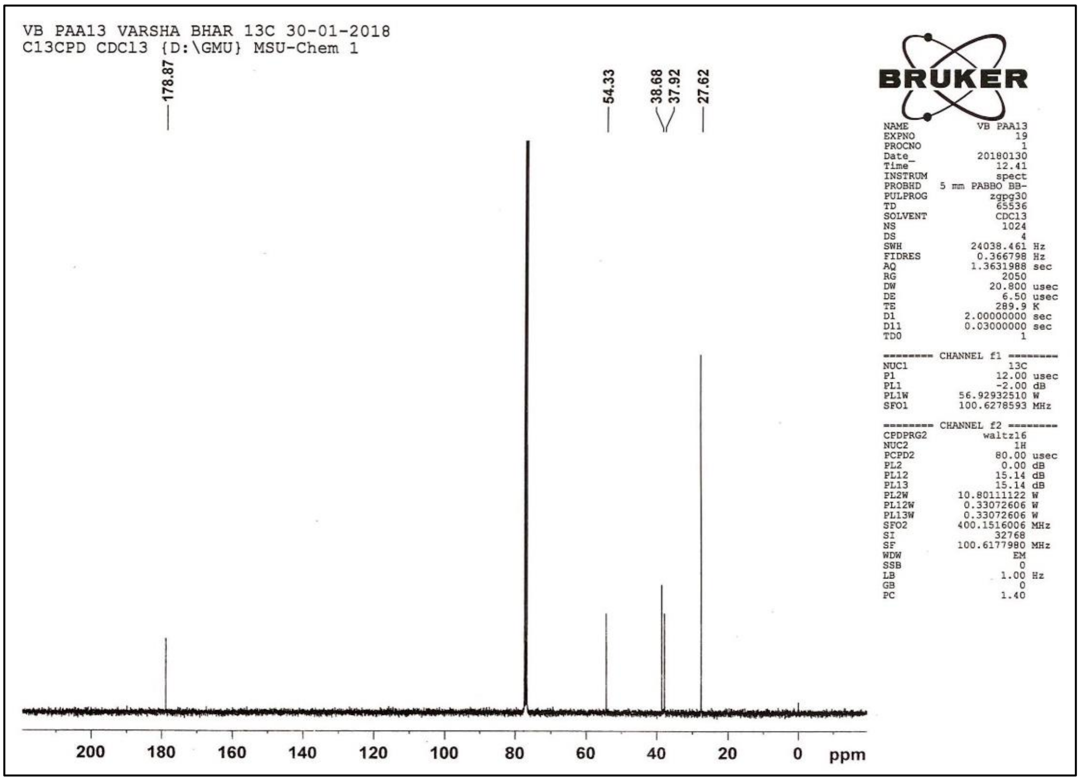
VB PAA13 VARSHA BHAR 13C 30-01-2018
C13CPD CDCl3 {D:\GMU} MSU-Chem 1
178.87
54.33
38.68
37.92
27.62
NAME VB PAA13
EXPNO 19
PROCNO 1
Date_ 20180130
Time 12.41
INSTRUM spect
PROBHD 5 mm PABBO BB-
PULPROG zgpg30
TD 65536
SOLVENT CDCl3
NS 1024
DS 4
SWH 24038.461 Hz
FIDRES 0.366798 Hz
AQ 1.3631988 sec
RG 2050
DW 20.800 usec
DE 6.50 usec
TE 289.9 K
D1 2.00000000 sec
D11 0.03000000 sec
TD0 1
======== CHANNEL f1 ========
NUC1 13C
P1 12.00 usec
PL1 -2.00 dB
PL1W 56.92932510 W
SFO1 100.6278593 MHz
======== CHANNEL f2 ========
CPDPRG2 waltz16
NUC2 1H
PCPD2 80.00 usec
PL2 0.00 dB
PL12 15.14 dB
PL13 15.14 dB
PL2W 10.80111122 W
PL12W 0.33072606 W
PL13W 0.33072606 W
SFO2 400.1516006 MHz
SI 32768
SF 100.6177980 MHz
WDW EM
SSB 0
LB 1.00 Hz
GB 0
PC 1.40
200 180 160 140 120 100 80 60 40 20 0 ppm

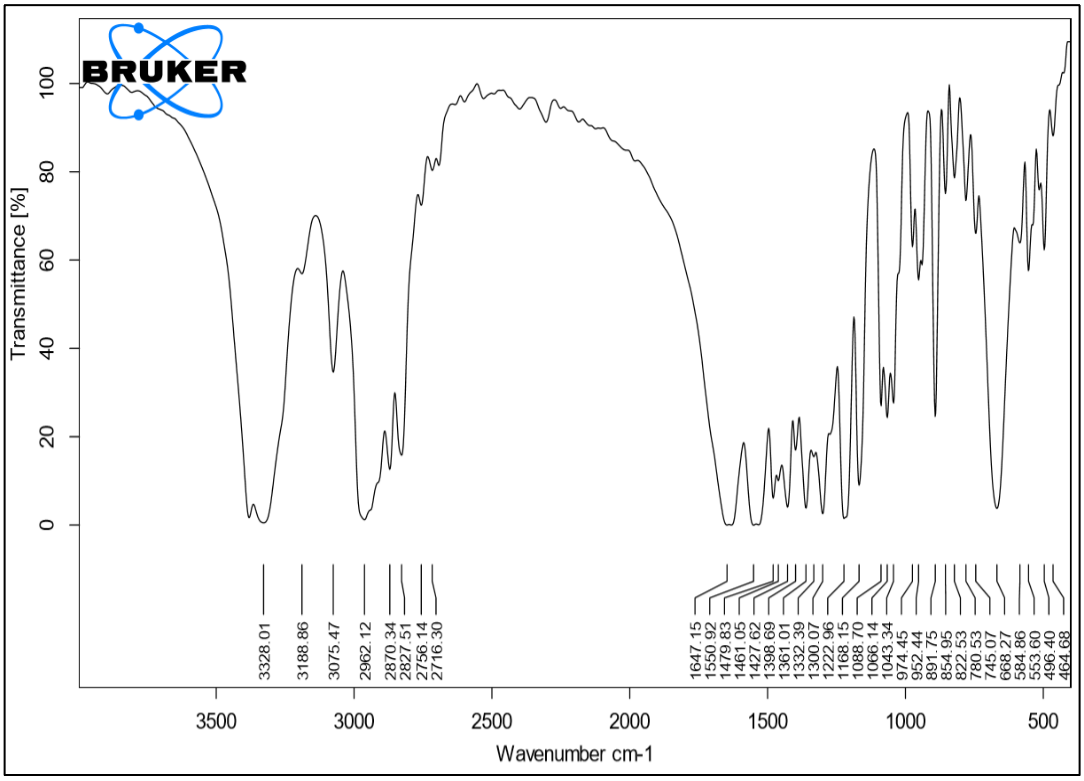
Transmittance [%]
0 20 40 60 80 100
3328.01
3188.86
3075.47
2962.12
2870.34
2827.51
2756.14
2716.30
1647.15
1550.92
1479.83
1461.05
1427.62
1398.69
1361.01
1332.39
1300.07
1222.96
1168.15
1088.70
1066.14
1043.34
974.45
952.44
891.75
854.95
822.53
780.53
745.07
668.27
584.86
553.60
496.40
464.68
3500 3000 2500 2000 1500 1000 500
Wavenumber cm-1

PIV9

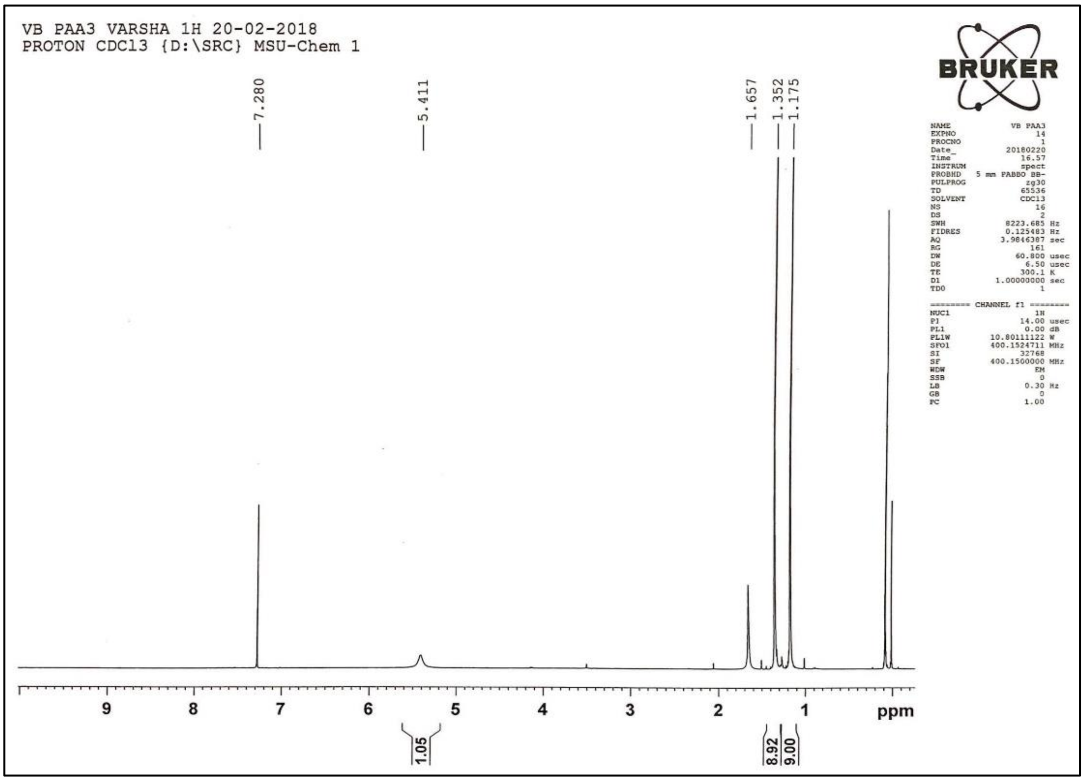
VB PAA3 VARSHA 1H 20-02-2018
PROTON CDCl3 {D:\SRC} MSU-Chem 1
BRUKER
7.280
5.411
1.657
1.352
1.175
9
8
7
6
5
4
3
2
1
ppm
1.05
8.92
9.00

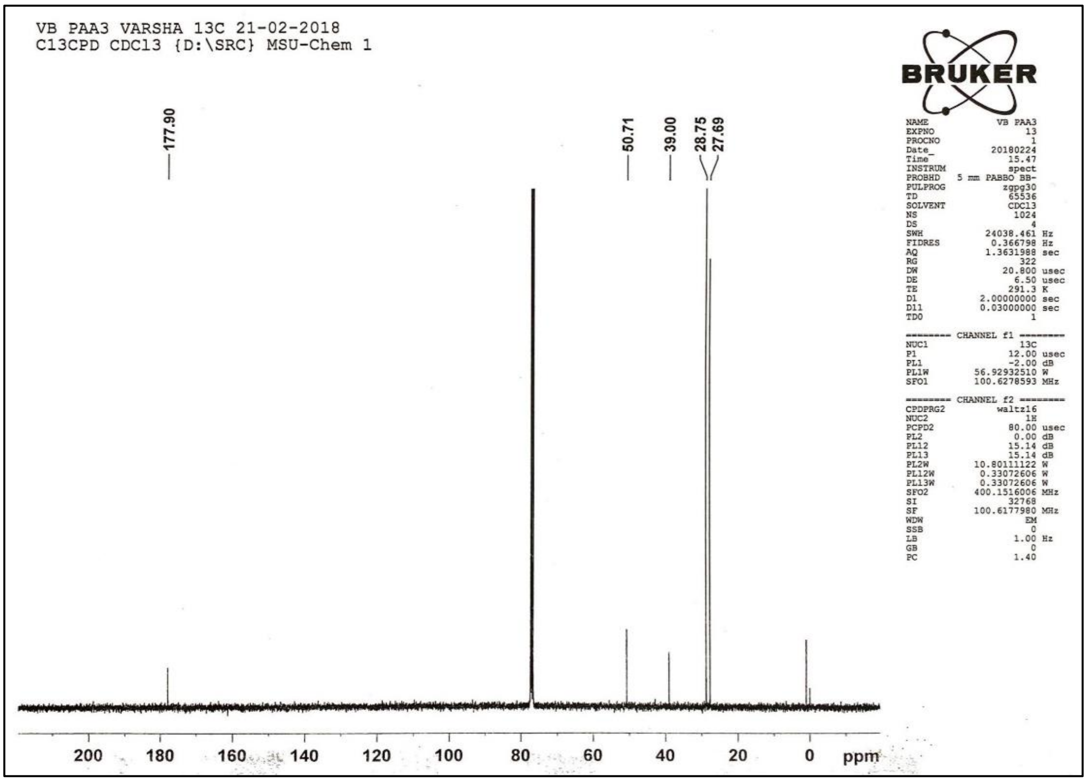
VB PAA3 VARSHA 13C 21-02-2018
C13CPD CDCl3 {D:\SRC} MSU-Chem 1
BRUKER
177.90
50.71
39.00
28.75
27.69
200
180
160
140
120
100
80
60
40
20
0
ppm

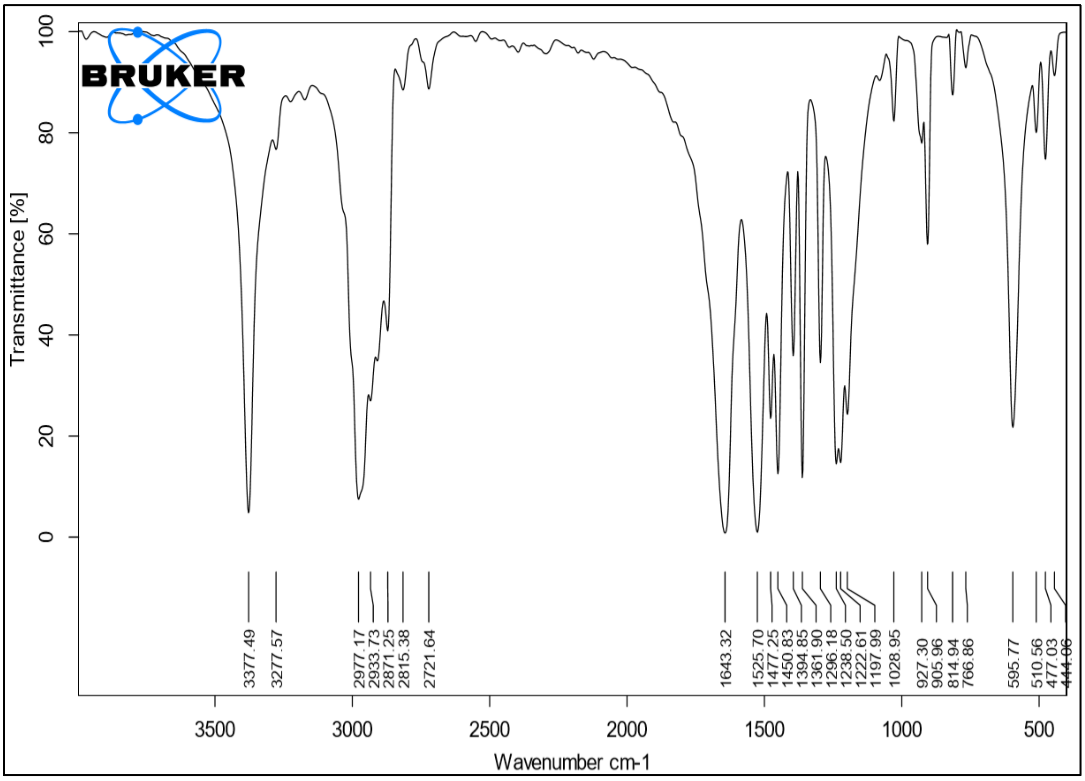
BRUKER
Transmittance [%]
Wavenumber cm-1
3377.49
3277.57
2977.17
2933.73
2871.25
2815.38
2721.64
1643.32
1525.70
1477.25
1450.83
1394.85
1361.90
1296.18
1238.50
1222.61
1197.99
1028.95
927.30
905.96
814.94
766.86
595.77
510.56
477.03
444.06

PIV10

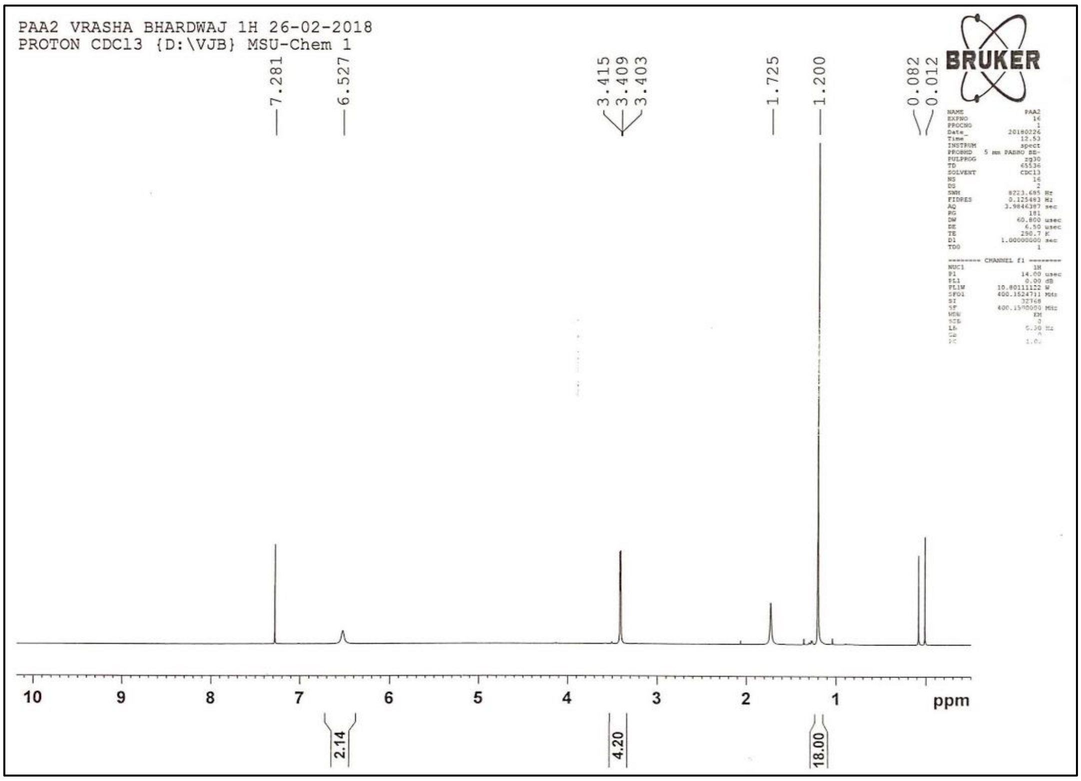
PAA2 VRASHA BHARDWAJ 1H 26-02-2018
PROTON CDCl3 {D:\VJB} MSU-Chem 1
BRUKER
7.281
6.527
3.415
3.409
3.403
1.725
1.200
0.082
0.012
2.14
4.20
18.00
ppm

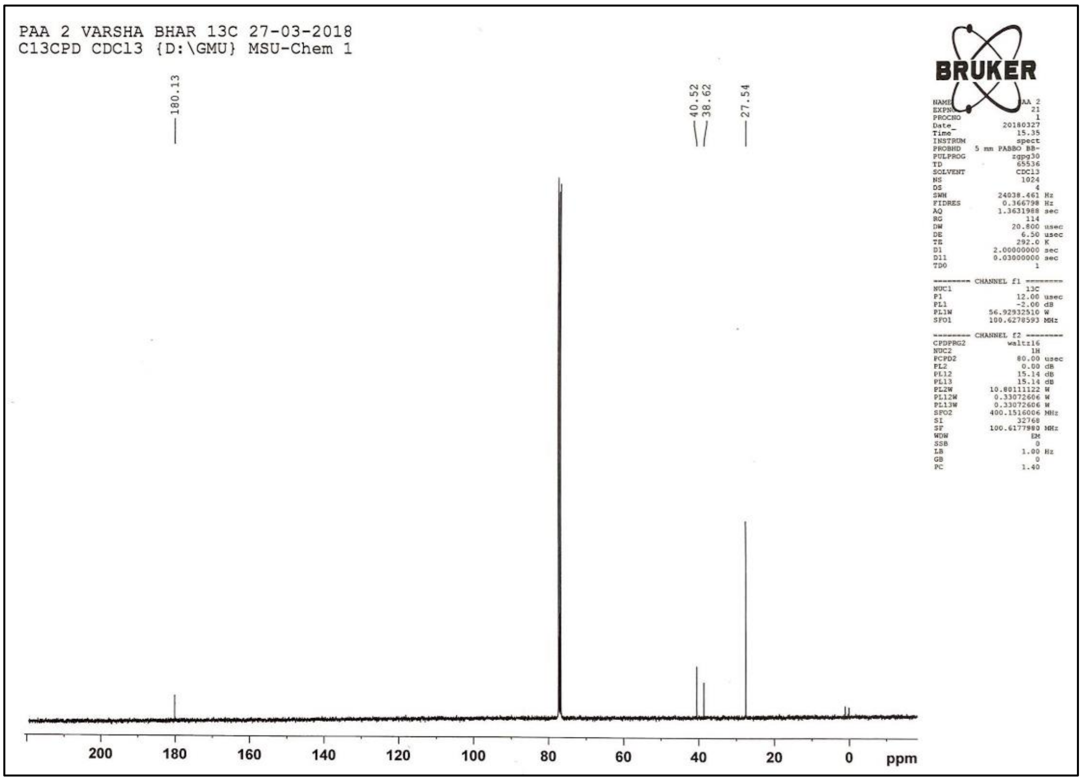

PAA 2 VARSHA BHAR 13C 27-03-2018
C13CPD CDCl3 {D:\GMU} MSU-Chem 1
180.13
40.52
38.62
27.54
NAME PAA 2
EXPNO 21
PROCNO 1
Date_ 20180327
Time 15.35
INSTRUM spect
PROBHD 5 mm PABBO BB-
PULPROG zgpg30
TD 65536
SOLVENT CDCl3
NS 1024
DS 4
SWH 24038.461 Hz
FIDRES 0.366798 Hz
AQ 1.3631988 sec
RG 114
DW 20.800 usec
DE 6.50 usec
TE 292.0 K
D1 2.00000000 sec
D11 0.03000000 sec
TD0 1
======== CHANNEL f1 ========
NUC1 13C
P1 12.00 usec
PL1 -2.00 dB
PL1W 56.92932510 W
SFO1 100.6278593 MHz
======== CHANNEL f2 ========
CPDPRG2 waltz16
NUC2 1H
PCPD2 80.00 usec
PL2 0.00 dB
PL12 15.14 dB
PL13 15.14 dB
PL2W 10.80111122 W
PL12W 0.33072606 W
PL13W 0.33072606 W
SFO2 400.1516006 MHz
SI 32768
SF 100.6177980 MHz
WDW EM
SSB 0
LB 1.00 Hz
GB 0
PC 1.40
200
180
160
140
120
100
80
60
40
20
0
ppm

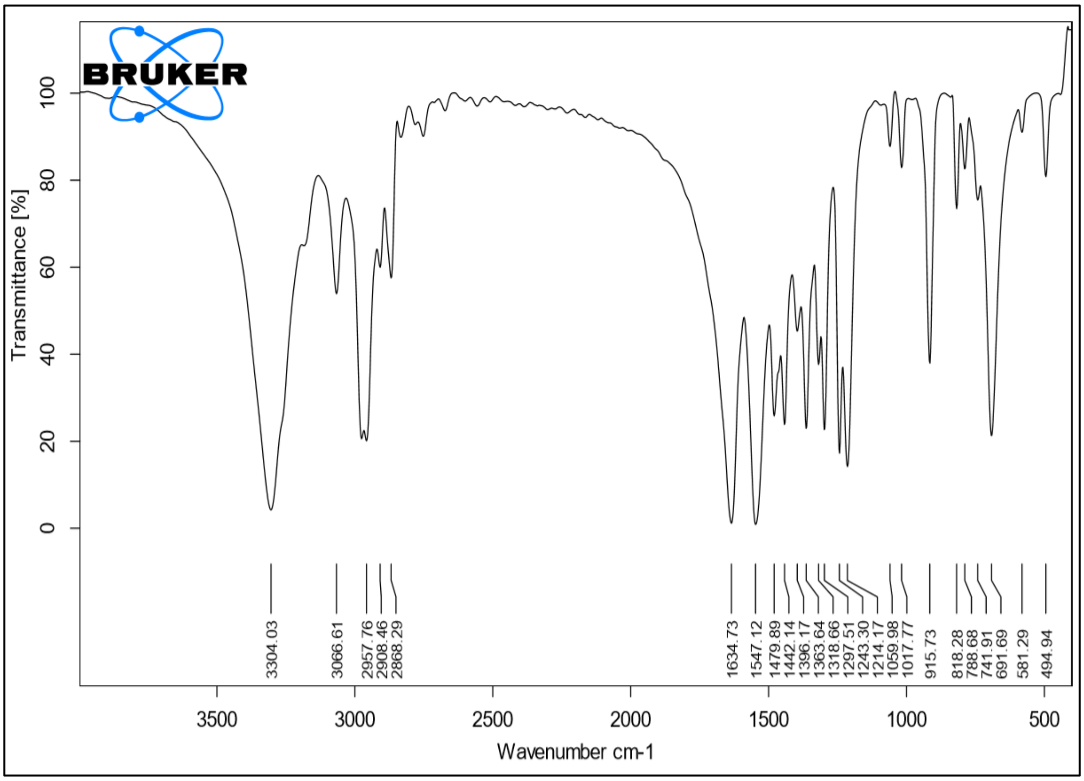

Transmittance [%]
100
80
60
40
20
0
3304.03
3066.61
2957.76
2908.46
2868.29
1634.73
1547.12
1479.89
1442.14
1396.17
1363.64
1318.66
1297.51
1243.30
1214.17
1059.98
1017.77
915.73
818.28
788.68
741.91
691.69
581.29
494.94
3500
3000
2500
2000
1500
1000
500
Wavenumber cm-1

PIV11

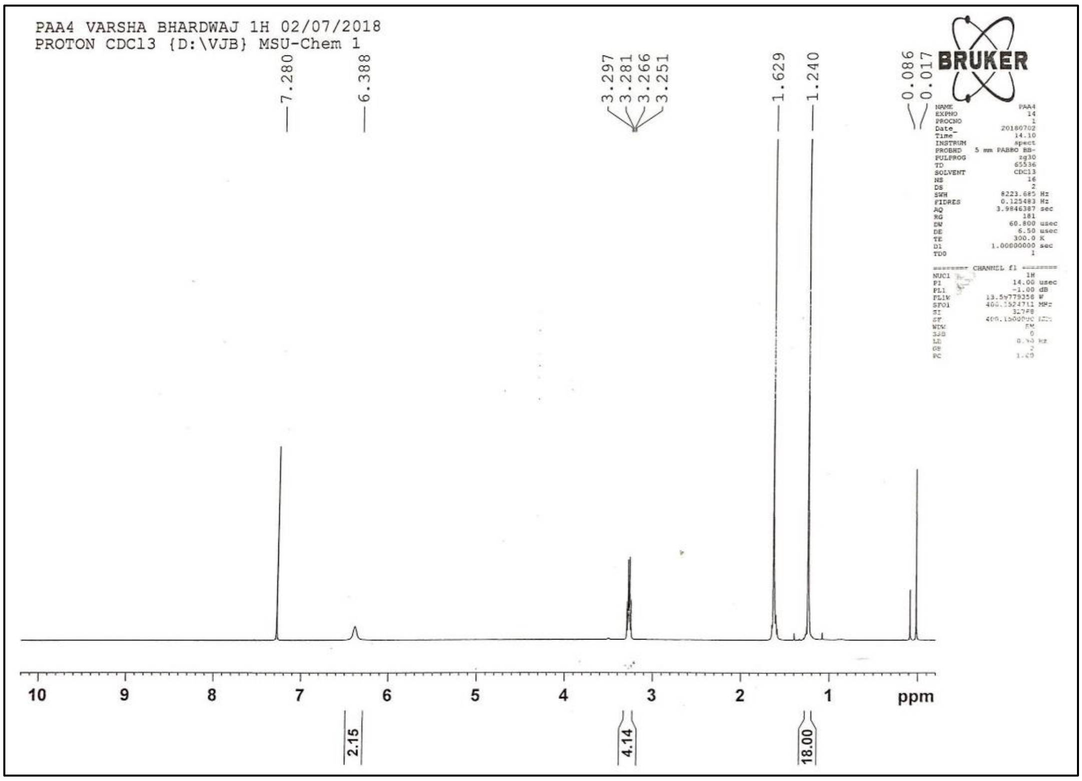
PAA4 VARSHA BHARDWAJ 1H 02/07/2018
PROTON CDCl3 {D:\VJB} MSU-Chem 1
7.280
6.388
3.297
3.281
3.266
3.251
1.629
1.240
0.086
0.017
BRUKER
ppm
2.15
4.14
18.00

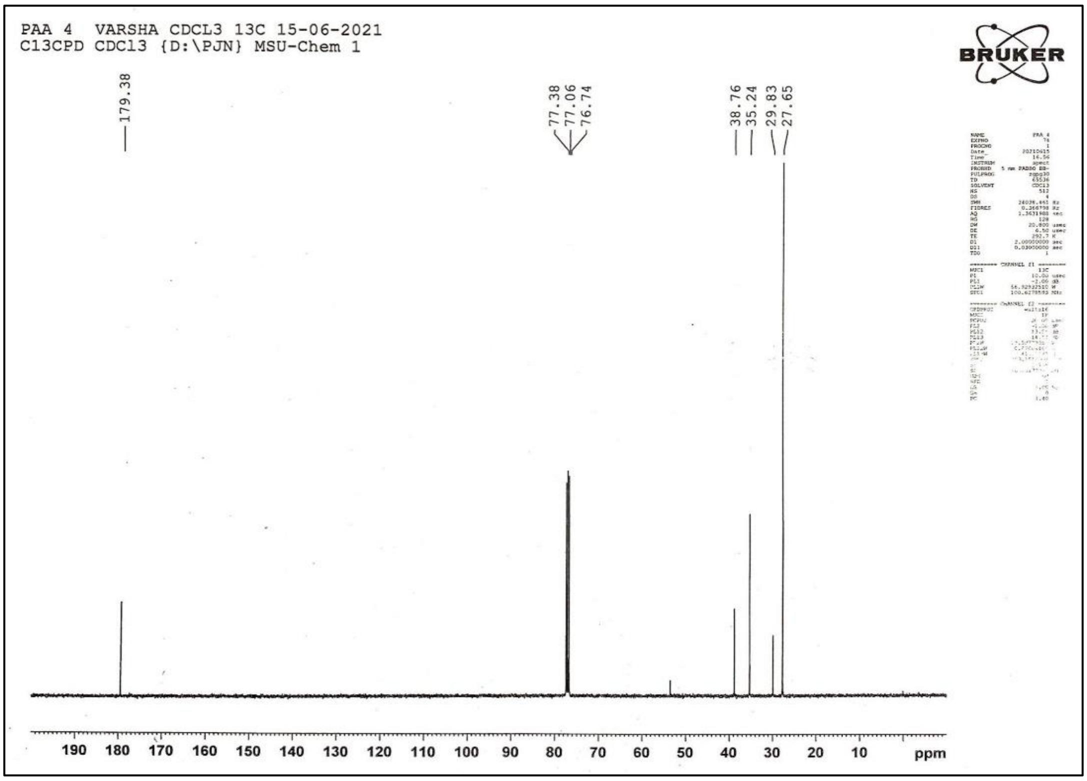
PAA 4 VARSHA CDCL3 13C 15-06-2021
C13CPD CDCl3 {D:\PJN} MSU-Chem 1
179.38
77.38
77.06
76.74
38.76
35.24
29.83
27.65
BRUKER
ppm

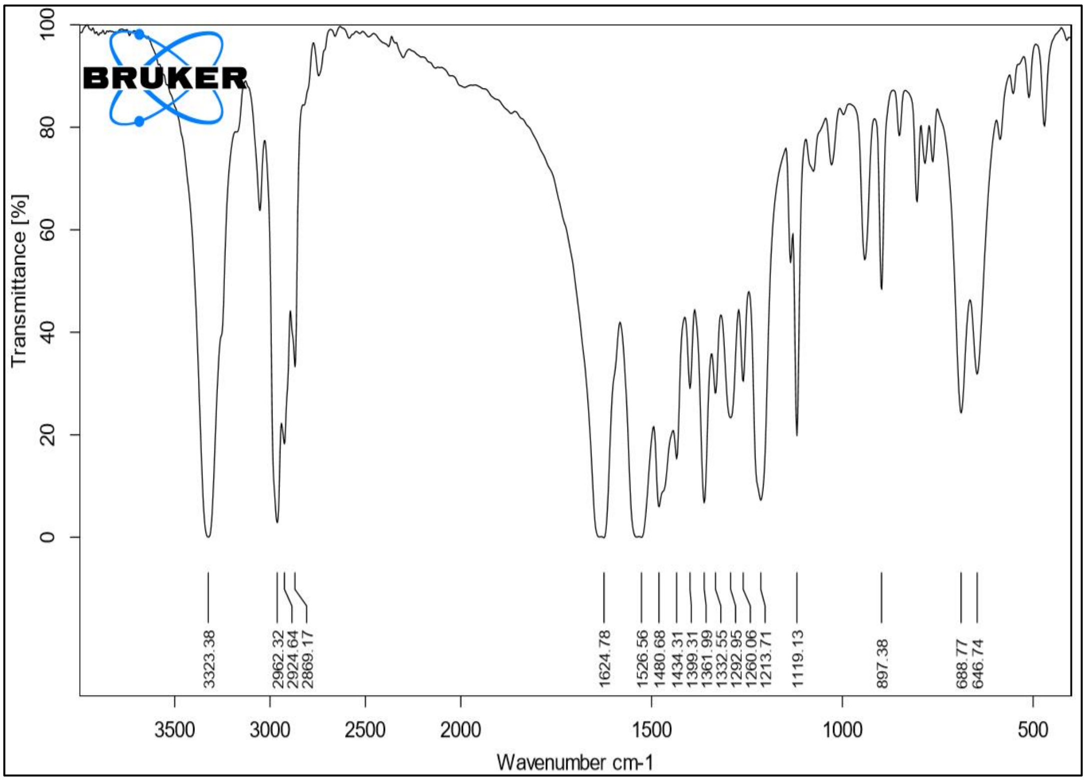
Transmittance [%]
Wavenumber cm-1
3323.38
2962.32
2924.64
2869.17
1624.78
1526.56
1480.68
1434.31
1399.31
1361.99
1332.55
1292.95
1260.06
1213.71
1119.13
897.38
688.77
646.74

PIV12

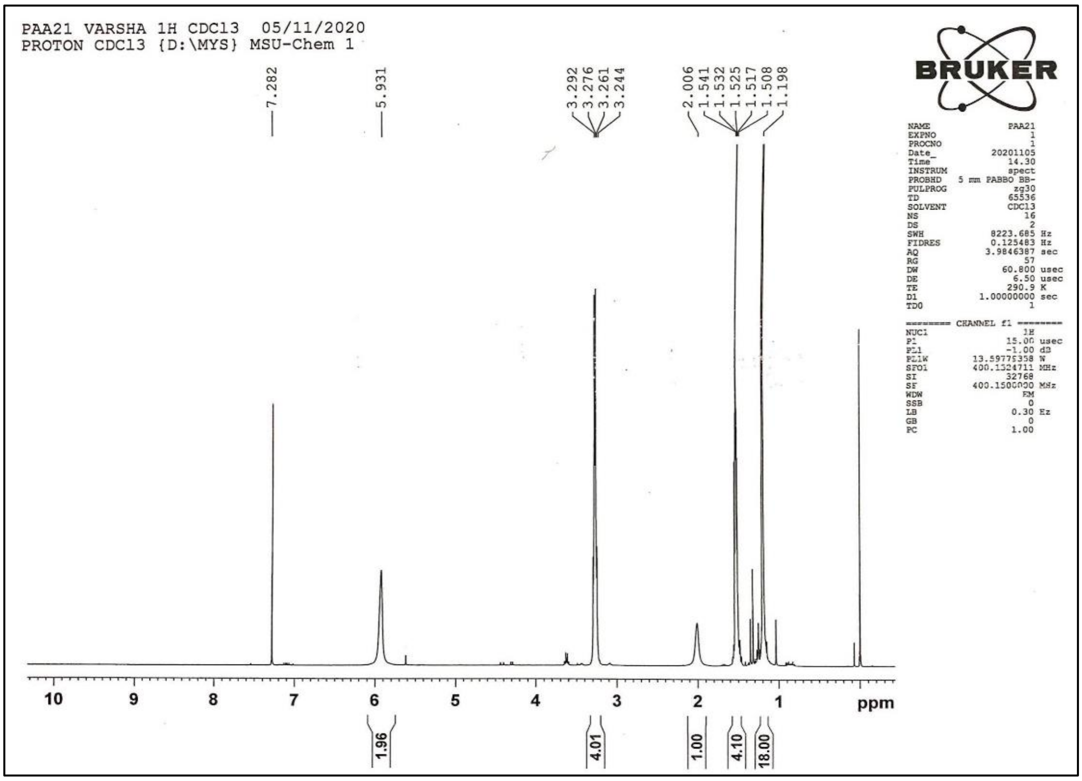
PAA21 VARSHA 1H CDCl3 05/11/2020
PROTON CDCl3 {D:\MYS} MSU-Chem 1
7.282
5.931
3.292
3.276
3.261
3.244
2.006
1.541
1.532
1.525
1.517
1.508
1.198
ppm
1.96
4.01
1.00
4.10
18.00

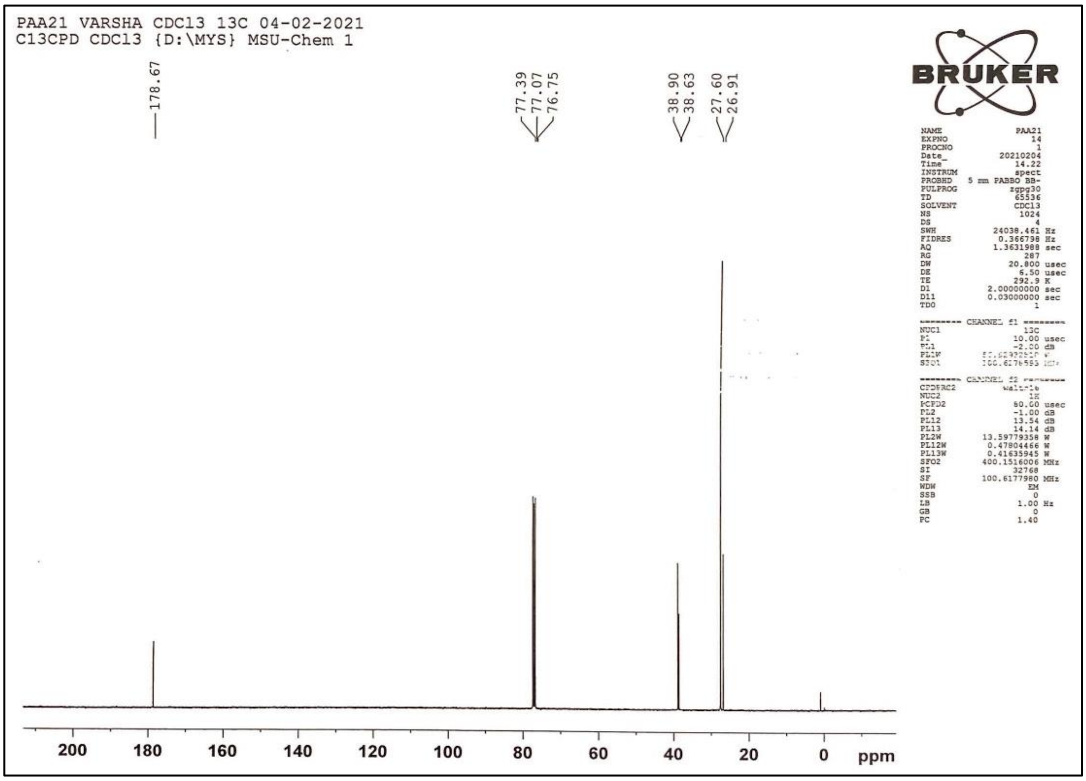
PAA21 VARSHA CDCl3 13C 04-02-2021
C13CPD CDCl3 {D:\MYS} MSU-Chem 1
178.67
77.39
77.07
76.75
38.90
38.63
27.60
26.91
BRUKER
200 180 160 140 120 100 80 60 40 20 0 ppm

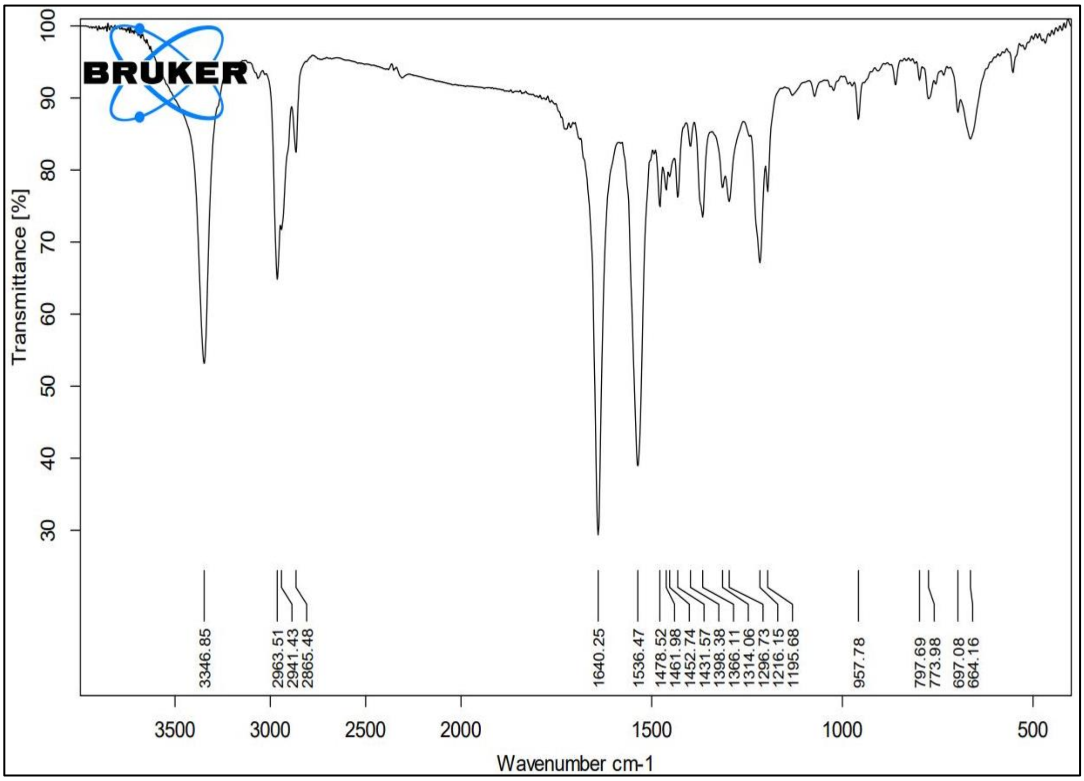
BRUKER
Transmittance [%]
100 90 80 70 60 50 40 30
3346.85
2963.51
2941.43
2865.48
1640.25
1536.47
1478.52
1461.98
1452.74
1431.57
1398.38
1366.11
1314.06
1296.73
1216.15
1195.68
957.78
797.69
773.98
697.08
664.16
3500 3000 2500 2000 1500 1000 500
Wavenumber cm-1

PIV13

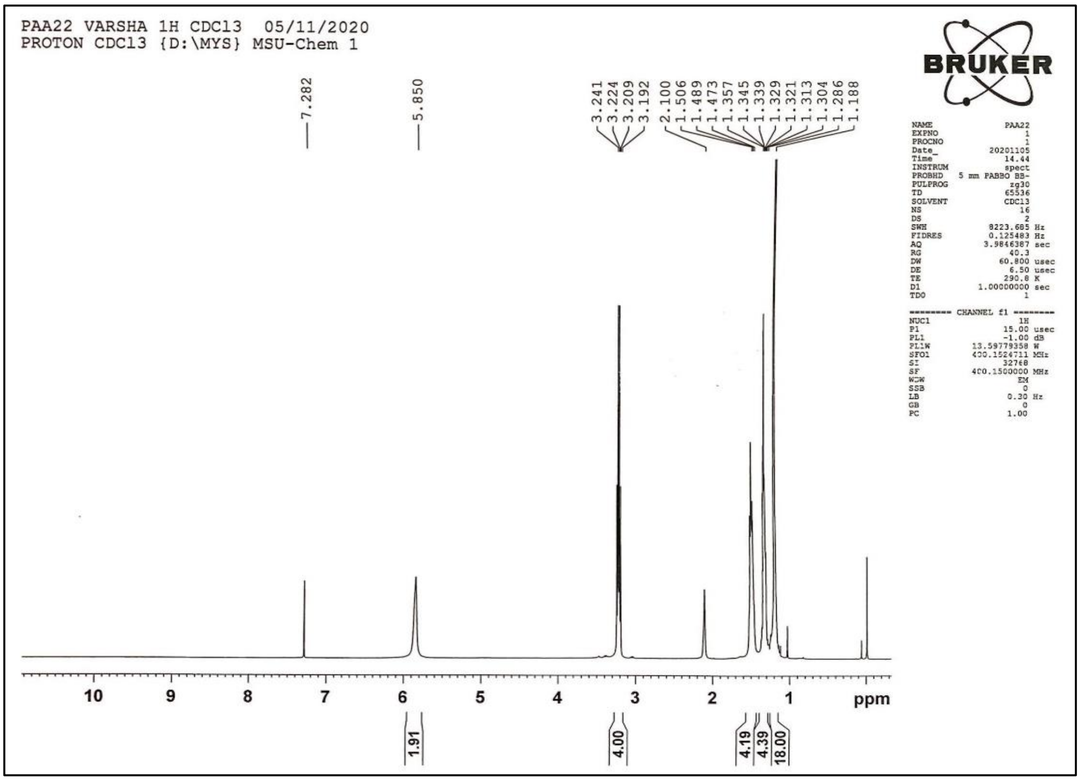
PAA22 VARSHA 1H CDCl3 05/11/2020
PROTON CDCl3 {D:\MYS} MSU-Chem 1
BRUKER
7.282
5.850
3.241
3.224
3.209
3.192
2.100
1.506
1.489
1.473
1.357
1.345
1.339
1.329
1.321
1.313
1.304
1.286
1.188
1.91
4.00
4.19
4.39
18.00
ppm

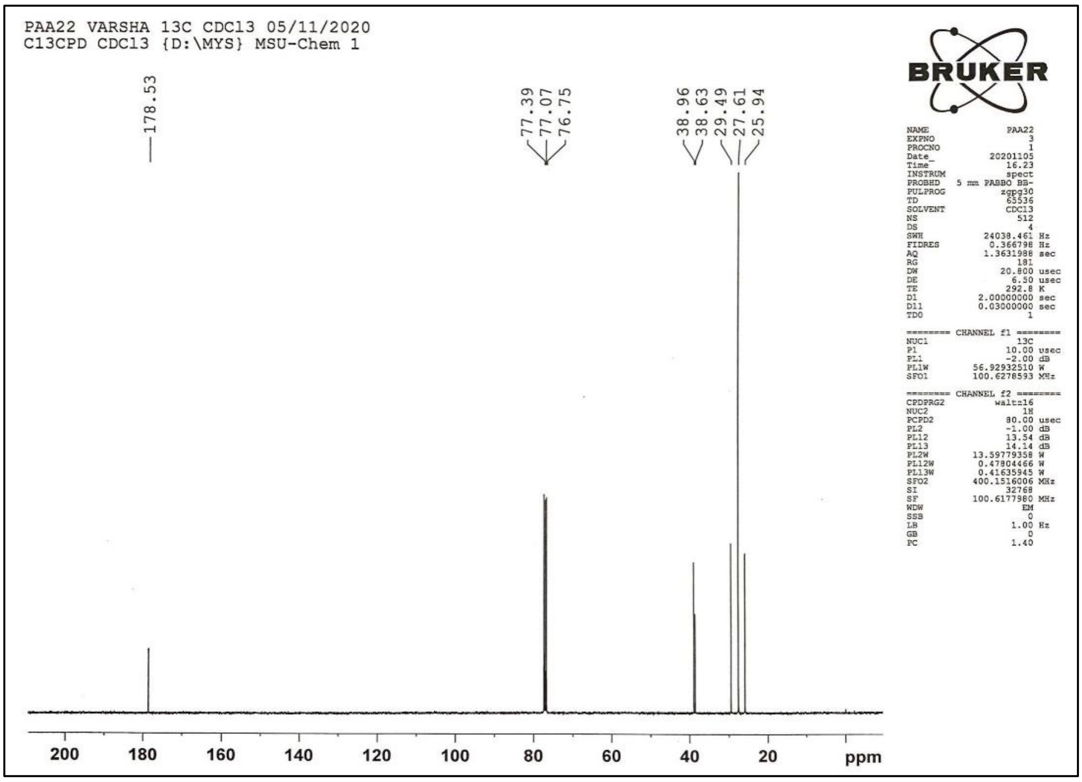
PAA22 VARSHA 13C CDCl3 05/11/2020
C13CPD CDCl3 {D:\MYS} MSU-Chem 1
BRUKER
178.53
77.39
77.07
76.75
38.96
38.63
29.49
27.61
25.94
ppm

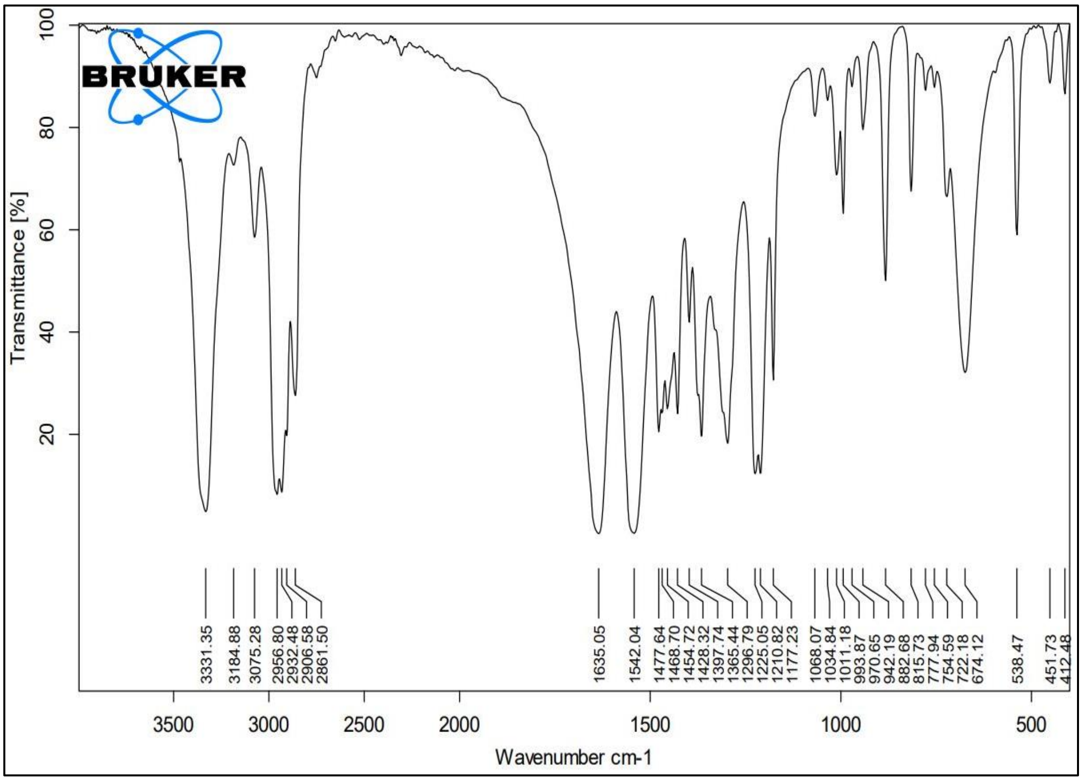
Transmittance [%]
100
80
60
40
20
3331.35
3184.88
3075.28
2956.80
2932.48
2906.58
2861.50
1635.05
1542.04
1477.64
1468.70
1454.72
1428.32
1397.74
1365.44
1296.79
1225.05
1210.82
1177.23
1068.07
1034.84
1011.18
993.87
970.65
942.19
882.68
815.73
777.94
754.59
722.18
674.12
538.47
451.73
412.48
3500
3000
2500
2000
1500
1000
500
Wavenumber cm-1

•

Chapter 4B

Supramolecular assemblies based on tert-butylacetic acid with potential applications in Phase Selective Organo-Gelation (PSOG), dye absorption and sensing studies

4.6 INTRODUCTION

Oil spill incidents can cause grave damage to the ecosystem and to counter this problem, PSOGs offer a viable method for uptake of oil from marine systems and the reversible gel-to-sol phase transition allows recyclability of organic solvent as well as the gelator.[1–6] PSOGs can cause selective partitioning of oil from oil-water biphasic mixtures and self-assemble into a network structure causing organogelation. They have emerged as a promising approach to contain oil spills in solution as well as powder form. They offer many advantages over the previously known conventional and destructive methods. They are thermoreversible, physical gels, driven by a complex interplay of complementary non-covalent intermolecular interactions. They allow safe transportation and recovery of the oil, without causing further distress to the marine environment. Ideally, an efficient PSOG must have the following attributes –

- selective and efficient gelation with spilled oil at room temperature without carrier solvents
- easy and low-cost synthesis
- environmentally compatible nature and mechanical stability
- efficient recoverability and recyclability

Based on these principles, several types of PSOG systems have been reported, with a variety of molecular backbones, ranging from bulky amino acid/peptides, sugar-based and cholesterol derivatives to amides and organic salts. Inspired from organogelation behavior of pivalamides, we synthesized a new series of *tert*-butylacetic acid (TBAA) based amides with the same set of amines which gave gels in Chapter 4A (Figure 4.24).

Additionally, these compounds were also explored for their interactions with heavy metal ions. Several toxic metals like cadmium, mercury, lead, arsenic, etc. can be detrimental to human and plant health if present in the biosphere. Exposure to these metals can occur through contaminated air, food, soil, and water. For example, lead is most commonly found in lead storage batteries, which remains one of most common sources of lead in polluting the environment. Lead poisoning (also called plumbism) can cause encephalopathy, impairment of cognitive function such as visuospatial ability, executive function, verbal memory, and dexterity among children. Lead is also known to cause osteoporosis and dental caries due to its ability to interact with vitamin D, thereby depleting active vitamin D level in the body.[7–9]

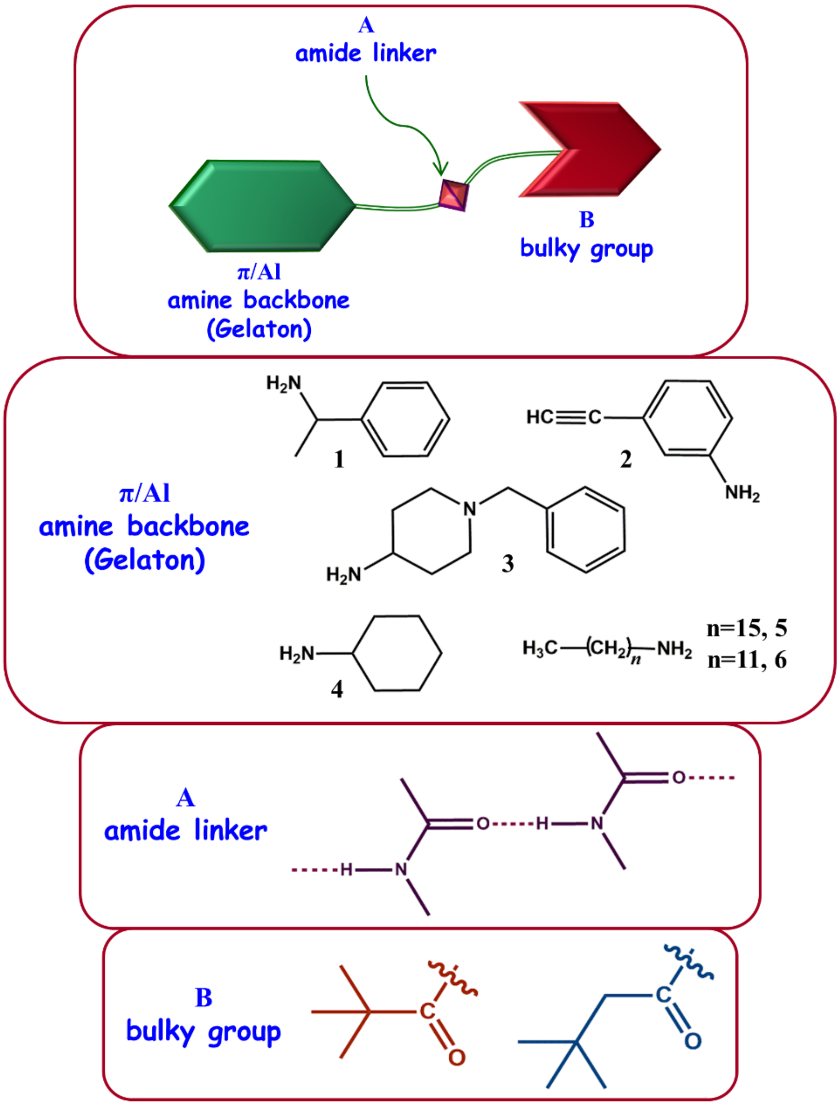

Figure 4.24 Illustration of the design strategy, π/Al-A-B

Just like lead, cadmium is a soft metal and finds applications in Ni-Cd batteries, electroplating, electro-galvanizing, plastic stabilizers, paints and pigments, electronics, etc. Cadmium is found as an active component in phosphate rocks, which are used in the preparation of phosphate fertilizers. Cadmium thus finds its way in the food chain as it gets absorbed and accumulates in the crops. Cadmium exposure is associated with oxidative stress, male infertility, hypertension, epigenetic change of DNA, impairment of mitochondrial related activities, kidney damage, cancer, diabetes and disruption of heme synthesis.[10–14]

Mercury is a unique metal, which exist in liquid state under standard conditions of temperature and pressure. It exists in +1 and +2 oxidation states. The organomercuric compounds are considered to be more toxic than the inorganic analogues. The use of mercury is rampant, ranging from fluorescent light bulbs, thermometers, barometers, diffusion pumps and electrodes to dental implants and batteries. The toxicity of mercury is known since ancient times and has caused devastating catastrophes like the Minamata Bay incident of Japan in 1957. Mercury poisoning can cause hearing loss, gait abnormality, ataxia, erosive bronchitis, respiratory insufficiency, tremor, excitability (also known as mercurial erethism), loss of memory, insomnia, excessive salivation, and tunnel vision, oxidative stress, kidney damage, lipid peroxidation and liver impairment.[15–18]

There is an increasing interest in reducing the heavy metal concentration in aqueous medium using low molecular weight gelators. In some cases, the use of metal ions can trigger the formation of a metallogels which can be useful in sensing as well as reducing their concentration. In other cases, the metal ions can interact with the molecules and can be simply used as sensors. There are various studies where reinforcement of organogels has been carried out by incorporating metal ions in the system. A strong metal-ligand interaction followed by complementary metal-metal bonding can be attributed to the enhancement in stability of metallo supramolecular gels. However, it is believed that many of the supramolecular gelators which hold promising potential for sequestration of dyes and heavy metal ions might be non-biocompatible. Parameters like removal efficiency, uptake ability, selectivity, absorption kinetics and thermodynamics, limit of removal, recyclability are also of paramount importance while dealing with enviro-supramolecular gels.

In the present study, six new compounds (**TBA1-TBA6**) were synthesized and characterized using various physico-chemical techniques. The organogels so formed were also employed for sequestering organic dyes from aqueous phase. We also carried out heavy metal sensing studies with all the synthesized compounds, out of which, **TBA1**, **TBA3** and **TBA4** showed impressive results. Single crystal studies of one compound were carried out and the intermolecular interactions were scrutinized.

4.7 EXPERIMENTAL PROCEDURES

4.7.1 Synthesis

Oxalyl chloride (0.9 mL, 10 mmol) was slowly added to a solution of *tert*-butylacetic acid (0.27 mL, 2 mmol) in dry dichloromethane under nitrogen atmosphere and the solution was subjected to continuous stirring at RT (~25°C) for 12 hours. Excess oxalyl chloride and the solvent were removed by distillation under reduced pressure. The acid chloride so formed was dissolved in dry dichloromethane (10 mL) and added to a solution of amine (1 mol equiv., **1-6**) and triethylamine (0.25 mL, 2 mmol) mixture in an RB flask. The mixture was stirred under N_2 atmosphere overnight. The reaction mixture was then added to dil. HCl (5%) and extracted with chloroform. The solvent was removed using rotary evaporator and the compounds (**TBA1-TBA6**, Scheme 4.2) were kept for recrystallization in various solvents (yield= 64-71%).

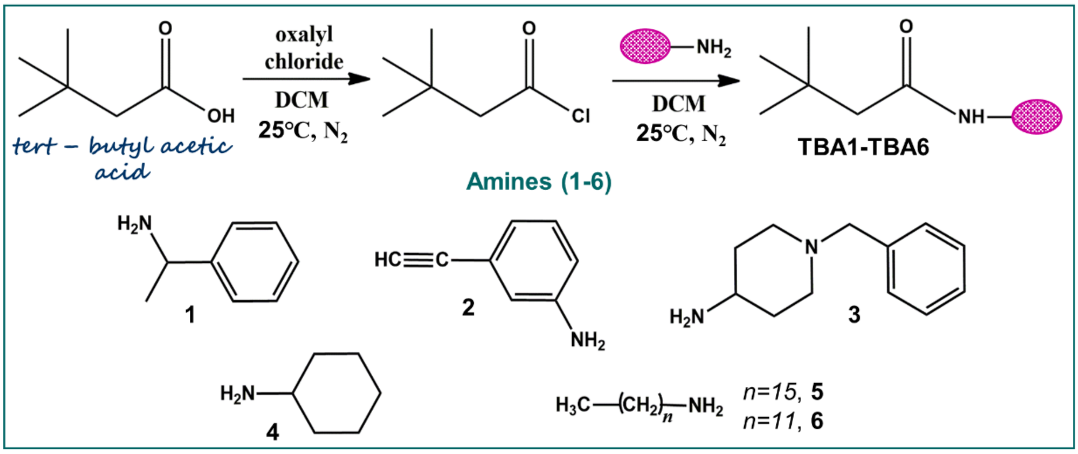

Scheme 4.2 Amides of *tert*-butylacetic acid, TBA1-TBA6 synthesized in the study

4.7.2 Gelation trials

The mgc values of all gelators were determined using dilution method. To a glass vial containing 10 mg gelator, 0.2 mL of solvent was added, and a heat-cool cycle was employed to observe gel formation. To this system, gradual dilution was carried out till no gelation was observed. The last concentration at which gelation was observed was recorded as mgc value (%wt/v or mg/mL). The same process was repeated in triplicates for each system and average values were reported as mgc values. The gelation behavior was also tested in presence of ultrasound waves.

T_{gel} (gel-to-sol conversion temperature) was also measured using the same method. The vials containing gels were heated in a temperature-controlled silicone oil bath at a steady rate of 0.5°C/min. The temperature at which first drop of gel melted was considered as $T_{gel.}$

4.7.3 Phase selective organo-gelation (PSOG)

A weighed amount of gelator was added to a biphasic mixture of water and organic solvent in dry or solution form. The system was subjected to heat, strong sunlight, or UV irradiation after which selective gelation of solvent was observed and recorded.

4.7.4 Dye removal studies

The ability of gels to uptake dyes from aqueous phase was determined using UV-vis studies. The concentration of dyes in the aqueous phase was calculated by Beer-Lambert law (A= αlc, where A= absorbance of dye at a certain concentration, α= extinction coefficient ($Lmg^{-1}cm^{-1}$, l= path length of incident light (cm), c= concentration of dye in solution). The maximum absorption wavelengths were monitored at 554 nm for Rhodamine B, 664 nm for Methylene Blue and 584 nm for Crystal Violet. The dye removal efficiencies were calculated using equation 4.2,

$$\textbf{Removal efficiency} = (C_0-C_t)/C_0 * 100\% \quad - (4.2)$$

where C_0= initial dye concentration, C_t= dye concentration at time t (mg/mL).

4.7.5 Heavy metal sensing

The metal ion responsive behavior of all compounds was studied in methanol. The binding interactions were followed through UV-vis spectroscopy. The experiments were performed with a fixed concentration of compounds (10 µM) and gradually increasing the concentration of metal ion (mercuric acetate, lead acetate and cadmium acetate) solutions (0-3 µM). An equal amount of metal ion solution was added to both the cuvettes, containing the test solution and the reference in order to eliminate the absorbance of metal acetate itself. A control study was also performed with sodium acetate to confirm whether the sensing was due to binding with metal ions or acetate ions.

Determination of binding constant. The binding constant (K_a) was determined by the Benesi−Hildebrand plot using the equation 4.3:

$$\frac{A_0}{\Delta A} = \left[\frac{\varepsilon_M}{\varepsilon_M - \varepsilon_C}\right]\left(K_a^{-1} C_g^{-1} + 1\right) \qquad \text{- (4.3)}$$

where ε_M and ε_C are molar extinction coefficients of the compound and the complex, respectively, at a selected wavelength; A_0 represents the absorbance of free compounds at that specific wavelength, and C_g is the concentration of the metal ions. The linear fit of $A_0/\Delta A$ with the inverse of the metal ion concentration indicated 1:1 stoichiometry of the complex. The ratio of the intercept to slope was used for binding constant (K_a) determination.[19,20]

Calculation of the Detection Limit. The detection limit was determined using the UV-vis titration data. The absorbance of the compounds was plotted against concentrations of metal ions to determine the slope. Then, detection limits were calculated using equation 4.4:

$$\textit{Detection limit} = \frac{3.3\,\sigma}{k} \qquad \text{- (4.4)}$$

where σ is the standard deviation of blank measurement and k refers to the slope.[21,22]

4.7.6 Materials and Methods

All the chemicals were obtained from Sigma Aldrich and TCI and the solvents were obtained from SD Fine Chemicals, India, and were used without any further purification.

4.7.6.1 NMR studies

NMR data was recorded on Bruker AVANCE, 400 MHz spectrometer in $CDCl_3$, with TMS as internal standard. The ^1H and ^{13}C NMR spectra of all compounds can be found in Supplementary Data* at the end of the chapter.

4.7.6.2 FT-IR studies

FT-IR studies were performed on Bruker Alpha FT-IR spectrometer in a solid-state as KBr pellets. The FT-IR spectra of all compounds can be found in Supplementary Data* at the end of the chapter. FT-IR spectra of **TBA1** in gel and solution phase (with n-octane as solvent) were recorded using CaF_2 discs.

4.7.6.3 Crystallography

Single crystal diffraction data of **TBA4** was collected on Bruker APEX-II CCD diffractometer with monochromatic Mo Kα radiation (0.71073 Å). The structure was solved and refined using the Olex2 software and ShelX refinement package. Graphics were generated using MERCURY, version 4.3.1. The structure was solved by direct methods and refined in a regular pattern. Non-hydrogen atoms were treated anisotropically. The hydrogen atoms were refined by locating on a difference Fourier map. The crystallographic parameters are tabulated in Table S4.3*.

4.7.6.4 Hirshfeld studies

The 3D Hirshfeld surface and 2D fingerprint plot were obtained using Crystal Explorer 3.1.

4.7.6.5 Rheology

Rheology studies of **TBA1** and **TBA4** were performed on an Anton Paar MCR 102 Modular Compact Rheometer at 38°C. The instrument has a parallel plate geometry with a plate diameter of 50 mm, maintained at a gap of 0.5 mm; the gel samples were subjected to oscillatory amplitude sweep range of 0 to 100 rad/s and values of G' (storage modulus) and G" (loss modulus) were evaluated.

4.7.6.6 Morphology

The frozen gel samples (in various solvents) were used directly for viewing images using HITACHI SUI510 Scanning Electron Microscope. POM analyses were performed using LEICADM2500P polarizing microscope. Images were captured using LEICADFC295 camera which is attached with the instrument. A thin layer of gel was formed on a glass slide and allowed to dry at RT, whose images were captured.

4.7.6.7 Powder XRD

Representative powder diffraction patterns of bulk (crystalline) gelator and xerogel samples (diesel) of **TBA1** and **TBA4** were recorded on an XPERT (Cu Kα radiation) diffractometer on a continuous scanning mode at 2θ value 5-50°.

4.7.6.8 UV-vis studies

Metal sensing studies were performed using Perkin Elmer Lambda 35 dual beam UV-vis spectrophotometer. Dye removal studies were performed on Agilent Cary 60 dual beam UV-vis spectrophotometer.

4.7.7 Analytical Data

Compound TBA1 (N-(1-phenylethyl)- 3,3-dimethylbutanamide). M.P.= 60°C, ^{1}H NMR (400 MHz, $CDCl_3$, TMS) = δ (ppm) 7.766-7.322 (*m*, 5H, 5(CH) ar), δ 5.660 (*s*, 1H, -CONH), δ 5.199-5.051 (*m*, 1H, (CH)), δ 2.063 (*s*, 2H, CH_2), δ 1.579-1.562 (*d*, 1H, CH), δ 1.517-1.499(*d*, 3H, CH_3), 1.040 (*s*, 9H, 3(CH_3)). ^{13}C = δ (ppm) 171, 159, 143, 142, 128, 127, 126, 50, 49, 48, 31, 29, 21.

FT-IR, cm^{-1} (KBr) – 3299, 3062. 3031, 2960, 2808, 1736, 1634, 1545, 1510, 1449, 1393, 1385, 1342, 1263, 1234, 1207, 1145, 1018, 907, 763, 697, 623, 541.

Compound TBA2 (N-(3-ethynylphenyl)-3,3-dimethylbutanamide). M.P.= 98°C, ^{1}H NMR (400 MHz, $CDCl_3$, TMS) = δ (ppm) 7.654 (*s*, 1H, (CH) ar), δ 7.572-7.553 (*d*, 1H, (CH) ar), δ 7.299-7.215 (*m*, 2H, 2(CH) ar), δ 3.077 (*s*, 1H, ≡CH), δ 2.237 (*s*, 2H, CH_2), δ 1.114 (*s*, 9H, 3(CH_3)). ^{13}C = δ (ppm) 170, 137, 129, 127, 123, 122, 120, 83, 51, 31, 29.

FT-IR, cm^{-1} (KBr) – 3431, 3292, 3067, 2961, 2361, 1651, 1580, 1554, 1474, 1419, 1366,1337, 1277, 1152, 1132, 1041, 976, 954, 885, 793, 763, 690, 665, 633.

Compound TBA3 (N-(1-benzylpiperidin-4-yl)-3,3-dimethylbutanamide). M.P.= 96°C, ^{1}H NMR (400 MHz, $CDCl_3$, TMS) = δ (ppm) 7.330-7.264 (*m*, 5H, 5(CH) ar), δ 5.311-5.292 (*d*, 1H, -CONH), δ 3.861-3.786 (*m*, 1H, (CH)), δ 3.500 (*s*, 2H, CH_2)), δ 2.839-2.811 (*d*, 2H, 2(C$\underline{H}_2$)), δ 2.149-2.095 (*m*, 2H, 2(C$\underline{H}_2$)), δ 2.026 (*s*, 2H, CH_2), δ 1.932-1.905 (*m*, 2H, 2(C$\underline{H}_2$)), δ 1.502-1.405 (*m*, 2H, 2(C$\underline{H}_2$)), δ 1.031 (*s*, 9H, 3(CH_3)). ^{13}C = δ (ppm) 171, 138, 129, 128, 127, 63, 52, 50, 48, 46, 35, 32, 30, 29.

FT-IR, cm^{-1} (KBr) – 3290, 3082, 3029, 2955, 2866, 2802, 1634, 1554, 1493, 1448, 1393, 1364, 1273, 1245,1201, 1154, 1141, 1092, 1028, 863, 791, 743, 731, 698, 643.

Compound TBA4 (N-cyclohexyl-3,3-dimethylbutanamide). M.P.= 88°C, ^{1}H NMR (400 MHz, $CDCl_3$, TMS) = δ (ppm) 5.478 (*s*, 1H, -CONH), δ 3.756-3.713 (*m*, 1H, (CH)), δ 1.987 (*s*, 2H, CH_2), δ 1.898-1.859 (*m*, 2H, 2(C$\underline{H}_2$)), δ 1.734-1.380 (*m*, 2H, 2(C$\underline{H}_2$)), δ 1.372-1.342 (*m*, 1H, C$\underline{H}_2$), δ 1.333-1.101 (*m*, 2H, 2(C$\underline{H}_2$)), δ 1.081-1.036 (*m*, 3H, 3(C$\underline{H}_2$)), δ 0.997 (*s*, 9H, 3(CH_3)). ^{13}C = δ (ppm) 170, 159, 50, 48, 47, 33, 32, 30, 29, 25, 24.

FT-IR, cm^{-1} (KBr) – 3307, 3077, 2952, 2933, 2853, 1637, 1547, 1447, 1365, 1346, 1300, 1273, 1256, 1239, 1202, 1153, 1100, 993, 891, 719, 622, 554.

Compound TBA5 (N-hexadecyl-3,3-dimethylbutanamide). M.P.= 54°C, ^1H NMR (400 MHz, $CDCl_3$, TMS) = δ (ppm) 5.431 (*s*, 1H, -CONH), δ 3.261-3.211 (*m*, 2H, CH_2), δ 2.042 (*s*, 2H, CH_2), δ 1.55-1.45 (*m*, 2H, CH_2), δ 1.288-1.258 (*m*, 28H, 14(CH_2)), δ 1.039 (*s*, 9H, 3(CH_3)), δ 0.886 (*t*, 3H, $C\underline{H}_3$). ^{13}C = δ (ppm) 171, 50, 39, 31, 30, 29.8-29.3, 26.9, 22, 14.

FT-IR, cm^{-1} (KBr) – 3301, 3062, 2915, 2849, 1633, 1543, 1474, 1393, 1365, 1333, 1265, 1232, 1201, 1145, 1039, 958, 716, 659, 620.

Compound TBA6 (N-dodecyl-3,3-dimethylbutanamide). M.P.= 43°C, ^1H NMR (400 MHz, $CDCl_3$, TMS) = δ (ppm) 5.409 (*s*, 1H, -CONH), δ 3.264-3.214 (*m*, 2H, CH_2), δ 2.717-2.683 (*m*, 2H, CH_2), δ 2.042 (*s*, 2H, CH_2), δ 1.511-1.264 (*m*, 20H, 10(CH_2)), δ 1.042 (*s*, 9H, 3(CH_3)), δ 0.905-0.871 (*t*, 3H, CH_3). ^{13}C = δ (ppm) 171, 50, 42, 39, 33, 31, 30, 29.8-29.2, 26, 22, 14.

FT-IR, cm^{-1} (KBr) – 3301, 2955, 2919, 2851, 1634, 1544, 1469, 1365, 1344, 1265, 1233, 1149, 817, 718, 663, 619.

4.8 RESULTS

All the synthesized compounds (**TBA1-TBA6**) were tested for their gelation performance. Compounds **TBA1** and **TBA4** displayed better gelation performance than rest of the compounds; gels were formed in in diesel, kerosene, engine oil, silicone oil and cooking oil, as well as in crude oil fractions (n>7 carbon atoms) (Table 4.4). None of the compounds could congeal petrol.

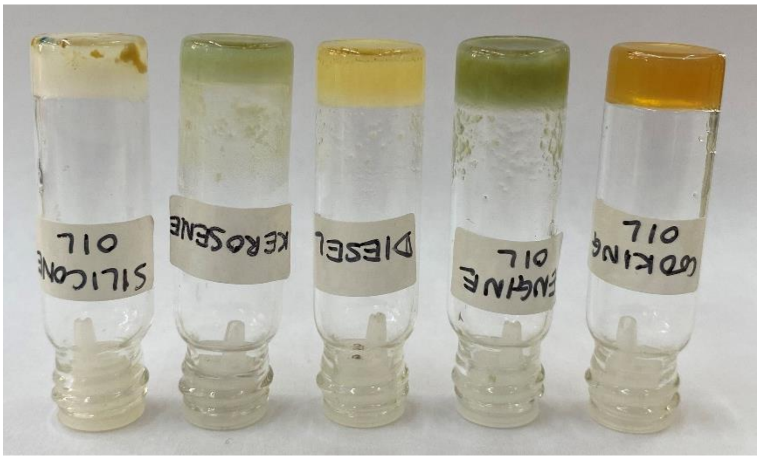

Figure 4.25 Gels of TBA1 in silicone oil, kerosene, diesel, engine oil and cooking oil

A conventional heat-cool cycle was employed to check the gelation behavior in a variety of solvents (Table 4.2). However, the solubility of these compounds was found to be compromised, as the gels could be formed only when the system was heated up to high temperature (65-70°C). No gelation was observed in presence of strong sunlight. A UV irradiation for atleast 15 minutes or ultrasonication for 15-20 minutes at 50°C was required to induce gelation.

The gels remained stable for several months, at RT (~25°C) as well as at low temperatures (4-10°C), which suggests the formation of a fairly efficient and stable self-assembly.

4.8.1 Gelation studies and effect of solvents on gelation

All synthesized compounds displayed a lack of gelation behavior in aromatic (protic as well as aprotic) solvents like benzene, toluene, nitrobenzene, halobenzenes, xylenes, benzyl alcohol, aniline, etc. Compounds **TBA1, TBA5** and **TBA5** formed gels in

DMSO and propan-1,2-diol along with aliphatic solvents and fuels which makes them versatile gelators. **TBA4** turned out to be the most versatile in terms of the number and types of solvents congealed.

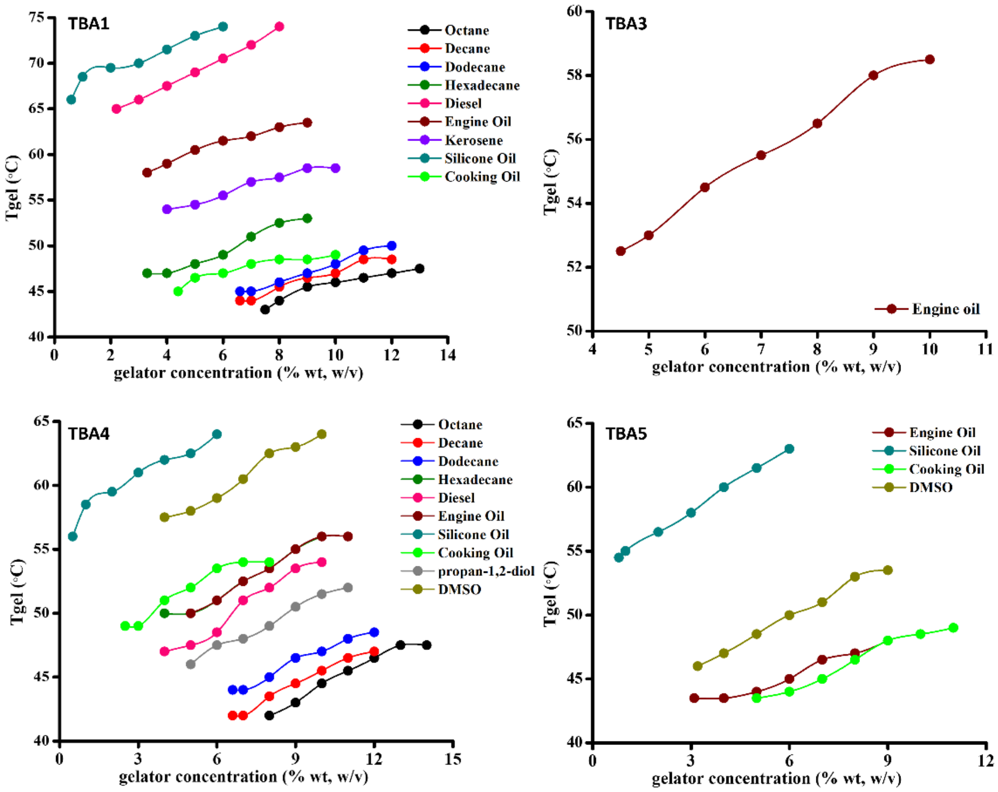

Figure 4.26 T_{gel} vs. concentration plots for all gels

Table 4.4 Gelation behavior of compounds TBA1-TBA6 in various solvents; mgc values are enclosed in parentheses

	TBA1	TBA2	TBA3	TBA4	TBA5	TBA6
n-octane	G (7.5)	S	S	G (8.0)	S	S
n-decane	G (6.6)	S	S	G (6.6)	S	S
Dodecane	G (6.6)	S	S	G (6.6)	S	S
Hexadecane	G (3.3)	S	S	G (4.0)	S	S
Diesel	G (2.2)	S	S	G (4.0)	S	S
Kerosene	G (4.0)	S	S	S	S	S
Engine oil	G (3.3)	S	G (4.5)	G (5.0)	G (3.1)	S
Cooking oil	G (4.0)	S	S	G (2.5)	G (5.0)	S
Silicone oil	G (0.6)	S	S	G (0.5)	G (0.8)	S
Propan-1,2-diol	S	S	S	G (5.0)	S	S
DMSO	G (3.3)	S	S	G (4.0)	G (3.2)	S

G - gel, WG - weak gel, S - solution, I – insoluble, ppt – precipitate.

TBA2 and **TBA6** are amides of 3-ethynyl aniline and dodecylamine failed to congeal any solvent. The gelation ability of **TBA5** and **TBA3** was found to be weaker than its pivalic acid analogues, possibly because of increase in van der Waals interactions and lipophilicity of the molecules which could have disturbed the hydrophilic-hydrophobic balance resulting in undermined gelation performance.

A semilog graph of mole fraction of gelator concentration plotted against 1/1000 T_{gel} (K^{-1}) for gels in alkane homologs and DMSO, propan-1,2-diol, etc. gave a nearly linear relationship according to the Schroeder-van Laar equation. ΔH_m values calculated from the plots fell within a range of 77-320 kJ/mol (Figure 4.27). This confirmed that the gel-to-sol transition can be considered a first-order transition.

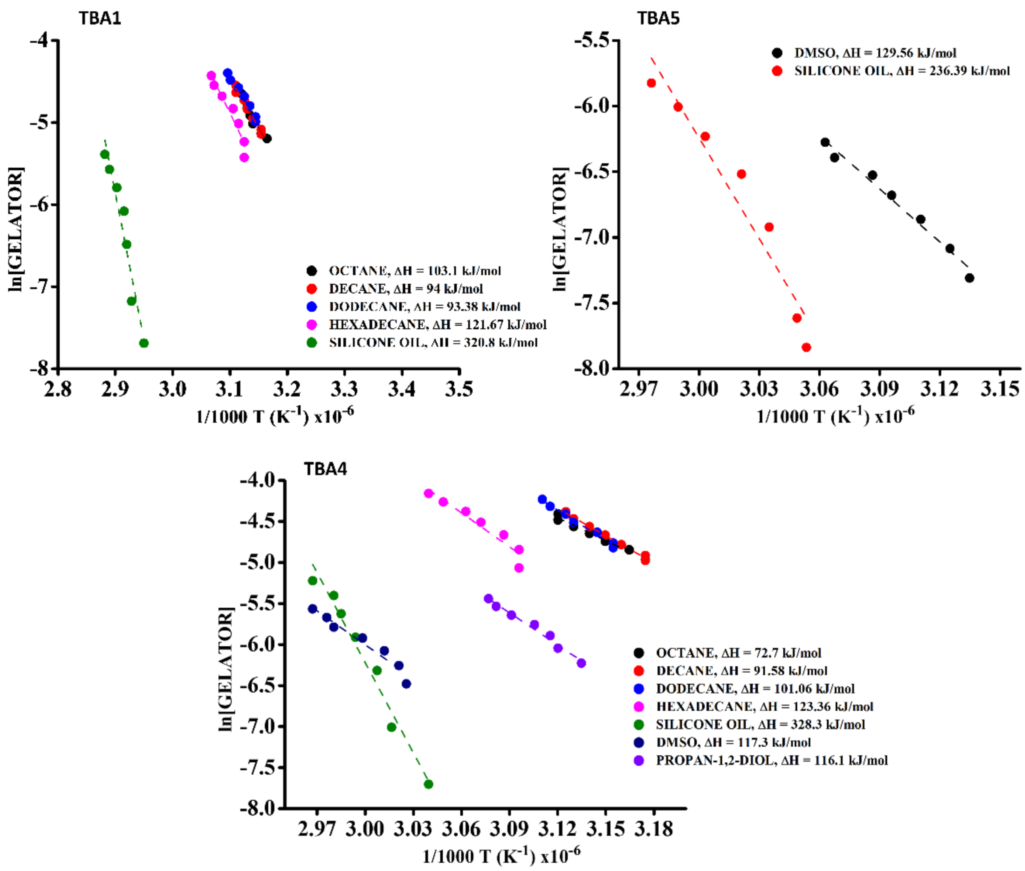

Figure 4.27 ΔH values for compounds according to the Schroeder-van Laar equation

4.8.2 Phase selective organo-gelation

All the gelators were screened for their ability to form gels in presence of aqueous phase (Figure 4.28). In a typical experiment, a glass vial containing mixture of water and organic solvent was taken and the gelator was added to it in solid form. Since all the gels in this series of compounds required a high temperature to be completely solubilized, the assembly had to be heated to a high temperature (60-65°C) which allowed the gelator to become soluble and form gel in presence of aqueous phase. All the organogels (with water immiscible solvents) could be formed in presence of aqueous phase, in presence of external heat. However, when external solvents were used, we observed improved performance. The gelator mixed in methanol or ethanol when added to the biphasic mixture readily formed a gel as the alcohols assisted in solubility of the gelator and allowed it to diffuse uniformly in the organic layer. However, employing water miscible solvents for the purpose of inducing better gelation performance can be detrimental to the water body in a typical environmental setting. Hence, a hot solution of the same solvent containing dissolved gelator was added to the biphasic mixture which elegantly served the purpose.

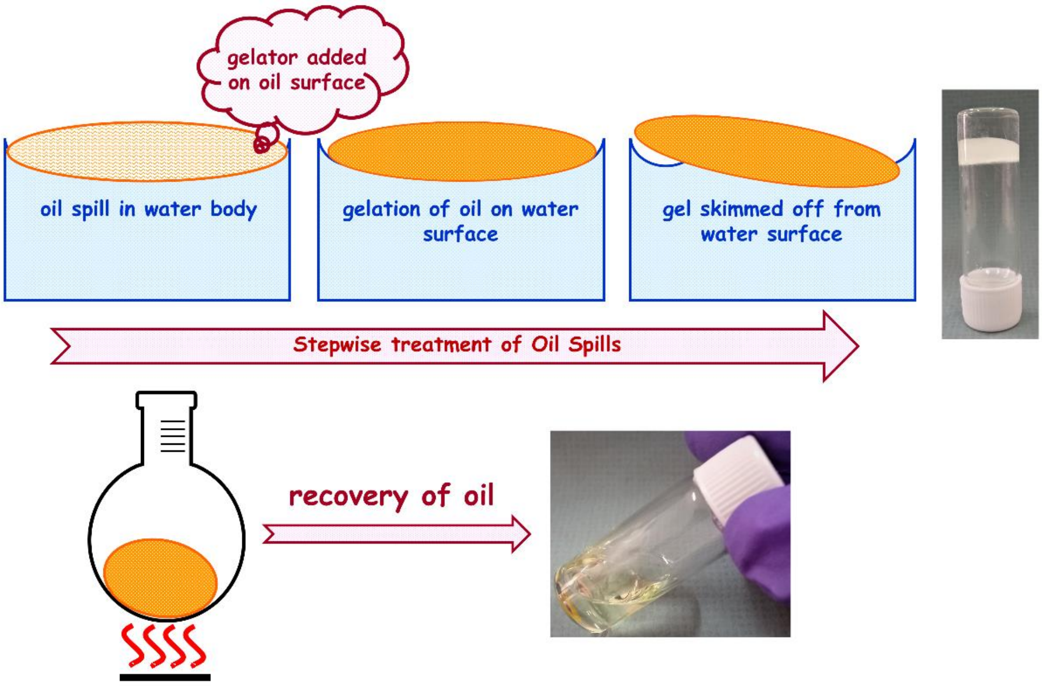

Figure 4.28 Demonstration of a PSOG experiment

The gels were formed with nearly the same mgc values in biphasic experiments as in neat solvents. This indicates that the gelation performance is not compromised biphasic systems. The experiments displayed similar results when carried out in presence of diesel-sea water mixtures (Figure 4.29). The organogel could be scooped out and distilled to retrieve the diesel back. The compounds, however, formed a sticky mass and could not be reused for another cycle.

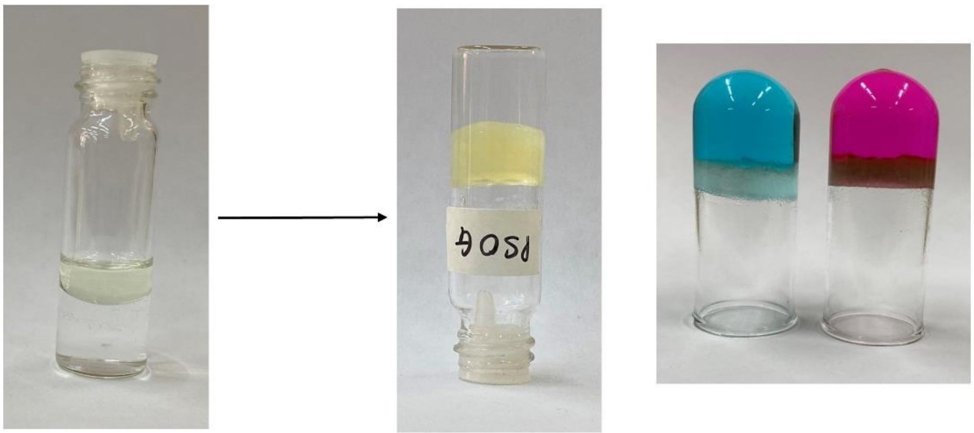

(a) (b)

Figure 4.29 (a) Selective gelation of organic phase in presence of sea water and (b) PSOG in presence of water containing dyes, $MgSO_4$, Na_2SO_4, NaCl and KCl

4.8.3 Dye removal studies

Organogels can be employed for sequestering dyes from water owing to their porous network and high surface area of contact. Furthermore, the gelators are amphiphilic in nature which allows their hydrophilic part to interact with the aqueous phase and the hydrophobic part to adsorb organic dyes. There are various factors held accountable for an ideal dye removal behavior of an organogel, such as, interaction of gelator fibers with dye molecules, backbone of the gelator, chemical structure and charge of dye, etc.

These environmentally benign supramolecular gels can be designed with pre-determined energetics and geometry from molecular level in order to exhibit high selectivity and uptake of a specific class of dyes. The paradigm is to effectively program the self-assembly *via* intermolecular interactions and molecular geometry.[23–25]

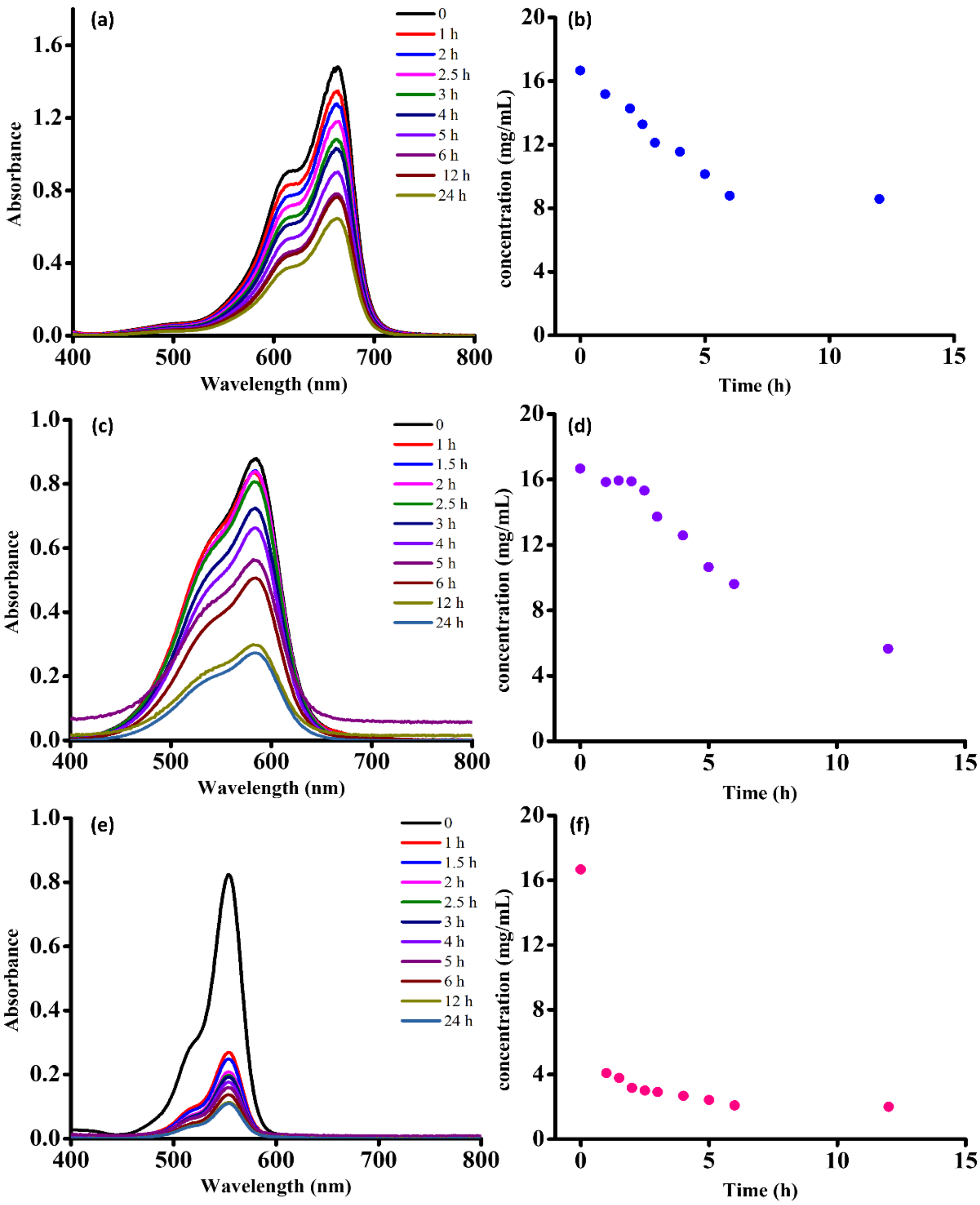

Figure 4.30 Time dependent absorption studies for TBA1 in an aqueous solution of 1.5 mL which contains (a) methylene blue dye at an initial concentration of 25mg/1.5 mL and (b) concentration-time correlation at 664 nm, (c) crystal violet dye at an initial concentration of 25mg/1.5 mL and (b) concentration-time correlation at 583 nm, (e) Rhodamine B dye at an initial concentration of 20mg/1.5mL, in presence of 1mL of diesel congealed on the water surface using 5% of TBA1 and (f) its concentration-time correlation at 554 nm.

In the present study, we employed **TBA1** and **TBA4** for removal of methylene blue, crystal violet and rhodamine B dyes. A biphasic mixture containing 1 mL diesel and 1.5 mL aqueous solution of dye (25 mg/1.5 mL methylene blue or 25 mg/1.5 mL crystal violet or 20 mg/1.5 mL rhodamine B) was formed, the gelator was added in powder form from the top, and the solution was gently heated to approx. 65°C to form a strong gel over the aqueous layer. The ability of gelator to adsorb these dyes was monitored at 664 nm (for methylene blue), 583 nm (for crystal violet) and 554 nm (for rhodamine B) by UV-vis spectroscopy.

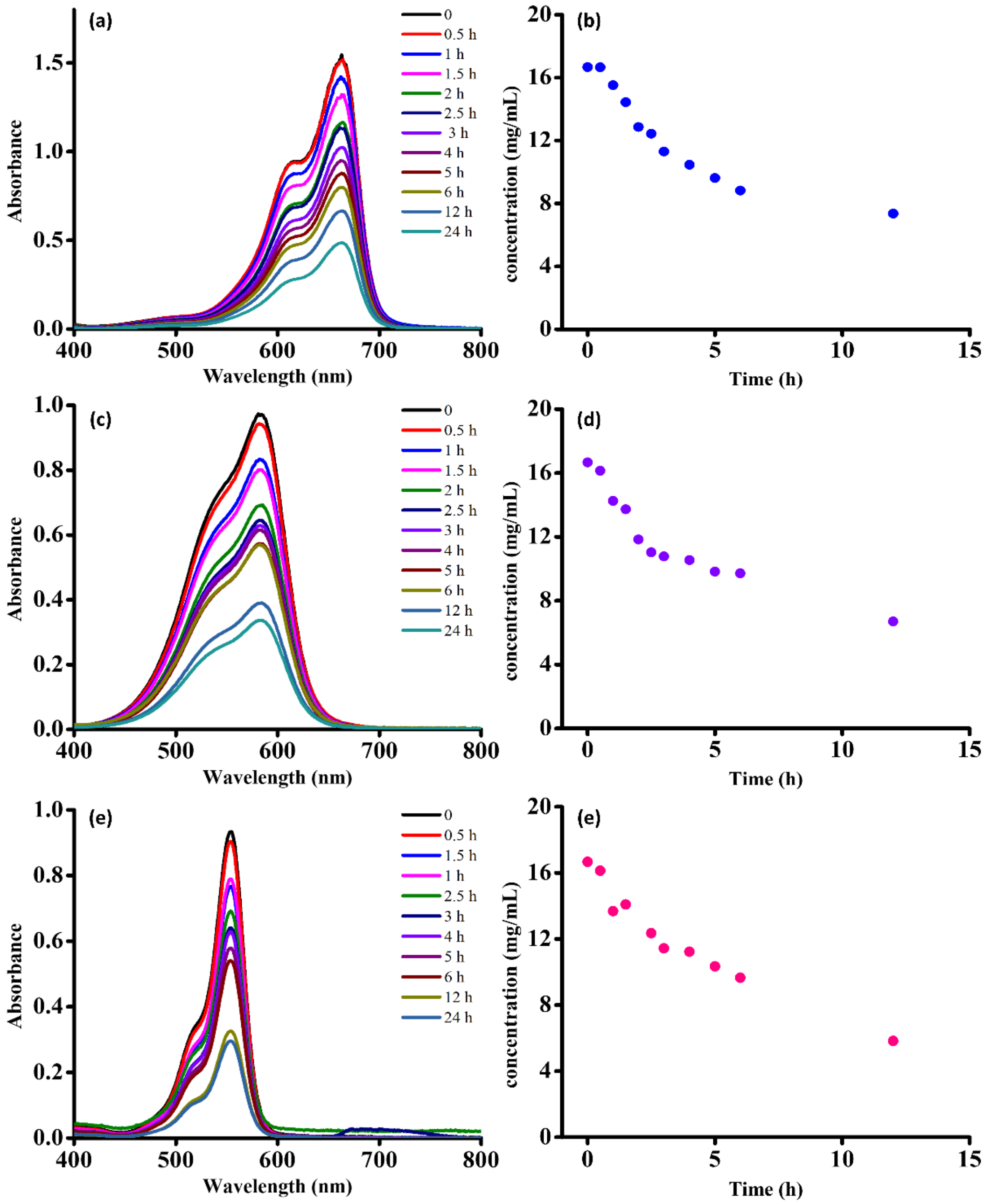

Figure 4.31 Time dependent absorption studies for TBA4 in an aqueous solution of 1.5 mL which contains (a) methylene blue dye at an initial concentration of 25mg/1.5 mL and (b) concentration-time correlation at 664 nm, (c) crystal violet dye at an initial concentration of 25mg/1.5 mL and (b) concentration-time correlation at 583 nm, (e) Rhodamine B dye at an initial concentration of 20mg/1.5mL, in presence of 1mL of diesel congealed on the water surface using 5% of TBA4 and (f) its concentration-time correlation at 554 nm.

The dye removal efficiencies were calculated from equation 4.2)

$$\textbf{Removal efficiency} = \left(\frac{C_0 - C_t}{C_0}\right) * 100\% \qquad - (4.2)$$

where C_0= initial dye concentration, C_t= dye concentration at time t (mg/mL)

Table 4.5 Removal efficiencies

	TBA1		TBA4	
	After 12h	**After 48h**	**After 12h**	**After 48h**
Methylene Blue	48.5	56.4	55.8	67.8
Crystal Violet	66.0	68.9	59.8	65.3
Rhodamine B	88.2	89.6	65.0	68.3

It was observed that compound **TBA1** showed better removal efficiency for rhodamine B and crystal violet after 12 hours. Both the compounds showed better removal efficiencies in rhodamine B (Table 4.5) than rest of the dyes, where maximum absorption could be achieved only after 12 hours. Dye absorption can be a time-consuming process and can take up to 24-48 hours for maximum absorption (Figures 4.30, 4.31). To ensure this, we monitored the system till 48 hours and found that the removal efficiencies did improve with increasing time. However, the maximum absorption must have occurred in the first 5-6 hours of the experiment, after which the spaces in the porous network of the gel must be essentially occupied with dye molecules, making further uptake rate rather sluggish.

4.8.4 Metal sensing studies

The metal-ion responsive behaviors of all compounds were studied in methanolic solutions with Cd^{2+}, Hg^{+} and Pb^{2+}. The binding interactions were followed using UV-vis spectroscopy. **TBA2**, **TBA5** and **TBA6** were found to be inactive towards any of the tested metal ions.

The change in absorbance of compounds was observed with gradual addition of metal ions to the compounds. With increasing concentrations of metal ions, the absorbance of the system systematically decreased. A control experiment with sodium acetate was also carried out with all the active compounds to ensure that acetate ions were not interacting with the compounds and causing the absorbance dip.

Table 4.6 LOD and K_a values for all the heavy metals tested in all compounds

	TBA1		TBA3		TBA4	
	Detection Limit x 10^{-6} M	K_a x 10^{5} M^{-1}	Detection Limit x 10^{-6} M	K_a x 10^{6} M^{-1}	Detection Limit x 10^{-5} M	K_a x 10^{5} M^{-1}
Cadmium	1.409	5.22	1.624	4.144	5.08	6.22
Mercury	0.931	9.92	1.757	1.474	2.03	2.08
Lead	1.530	2.82	1.007	4.432	3.81	6.94

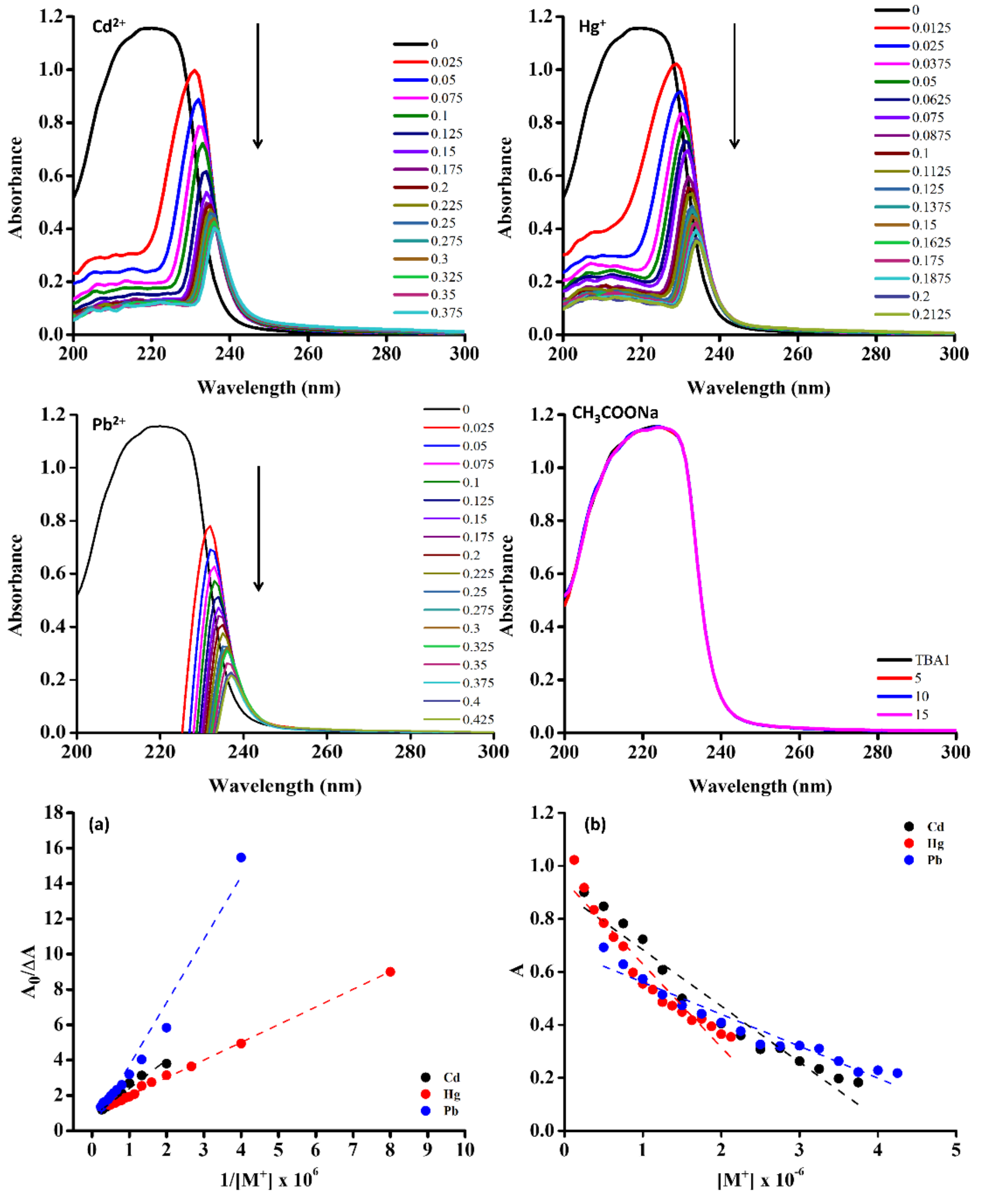

Figure 4.32 Change in absorbance of TBA1 with increasing concentrations of cadmium(II), mercury(I) and lead (II), control experiment with sodium acetate; (a) Benesi–Hildebrand plot and (b) detection limit of all metal ions with TBA1

The original spectra of all the compounds displayed a broad peak between 220-240 nm, but addition of metal ions caused it to transform into a sharp peak. The association constant, K_a was calculated from Benesi-Hildebrand plots. The linear fit of $A_0/\Delta A$ with the inverse of the metal ions concentration indicated 1:1 stoichiometry of the complexes (Figures 4.32-4.34 (a)). The values of detection limit were calculated from the plot of absorbance vs. concentration of metal ion (Figures 4.32-4.34 (b)).

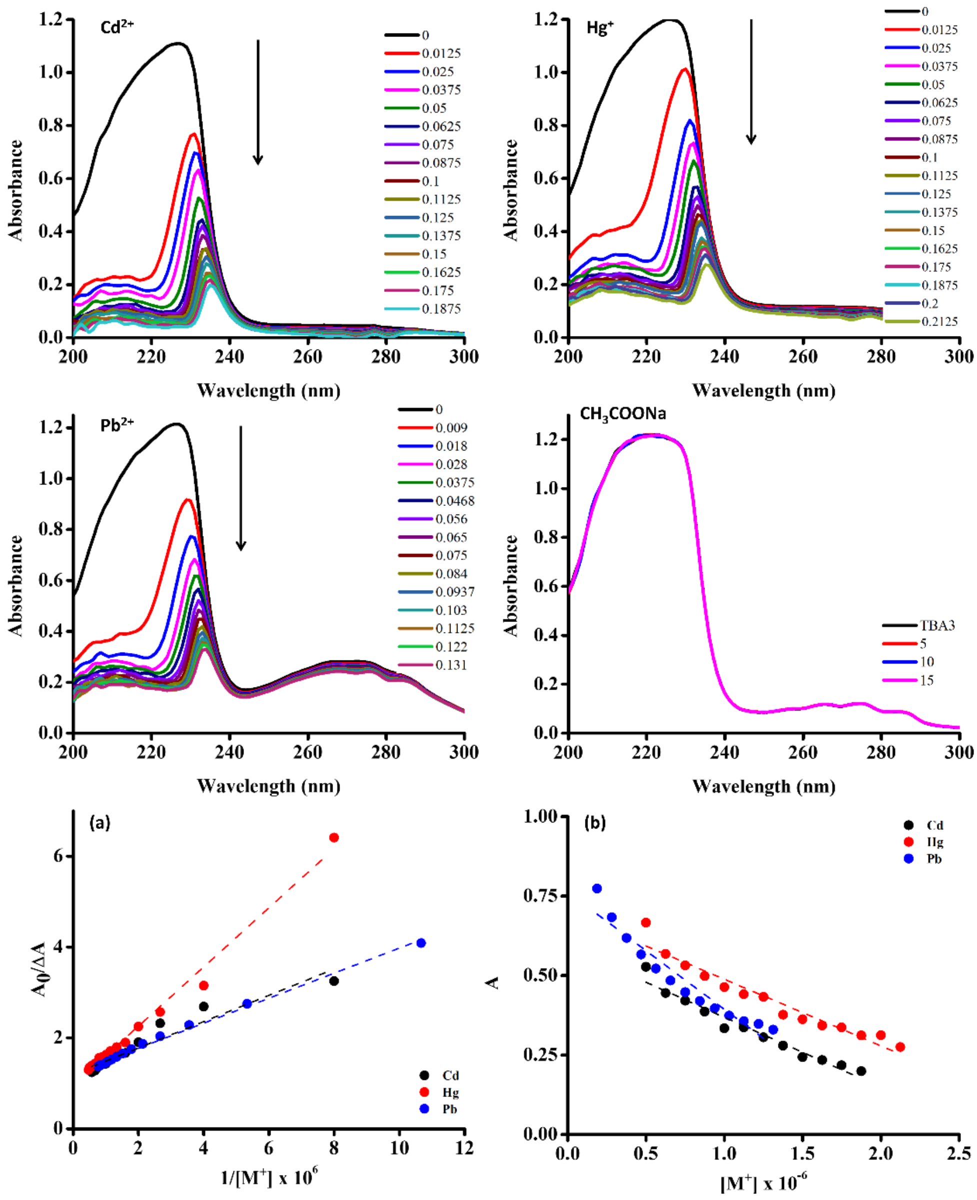

Figure 4.33 Change in absorbance of TBA3 with increasing concentrations of cadmium(II), mercury(I) and lead (II), control experiment with sodium acetate; (a) Benesi–Hildebrand plot and (b) detection limit of all metal ions with TBA3

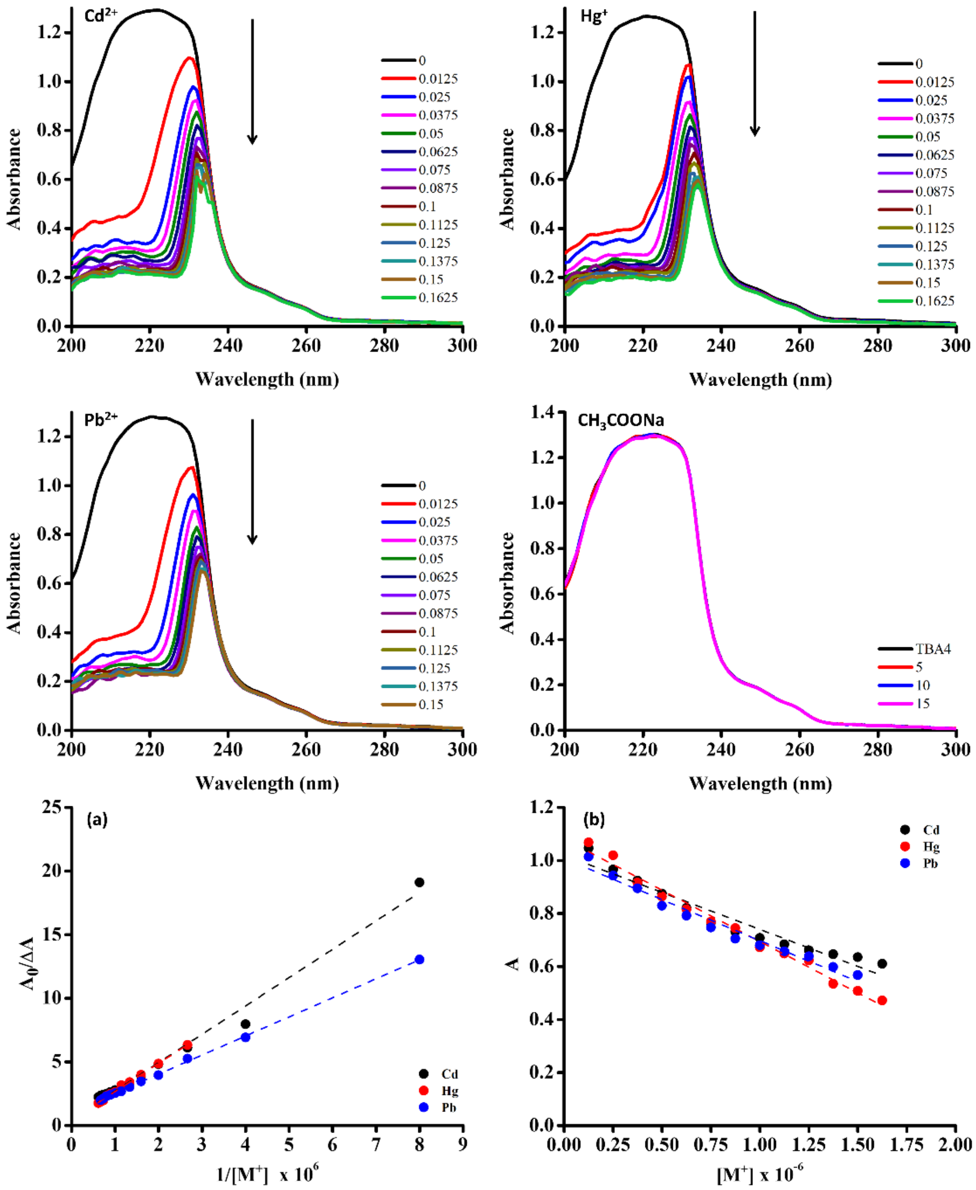

Figure 4.34 Change in absorbance of TBA4 with increasing concentrations of cadmium(II), mercury(I) and lead (II), control experiment with sodium acetate; (a) Benesi–Hildebrand plot and (b) detection limit of all metal ions with TBA4

Three compounds, **TBA1**, **TBA3** and **TBA4** were found to be sensitive towards all the three tested heavy metal ions. In **TBA1**, lowest detection limit was observed for mercury(I) ions at 0.931 x 10^{-6} M, with a K_a value of 9.92 x 10^5 M^{-1}. Similar trend was observed in **TBA4**; while in **TBA3**, lead(II) showed a lower detection limit of 1.007 x 10^{-6} M, with a K_a value of 4.43 x 10^6 M^{-1}.

4.8.5 Rheology

The mechanical strength of the gels was probed using rheology. The diesel gels of **TBA1** and **TBA4** were utilized for the shear stress amplitude sweep measurements. The values of G′ and G′′ remained between 10^3 and 10^5 for both the compounds. A crossover was observed in **TBA4** gel while the lines in **TBA1** gel appeared to be coming closer as the τ value approached 100.

All the gels remained stable for months and displayed shear thinning behavior when subjected to stress. This indicates a high degree of elasticity in the gels.

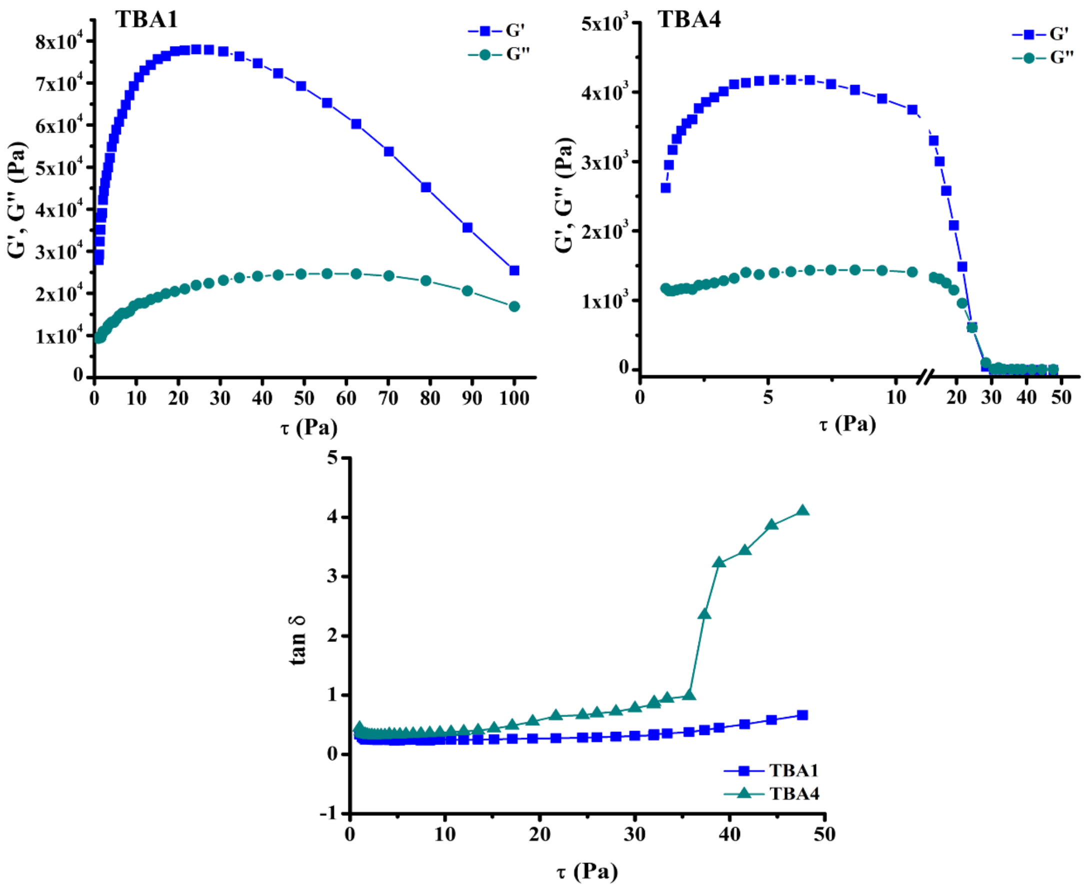

Figure 4.35 Rheological behavior of the gels in diesel and trends in tan δ values

4.8.6 Morphology

The surface morphology of frozen gels was assessed using SEM studies. The diesel gel of **TBA1** displayed hollow tunnel-like formations which could have assisted in better gelation behavior (Figure 4.36 (a), (b)). Similar formations were observed in diesel gel of **TBA4**. **TBA3** displayed a leafy pattern in the diesel gel. Since all the images were captured in frozen gels, there is a chance we could freeze the fibrous assembly in the gel form, and we believe that this could be one of the best suited methods to probe into the individual gelator fibers.

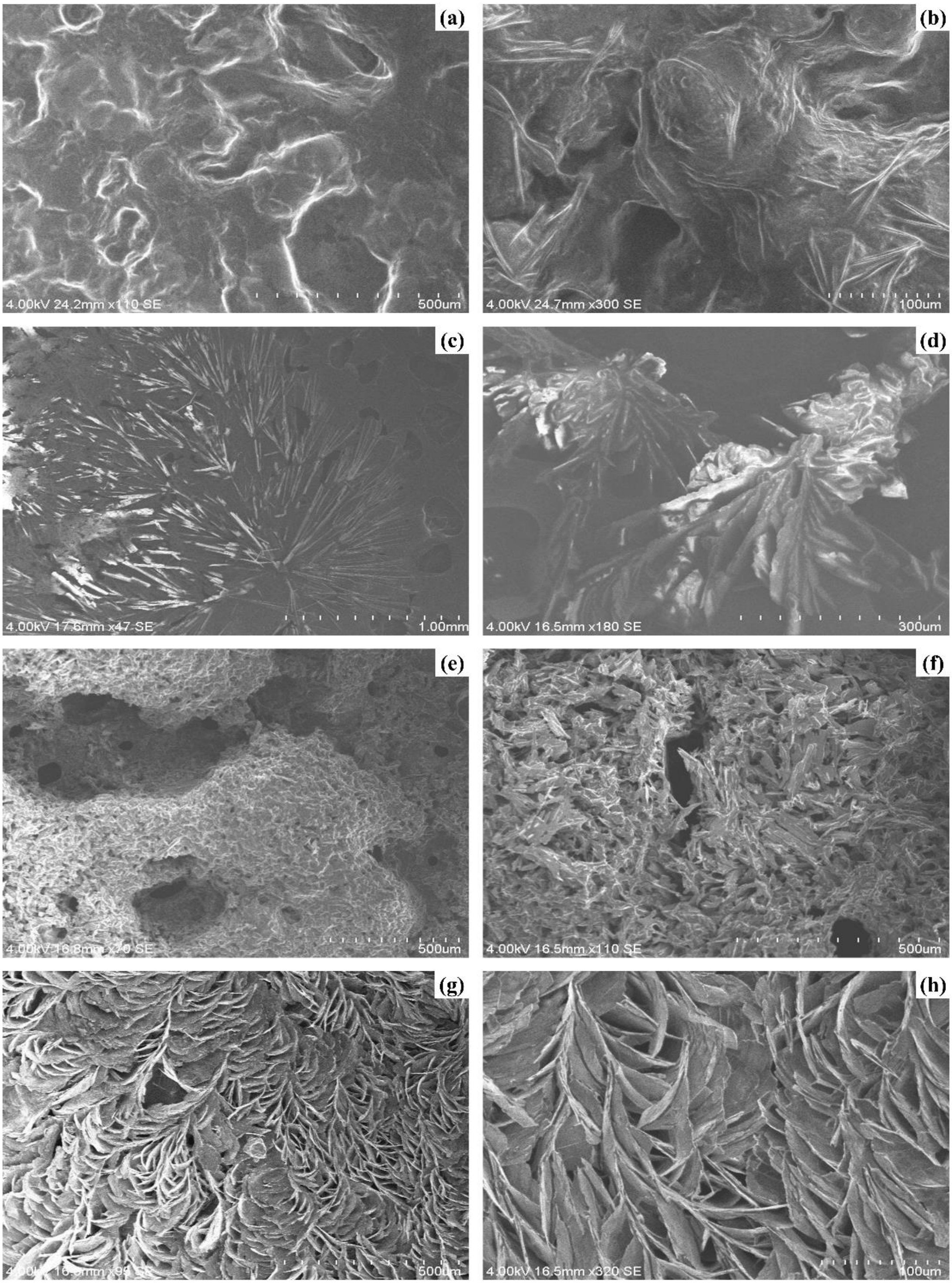

Figure 4.36 Surface morphology of frozen gels TBA1 in (a) diesel, (b) diesel, (c) decane; TBA3 in (d) diesel; TBA4 in (e) diesel, (f) diesel and TBA5 in (g) diesel, (h) diesel; at various magnifications

4.8.7 Single crystal and Hirshfeld studies

Single crystals of **TBA4** were obtained from a mixture of ethanol and acetonitrile at 10℃. The molecule crystallizes in monoclinic, *$P2_1/c$* space group and contains two molecules in its asymmetric unit. The molecule exhibits one dimensional network *via* N-H…O bonds. Interestingly, no other specific non-covalent interactions were found in the structure. The strategy of design is remarkably pertinent in this case, as the bulky *tert*-butyl group impedes the formation of 2D, or 3D network, and the amine functionality allows an alternate arrangement of the head group attached to it in order to assist the formation of 1D network. This arrangement is primarily the cause behind exceptional gelation behavior of the compound.

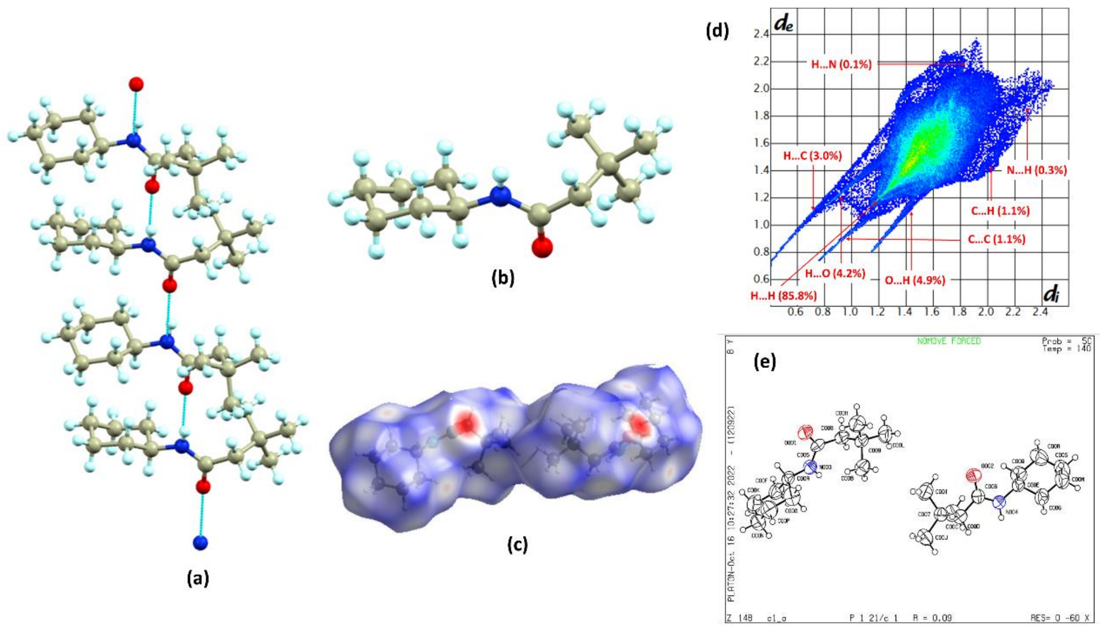

Figure 4.37 (a) 1D network and (b) discrete molecule of TBA4, (c) 3D Hirshfeld surface, (d) Fingerprint plot indicating various interactions observed in TBA4, where d_i is internal distance and d_e, external distance from the Hirshfeld surface to the nearest molecule (e) ORTEP image

The Hirshfeld studies indicate a high amount of van der Waals interactions in the structure. The H…H interactions amount to 85.8% of the total interactions in addition to the O…H and N…H interactions. The fingerprint plot uniquely displays four distinct spikes corresponding to H…C (d_i= 0.8 Å, d_e= 1.0 Å), H…O (d_i= 0.8 Å, d_e= 1.1 Å), C…C (d_i= 1.0 Å, d_e= 0.9 Å) and O…H (d_i= 1.3 Å, d_e= 1.1 Å). The middle region corresponds to the most prominent, H…H interactions (d_i= 1.2 Å, d_e= 1.2 Å) (Figure 4.37).

4.8.8 Powder X-ray diffraction studies

To confirm whether the packing was retained after gelation, PXRD was performed for **TBA1** in bulk form and xerogel obtained after gel formation in diesel. The peaks at 11.3, 12.8, 15.0, 16.7, 18.7, 20.0, 21.7 and 22.6 were found to be present in both the bulk and xerogel forms, with slight shifts. The peaks at 6.9 and 7.3 in bulk were not present in xerogel and new peaks at 25.0 and 29.3 were observed in xerogel form.

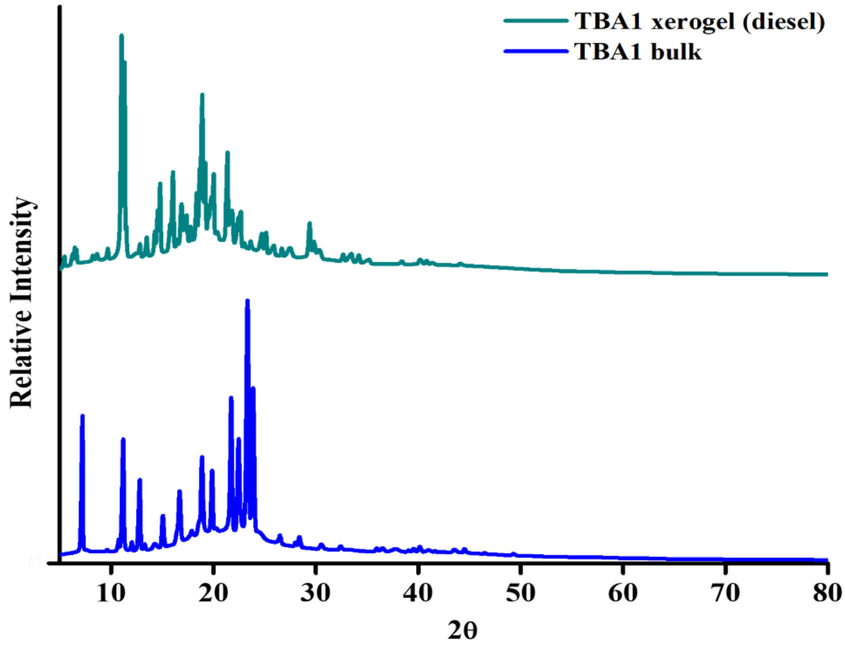

Figure 4.38 Comparative PXRD spectra of TBA1

The overall pattern did not appear to be matching in both the cases. A change in packing after gel formation can alter the packing of the solid post formation of a fibrous assembly as a result of enhanced interactions between solute and solvent.

4.8.9 Comparative FT-IR studies

Similar comparative FT-IR studies were performed for **TBA1** in bulk, xerogel, gel and solution form. The C=O stretching vibration observed at 1634 cm^{-1} in bulk was retained at 1639 cm^{-1} in xerogel and 1633 cm^{-1} in the gel and solution phase (Figure 4.39). The N-H bending vibration band at 1546 cm^{-1} was found to be overlapping in gel and solution phase, although it was shifted to 1527 cm^{-1} in the xerogel form. The N-H stretching band at 3297 cm^{-1} in bulk was retained at 3335 cm^{-1} in xerogel and a broad hump at 3289 cm^{-1} in gel and solution phases was observed.

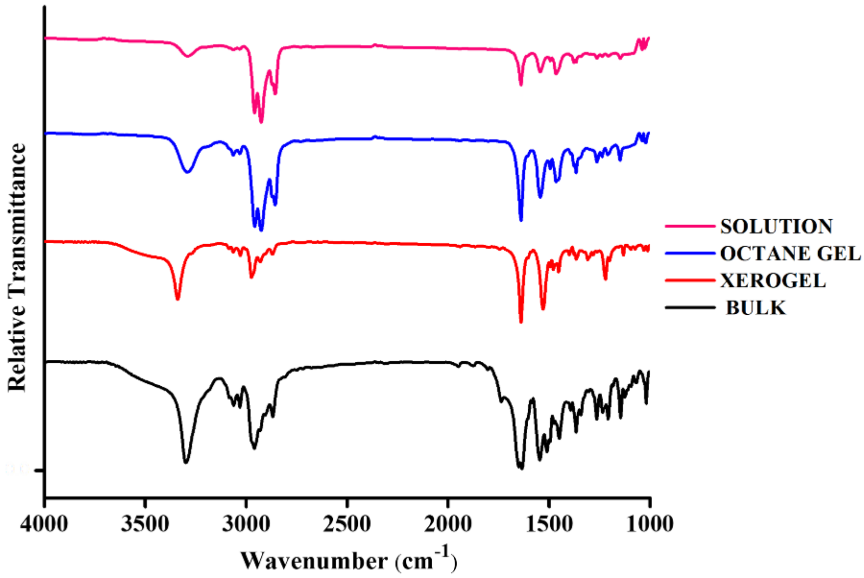

Figure 4.39 Comparison of FT-IR spectra between different forms of TBA1

The slight shifts observed in the respective fingerprint regions correspond to intermolecular hydrogen bonding between the -NH and carbonyl of the adjoining amides, which was confirmed from the structural studies. Overall, the FT-IR spectra in xerogel and gel form resembled with that of the bulk solid, indicating the basic form of **TBA1** was retained after gelation.

4.9 SUMMARIZING DISCUSSION AND CONCLUSIONS

In conclusion, we report a series of six compounds, inspired by the design strategy of **π/Al-A-B** (aromatic/aliphatic-amide linker-bulky group) type backbone. The amides of ethynyl aniline and dodecyl amine (**TBA2** and **TBA6**) failed to exhibit any gelation behavior, while rest of the compounds showed organo-gelation. **TBA1** and **TBA4** displayed splendid gelation behavior in all the tested solvents. The compounds were found to be capable of congealing crude oil fractions (n>7 carbons), kerosene, diesel, silicone oil, cooking oil, and engine oil. The behavior of **TBA5** (containing hexadecyl carbon chain) remained far less than expected, and inferior to that of pivalamide analogue. The mgc values appeared to be much higher in case of TBAA based gels, with a higher temperature required to instigate gelation. But once formed, these gels displayed better thermal stability and also remained stable for several months at room temperature.

The compounds displayed phase selective organo-gelation in presence of biphasic mixtures containing oil phase and sea water. When added in powder form, the system required to be heated to a high temperature on account of low solubility, but when added in solution form, the system instantly solidified on the surface of water. These compounds were also employed for successful removal of dyes from aqueous medium. Out of the three dyes tested for the study, crystal violet and rhodamine B showed better removal efficiencies. The absorption of dyes present in aqueous medium from a biphasic mixture can depend on various factors, such as, pH of the solution, nature of organic phase, hydrophobicity of gel fibers, interaction of dye molecules with the gel fibers, etc. Ideally, claiming which of the factors can play a decisive role in controlling the dye removal behavior for a specific set of compounds is easier said than done, but we could well establish that organogels hold a potential to absorb dyes dissolved in aqueous media.

Sensing of heavy metals was also observed in the compounds, with impressive detection limits. Although no visual gelation enhancement or fluorescent nature was found in presence of metal salts, the sensing behavior in solution form can be further improved with necessary improvisations in the structure and backbone.

Interestingly, we did not observe any gelation behavior in petrol in both the series. It seems probable since the composition of petrol mainly comprises of 4-8% alkanes only.

Other elements are approximately 2-5% alkenes, 25-40% isoalkanes, 3-7% cycloalkanes, l-4% cycloalkenes, and 20-50% total aromatics (0.5-2.5% benzene) by volume. Since most of the gelation behavior has been observed in alkanes, their lower percentage in petrol may not be sufficient to induce gelation. Additionally, presence of unsaturated hydrocarbons, like alkenes and aromatics, along with additives like anti-knock agents, antioxidants, metal deactivators, lead scavengers, anti-rust agents, detergents, dyes, anti-icing agents, upper-cylinder lubricants, etc. might be playing an important role in hindering the formation of an effective self-assembly. Since no gelation was observed in aromatic solvents, their high percentage in petrol could also be one of the reasons behind this anomaly.

The idea of associating an increase in methylene group with a better gelation behavior ideally involves many factors to be considered. In this case, probably a disturbed balance between the hydrophobic and hydrophilic forces caused the gelation behavior to be compromised, even though the overall structural arrangement of compounds in both the series remained essentially similar. Additionally, the *tert*-butyl group in pivalic acid backbone is attached to sp^2 hybridised carbonyl carbon, which behaves similar to toluene, while in TBAA, it is attached to sp^3 hybridised methylene group, which ideally has more freedom of rotation. Although the presence of bulky group allows the molecular arrangement to adapt a one-dimensional arrangement in both the series, the compounds display varied gelation behavior.

Nevertheless, we believe that the two sets of compounds studied in this chapter represent a class of smallest systems ever exploited for phase selective organogelation. We hope to design better systems, with enhanced applications, which can open new avenues in the area of functional soft materials.

REFERENCES

1. Bi, H., An, C., Mulligan, C. N., Chen, Z., Lee, K., Wen, J., Qu, Z. & Chen, X. Application of Phase-Selective Organogelators (PSOGs) for Marine Oil Spill Remediation. *J. Mar. Sci. Eng.* **10**, 1111 (2022).
2. Kim, H., Zhang, G., Chung, T. C. M. & Nam, C. A Role for Newly Developed Sorbents for Remediating Large-Scale Oil Spills - Reviewing Recent Advances and Beyond. *Adv. Sustain. Syst.* **6**, 1–24 (2022).
3. Ge, J., Zhao, H. Y., Zhu, H. W., Huang, J., Shi, L. A. & Yu, S. H. Advanced Sorbents for Oil-Spill Cleanup: Recent Advances and Future Perspectives. *Adv. Mater.* **28**, 10459–10490 (2016).
4. Fan, K., Wang, X., Wang, X., Yang, H., Han, G., Zhou, L. & Fang, S. One-step-synthesized D-gluconic acetal-based supramolecular organogelators with effective phase-selective gelation. *RSC Adv.* **10**, 37080–37085 (2020).
5. Colak, M. Glutamic acid-based novel effective phase-selective organogelators for fuel pollution control. *J. Mater. Sci.* **57**, 1044–1057 (2022).
6. Ren, C., Shen, J., Chen, F. & Zeng, H. Rapid Room-Temperature Gelation of Crude Oils by a Wetted Powder Gelator. *Angew. Chemie - Int. Ed.* **56**, 3847–3851 (2017).
7. Neal, A. P. & Guilarte, T. R. Mechanisms of lead and manganese neurotoxicity. *Toxicol Res (Camb).* **2**, 99–114 (2013).
8. Shih, R. A., Hu, H., Weisskopf, M. G. & Schwartz, B. S. Cumulative lead dose and cognitive function in adults: a review of studies that measured both blood lead and bone lead. *Environ. Heal. Perspect.* **115**, 483–492 (2007).
9. Orisakwe, O. Lead and cadmium in public health in Nigeria: physicians neglect and pitfall in patient management. *N. Am. J. Med. Sci.* **6**, 61–70 (2014).
10. Mao, W. P., Zhang, N. N., Zhou, F. Y., Li, W. X., Liu, H. Y., Feng, J., Zhou, L., Wei, C. J., Pan, Y. B. & He, Z. J. Cadmium directly induced mitochondrial dysfunction of human embryonic kidney cells. *Hum. Exp. Toxicol.* **30**, 920–929 (2011).
11. Schwartz, G. G., Il'yasova, D. & Ivanova, A. Urinary cadmium, impaired fasting glucose, and diabetes in the NHANES III. *Diabetes Care* **26**, 468–470 (2003).
12. Longo, A., Librizzi, M. & Luparello, C. Effect of transfection with PLP2 antisense oligonucleotides on gene expression of cadmium-treated MDA-MB231 breast cancer cells. *Anal. Bioanal. Chem.* **405**, 1893–1901 (2013).
13. Kim, Y.-D., Yim, D.-H., Eom, S.-Y., Moon, S.-I., Park, C.-H., Kim, G.-B., Yu, S.-D., Choi, B.-S., Park, J.-D. & Kim, H. Differences in the susceptibility to cadmium-induced renal tubular damage and osteoporosis according to sex. *Environ. Toxicol. Pharmacol.* **38**, 272–278 (2014).
14. Cheng, H., Yang, B., Ke, T., Li, S., Yang, X., Aschner, M. & Chen, P. Mechanisms of metal-induced mitochondrial dysfunction in neurological disorders. *Toxics* **9**, 1–26 (2021).
15. Manzolli, E. S., Serpeloni, J. M., Grotto, D., Bastos, J. K., Antunes, L. M. G., Barbosa Junior, F. & Barcelos, G. R. M. Protective effects of the flavonoid chrysin against methylmercury-induced genotoxicity and alterations of antioxidant status, in vivo. *Oxid. Med. Cell. Longev.* **2015**, 602360 (2015).
16. Satoh, H. CHAPTER 5 Mercury. in *Aging and Vulnerability to Environmental Chemicals: Age-related Disorders and Their Origins in Enviromental Exposures* 125–150 (The Royal Society of Chemistry, 2013). doi:10.1039/9781849734660-00125.

17. Saunders, J. E., Jastrzembski, B. G., Buckey, J. C., Enriquez, D., MacKenzie, T. A. & Karagas, M. R. Hearing loss and heavy metal toxicity in a Nicaraguan mining community: audiological results and case reports. *Audiol. Neurootol.* **18**, 101–113 (2013).
18. Aaseth, J., Alexander, J., Alehagen, U., Tinkov, A., Skalny, A., Larsson, A., Crisponi, G. & Nurchi, V. M. The aging kidney—as influenced by heavy metal exposure and selenium supplementation. *Biomolecules* **11**, 1–11 (2021).
19. Chou, P.-T., Wu, G.-R., Wei, C.-Y., Cheng, C.-C., Chang, C.-P. & Hung, F.-T. Excited-State Amine−Imine Double Proton Transfer in 7-Azaindoline. *J. Phys. Chem. B* **104**, 7818–7829 (2000).
20. Panja, S., Mondal, S., Ghosh, S., Ghosh, U. & Ghosh, K. Effect of Substitution at Amine Functionality of 2,6-Diaminopyridine-Coupled Rhodamine on Metal-Ion Interaction and Self-Assembly. *ACS Omega* **5**, 13984–13993 (2020).
21. Panja, S., Debnath, S. & Ghosh, K. Fluorophore inserted bisbenzimidazole clefts in selective sensing of Ag^{+} and Cu^{2+} ions. *J. Photochem. Photobiol. A Chem.* **348**, 110–117 (2017).
22. Ghosh, S., Baildya, N., Ghosh, N. N. & Ghosh, K. Naphthalimide-decorated imino-phenol: supramolecular gelation and selective sensing of Fe^{3+} and Cu^{2+} ions under different experimental conditions. *New J. Chem.* **45**, 5213–5220 (2021).
23. Okesola, B. O. & Smith, D. K. Applying low-molecular weight supramolecular gelators in an environmental setting – self-assembled gels as smart materials for pollutant removal. *Chem. Soc. Rev.* **45**, 4226–4251 (2016).
24. Yang, Y. S., Yang, C., Zhang, Y. P., Niu, W. Y. & Xue, J. J. Synthesis and self-assembly of coumarin-chalcone derivatives organogels. *Colloids Interface Sci. Commun.* **41**, 1–7 (2021).
25. Zhang, Y., Ma, Y., Deng, M., Shang, H., Liang, C. & Jiang, S. An efficient phase-selective gelator for aromatic solvents recovery based on a cyanostilbene amide derivative. *Soft Matter* **11**, 5095–5100 (2015).

*SUPPLEMENTARY DATA

Crystallographic parameters

Table S4.3 Crystallographic parameters of TBA4

Code	TBA4
Empirical formula	$C_{48}H_{92}N_4O_4$
Formula weight	789.25
Temperature/K	140.00
Crystal system	monoclinic
Space group	$P2_1/c$
a/Å	23.20(3)
b/Å	10.861(13)
c/Å	10.066(13)
α/°	90
β/°	90.07(4)
γ/°	90
Volume/Å^3	2537(6)
Z	2
ρ_{calc}g/cm^3	1.033
μ/mm^{-1}	0.064
F(000)	880.0
Crystal size/mm^3	0.7 x 0.5 x 0.3
Radiation	MoKα (λ = 0.71073)
2Θ range for data collection/°	4.14 to 50.49
Index ranges	$-27 \leq h \leq 27$, $-12 \leq k \leq 12$, $-11 \leq l \leq 9$
Reflections collected	14743
Independent reflections	4443 [Rint = 0.2156, Rsigma = 0.2625]
Data/restraints/parameters	4443/0/260
Goodness-of-fit on F^2	0.867
Final R indexes [I>=2σ (I)]	R1 = 0.0771, wR2 = 0.1694
Final R indexes [all data]	R1 = 0.2538, wR2 = 0.2612
Largest diff. peak/hole / e Å^{-3}	0.17/-0.17
CCDC No.	2221607

Spectral Data - ^{1}H and ^{13}C NMR

TBA1

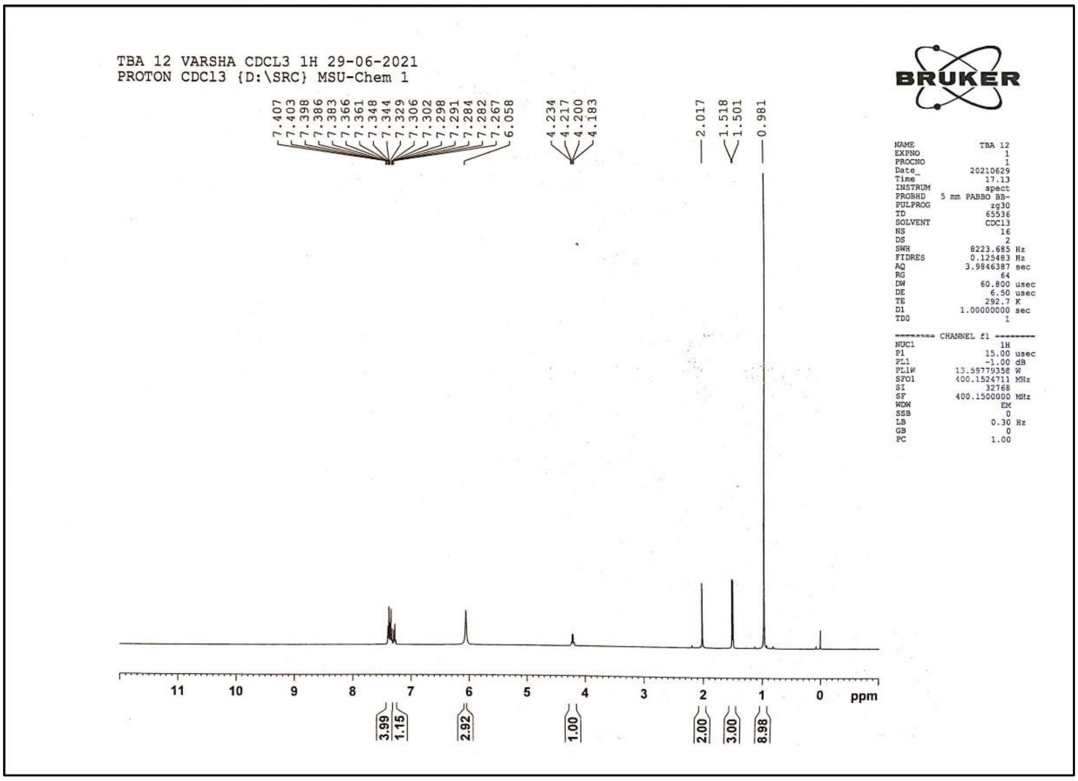

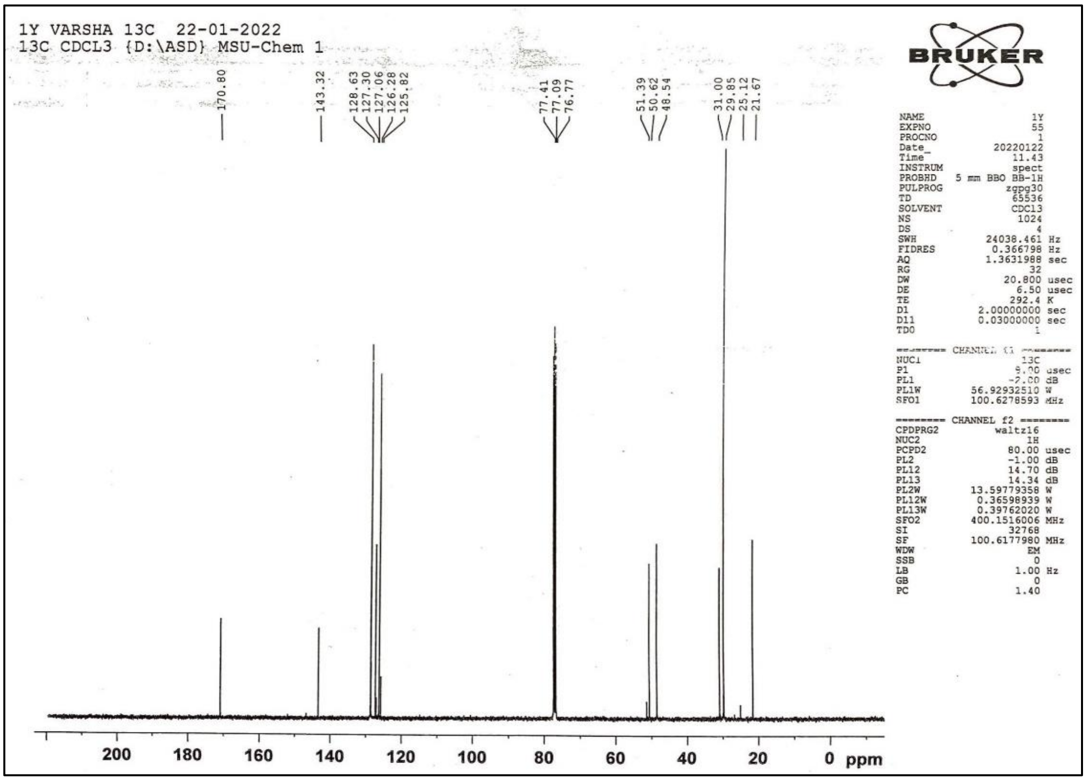

TBA2

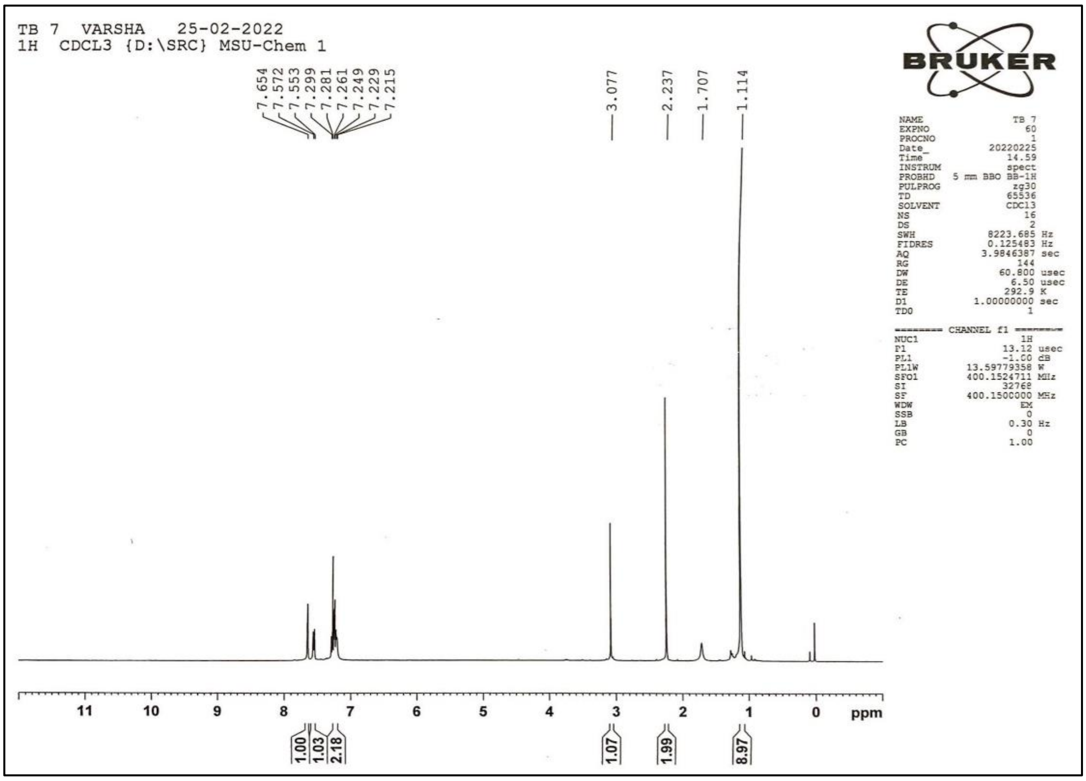
TB 7 VARSHA 25-02-2022
1H CDCL3 {D:\SRC} MSU-Chem 1
7.654
7.572
7.553
7.299
7.281
7.261
7.249
7.229
7.215
3.077
2.237
1.707
1.114
BRUKER
1.00
1.03
2.18
1.07
1.99
8.97
ppm

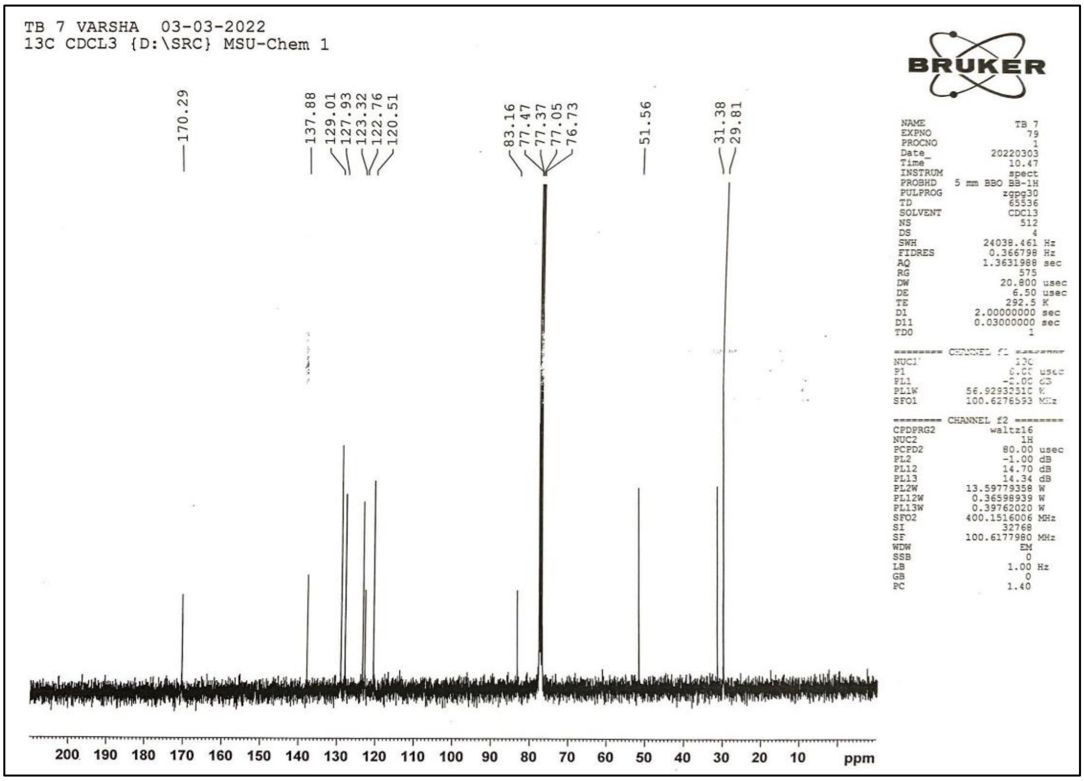
TB 7 VARSHA 03-03-2022
13C CDCL3 {D:\SRC} MSU-Chem 1
170.29
137.88
129.01
127.93
123.32
122.76
120.51
83.16
77.47
77.37
77.05
76.73
51.56
31.38
29.81
BRUKER
ppm

TBA3

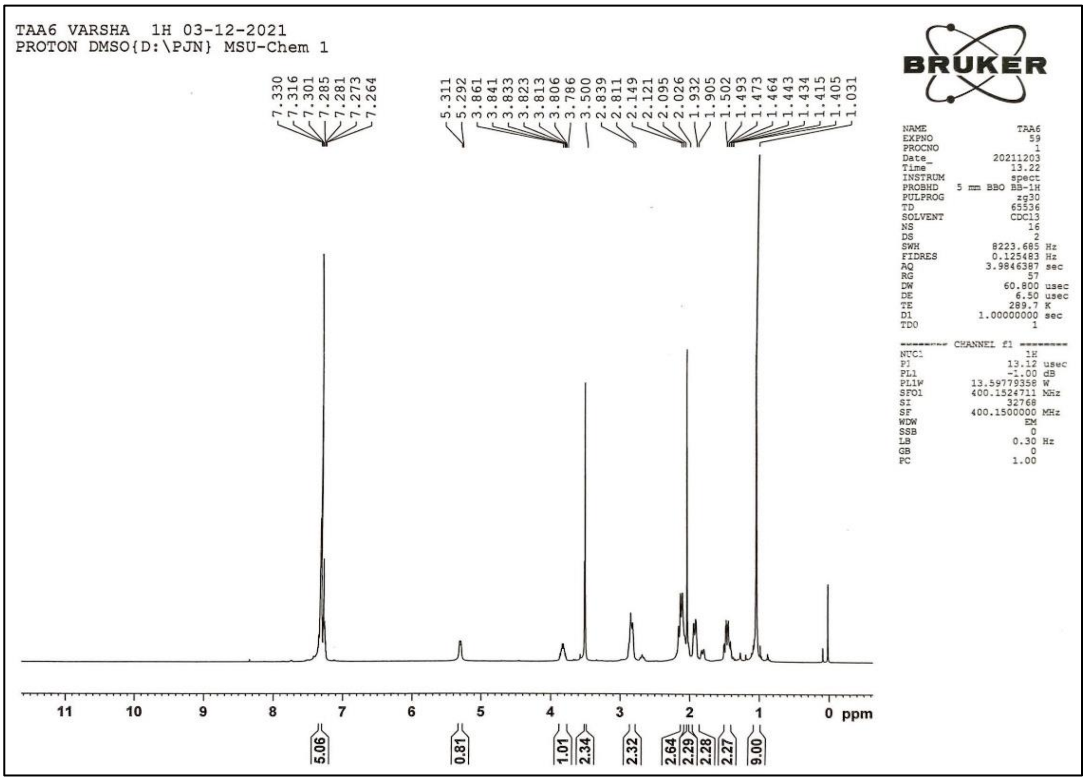
TAA6 VARSHA 1H 03-12-2021
PROTON DMSO{D:\PJN} MSU-Chem 1
BRUKER
ppm

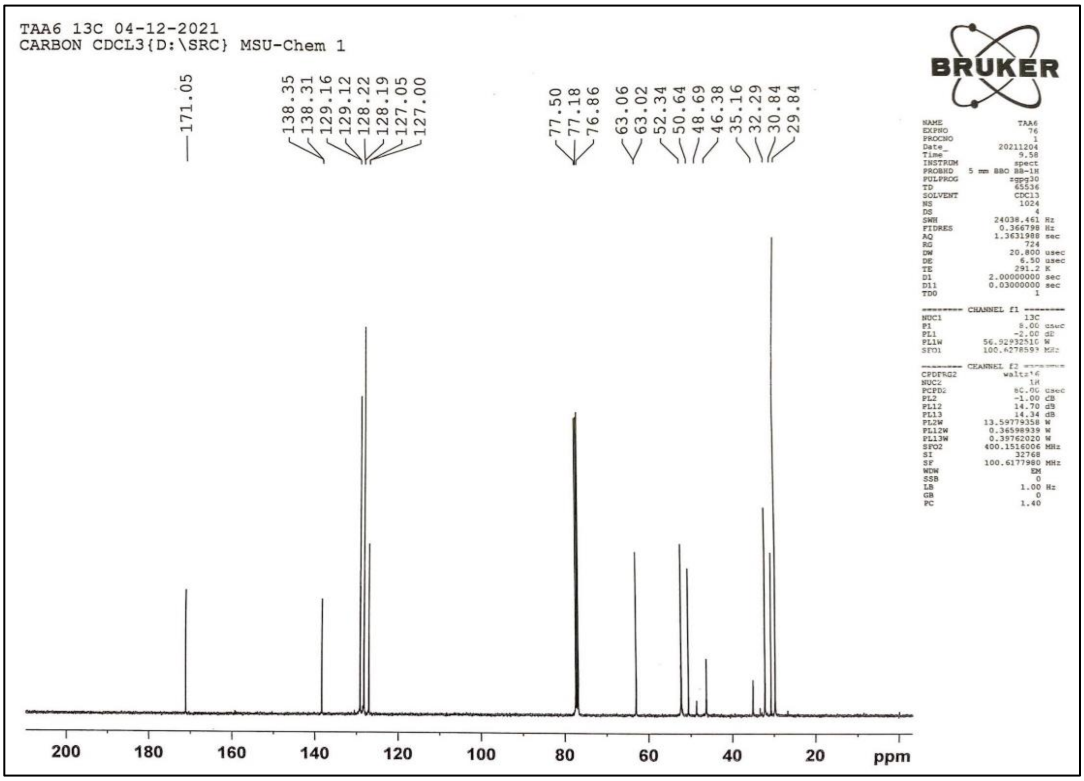
TAA6 13C 04-12-2021
CARBON CDCL3{D:\SRC} MSU-Chem 1
BRUKER
ppm

TBA4

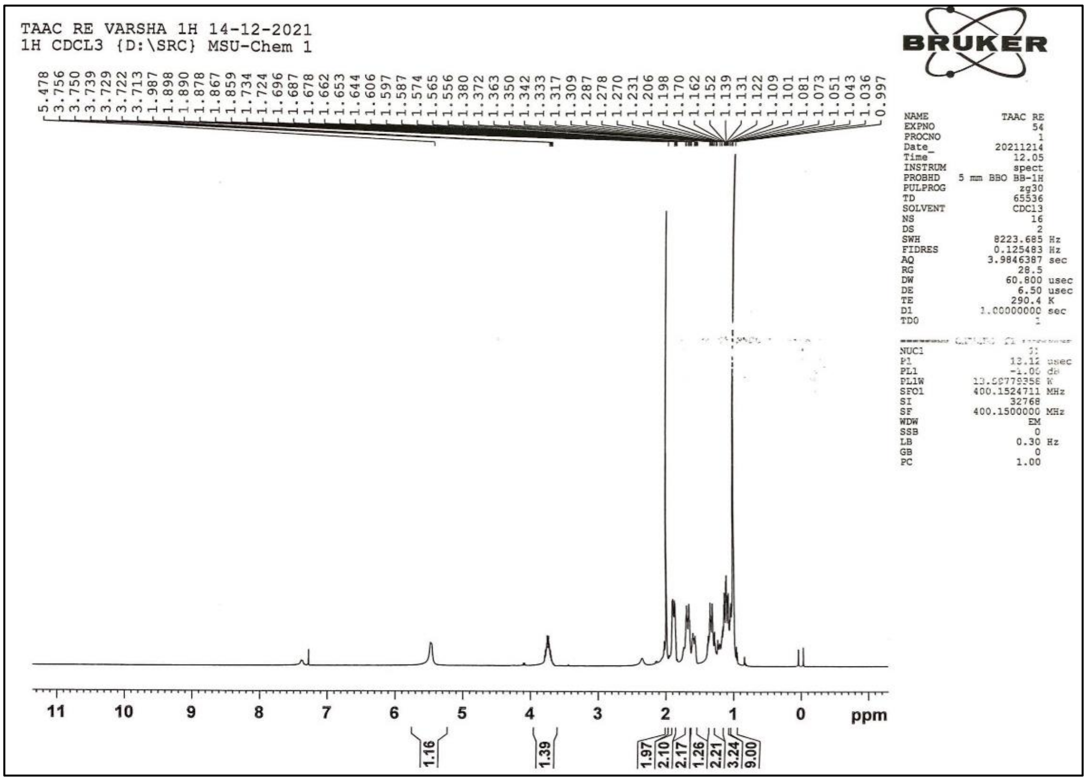

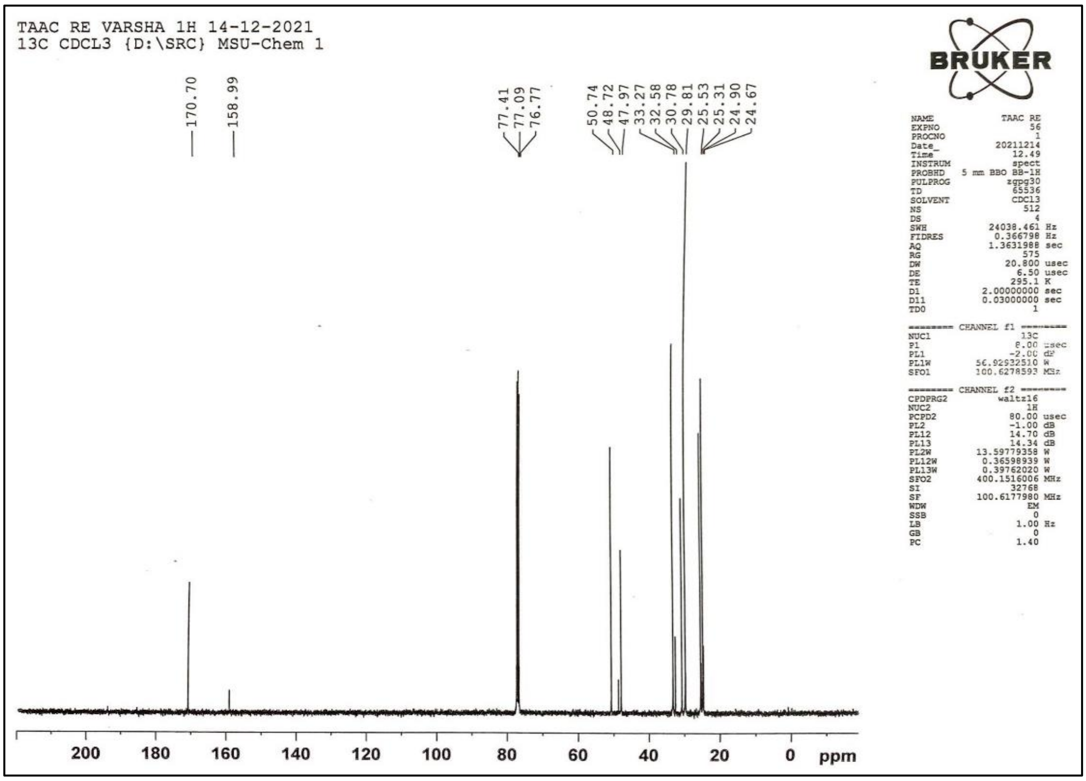

TBA5

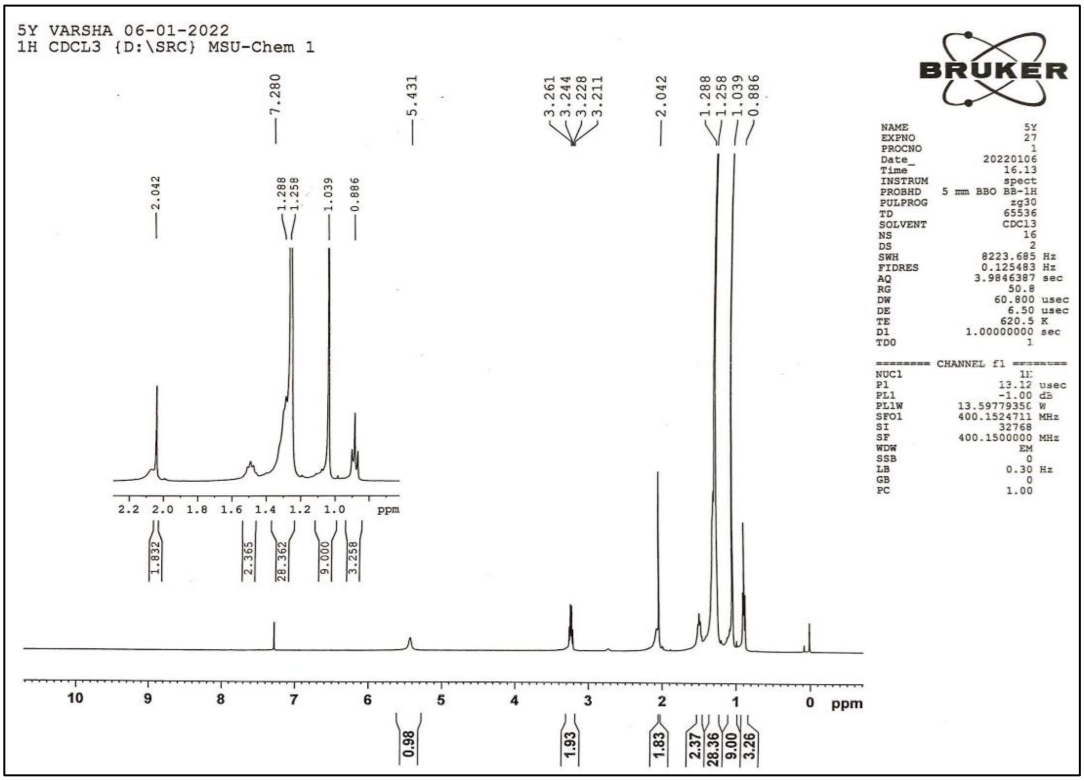

5Y VARSHA 06-01-2022
1H CDCL3 {D:\SRC} MSU-Chem 1
7.280
5.431
3.261
3.244
3.228
3.211
2.042
1.288
1.258
1.039
0.886
BRUKER
NAME 5Y
EXPNO 27
PROCNO 1
Date_ 20220106
Time 16.13
INSTRUM spect
PROBHD 5 mm BBO BB-1H
PULPROG zg30
TD 65536
SOLVENT CDCl3
NS 16
DS 2
SWH 8223.685 Hz
FIDRES 0.125483 Hz
AQ 3.9846387 sec
RG 50.8
DW 60.800 usec
DE 6.50 usec
TE 620.5 K
D1 1.00000000 sec
TD0 1
======== CHANNEL f1 ========
NUC1 1H
P1 13.12 usec
PL1 -1.00 dB
PL1W 13.59779350 W
SFO1 400.1524711 MHz
SI 32768
SF 400.1500000 MHz
WDW EM
SSB 0
LB 0.30 Hz
GB 0
PC 1.00
2.2 2.0 1.8 1.6 1.4 1.2 1.0 ppm
1.832
2.365
28.362
9.000
3.258
10 9 8 7 6 5 4 3 2 1 0 ppm
0.98
1.93
1.83
2.37
28.36
9.00
3.26

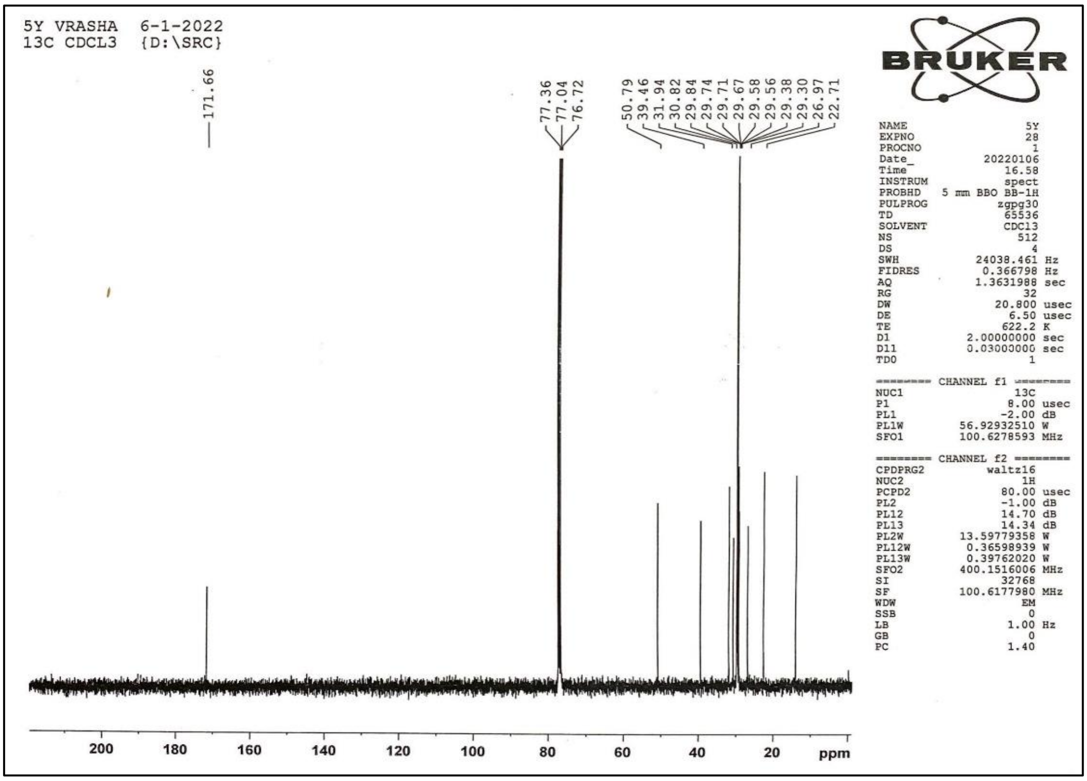

5Y VRASHA 6-1-2022
13C CDCL3 {D:\SRC}
171.66
77.36
77.04
76.72
50.79
39.46
31.94
30.82
29.84
29.74
29.71
29.67
29.58
29.56
29.38
29.30
26.97
22.71
BRUKER
NAME 5Y
EXPNO 28
PROCNO 1
Date_ 20220106
Time 16.58
INSTRUM spect
PROBHD 5 mm BBO BB-1H
PULPROG zgpg30
TD 65536
SOLVENT CDCl3
NS 512
DS 4
SWH 24038.461 Hz
FIDRES 0.366798 Hz
AQ 1.3631988 sec
RG 32
DW 20.800 usec
DE 6.50 usec
TE 622.2 K
D1 2.00000000 sec
D11 0.03000000 sec
TD0 1
======== CHANNEL f1 ========
NUC1 13C
P1 8.00 usec
PL1 -2.00 dB
PL1W 56.92932510 W
SFO1 100.6278593 MHz
======== CHANNEL f2 ========
CPDPRG2 waltz16
NUC2 1H
PCPD2 80.00 usec
PL2 -1.00 dB
PL12 14.70 dB
PL13 14.34 dB
PL2W 13.59779358 W
PL12W 0.36598939 W
PL13W 0.39762020 W
SFO2 400.1516006 MHz
SI 32768
SF 100.6177980 MHz
WDW EM
SSB 0
LB 1.00 Hz
GB 0
PC 1.40
200 180 160 140 120 100 80 60 40 20 ppm

TBA6

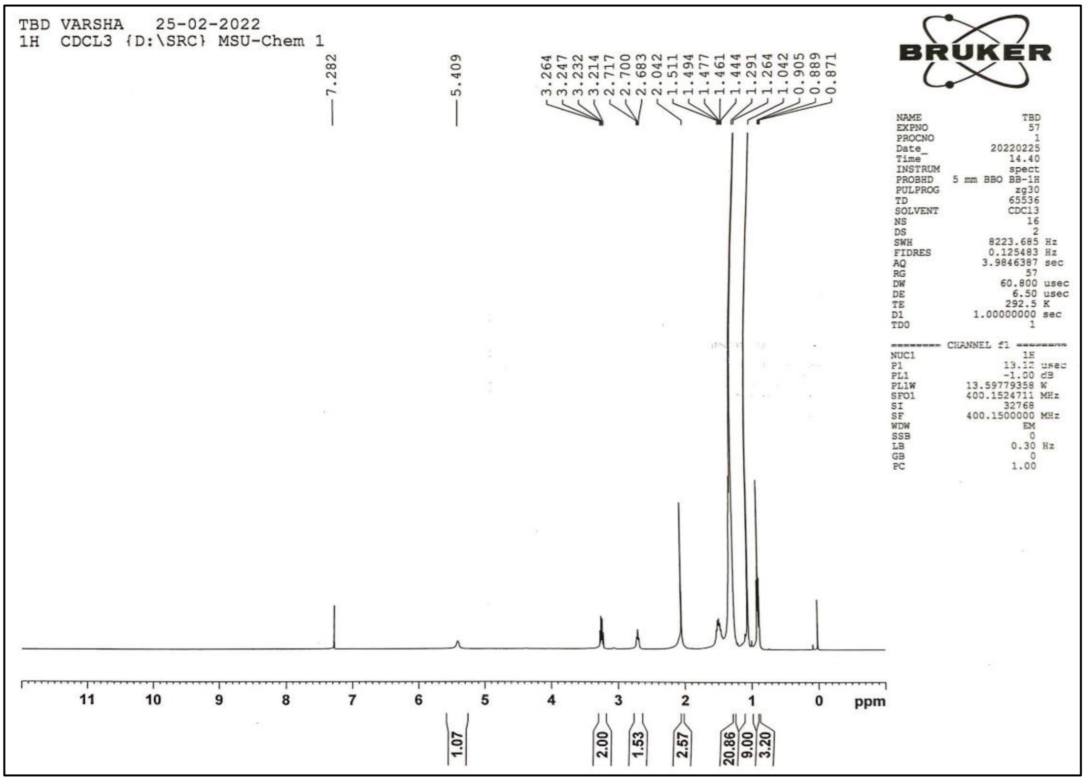
TBD VARSHA 25-02-2022
1H CDCL3 {D:\SRC} MSU-Chem 1
7.282
5.409
3.264
3.247
3.232
3.214
2.717
2.700
2.683
2.042
1.511
1.494
1.477
1.461
1.444
1.291
1.264
1.042
0.905
0.889
0.871
BRUKER
NAME TBD
EXPNO 57
PROCNO 1
Date_ 20220225
Time 14.40
INSTRUM spect
PROBHD 5 mm BBO BB-1H
PULPROG zg30
TD 65536
SOLVENT CDCl3
NS 16
DS 2
SWH 8223.685 Hz
FIDRES 0.125483 Hz
AQ 3.9846387 sec
RG 57
DW 60.800 usec
DE 6.50 usec
TE 292.5 K
D1 1.00000000 sec
TD0 1
======== CHANNEL f1 ========
NUC1 1H
P1 13.12 usec
PL1 -1.00 dB
PL1W 13.59779358 W
SFO1 400.1524711 MHz
SI 32768
SF 400.1500000 MHz
WDW EM
SSB 0
LB 0.30 Hz
GB 0
PC 1.00
11 10 9 8 7 6 5 4 3 2 1 0 ppm
1.07
2.00
1.53
2.57
20.86
9.00
3.20

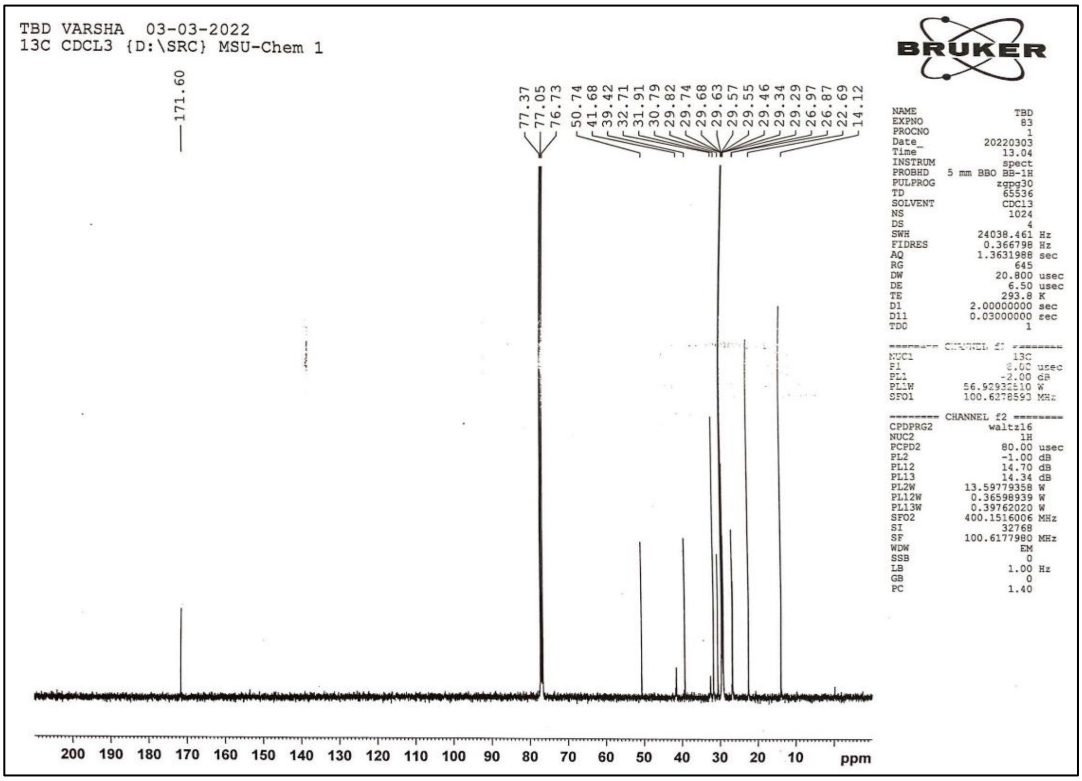
TBD VARSHA 03-03-2022
13C CDCL3 {D:\SRC} MSU-Chem 1
171.60
77.37
77.05
76.73
50.74
41.68
39.42
32.71
31.91
30.79
29.82
29.74
29.68
29.63
29.57
29.55
29.46
29.34
29.29
26.97
26.87
22.69
14.12
BRUKER
NAME TBD
EXPNO 83
PROCNO 1
Date_ 20220303
Time 13.04
INSTRUM spect
PROBHD 5 mm BBO BB-1H
PULPROG zgpg30
TD 65536
SOLVENT CDCl3
NS 1024
DS 4
SWH 24038.461 Hz
FIDRES 0.366798 Hz
AQ 1.3631988 sec
RG 645
DW 20.800 usec
DE 6.50 usec
TE 293.8 K
D1 2.00000000 sec
D11 0.03000000 sec
TD0 1
NUC1 13C
PL1 -2.00 dB
SFO1 100.6278593 MHz
======== CHANNEL f2 ========
CPDPRG2 waltz16
NUC2 1H
PCPD2 80.00 usec
PL2 -1.00 dB
PL12 14.70 dB
PL13 14.34 dB
PL2W 13.59779358 W
PL12W 0.36598939 W
PL13W 0.39762020 W
SFO2 400.1516006 MHz
SI 32768
SF 100.6177980 MHz
WDW EM
SSB 0
LB 1.00 Hz
GB 0
PC 1.40
200 190 180 170 160 150 140 130 120 110 100 90 80 70 60 50 40 30 20 10 ppm

FT-IR

TBA1

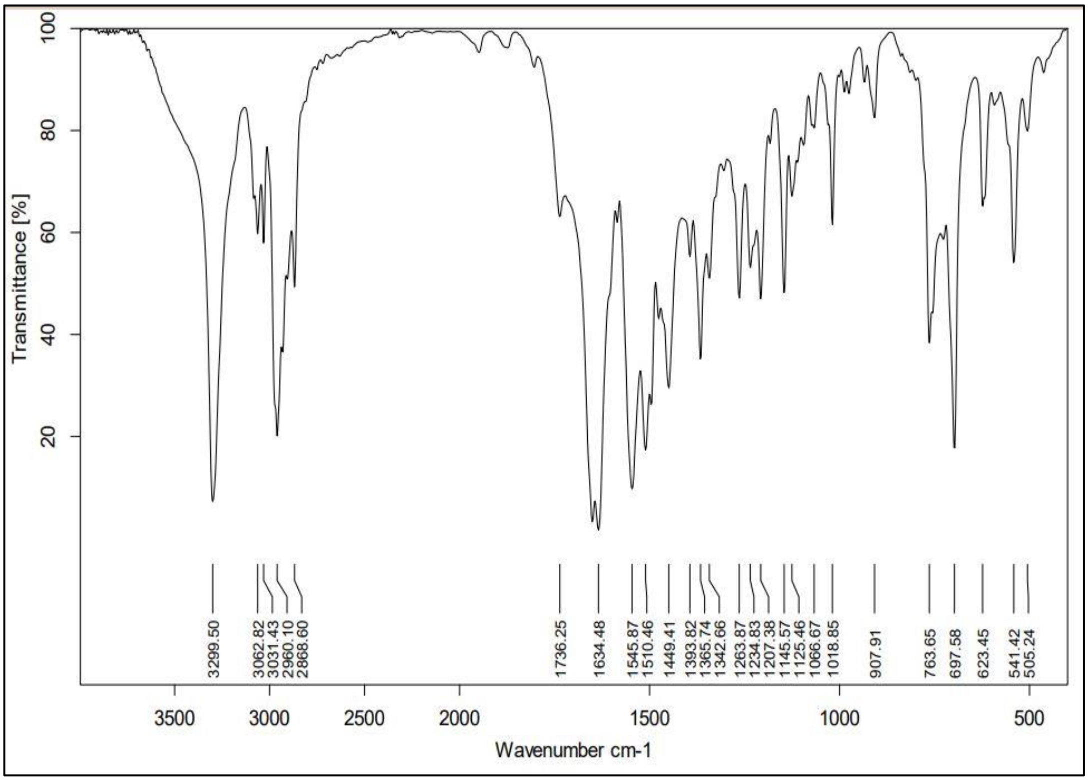

TBA2

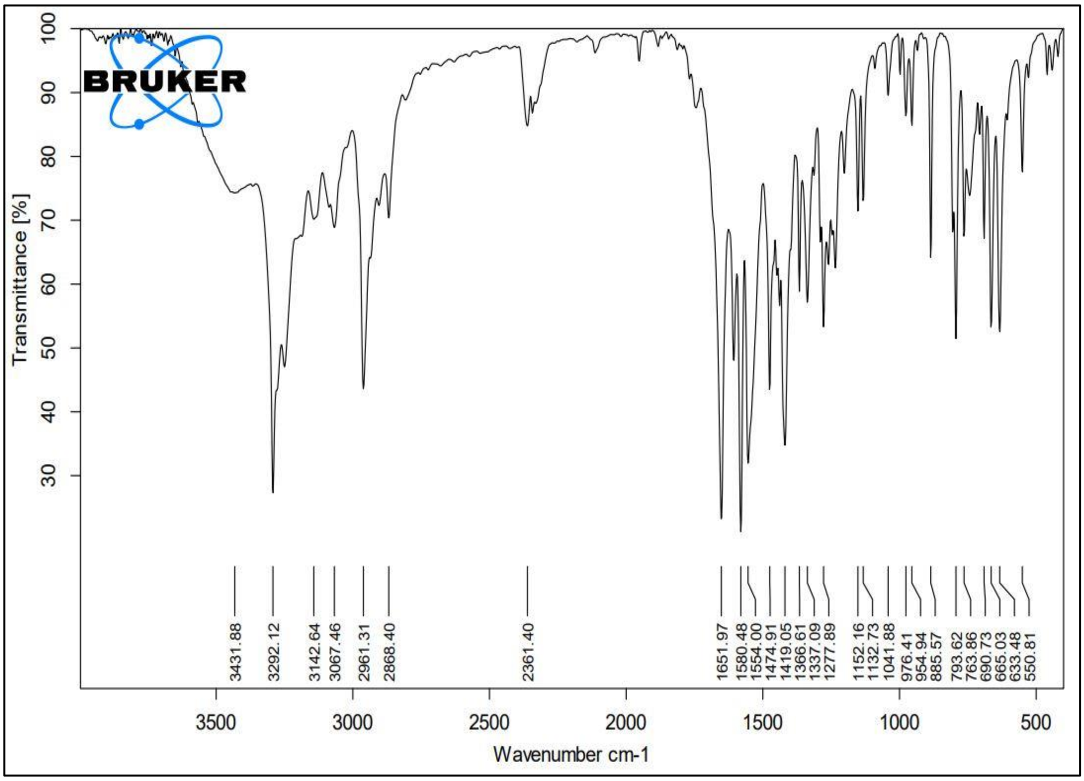

TBA3

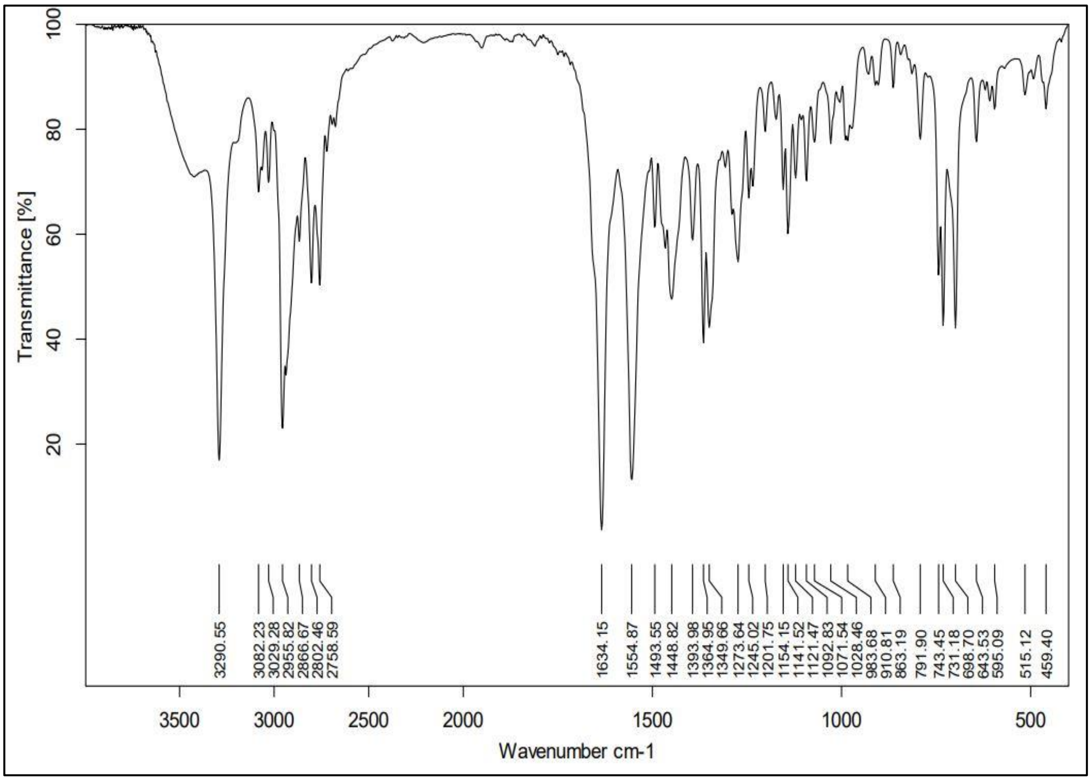
Transmittance [%]
20
40
60
80
100
3290.55
3082.23
3029.28
2955.82
2866.67
2802.46
2758.59
1634.15
1554.87
1493.55
1448.82
1393.98
1364.95
1349.66
1273.64
1245.02
1201.75
1154.15
1141.52
1121.47
1092.83
1071.54
1028.46
983.68
910.81
863.19
791.90
743.45
731.18
698.70
643.53
595.09
515.12
459.40
3500
3000
2500
2000
1500
1000
500
Wavenumber cm-1

TBA4

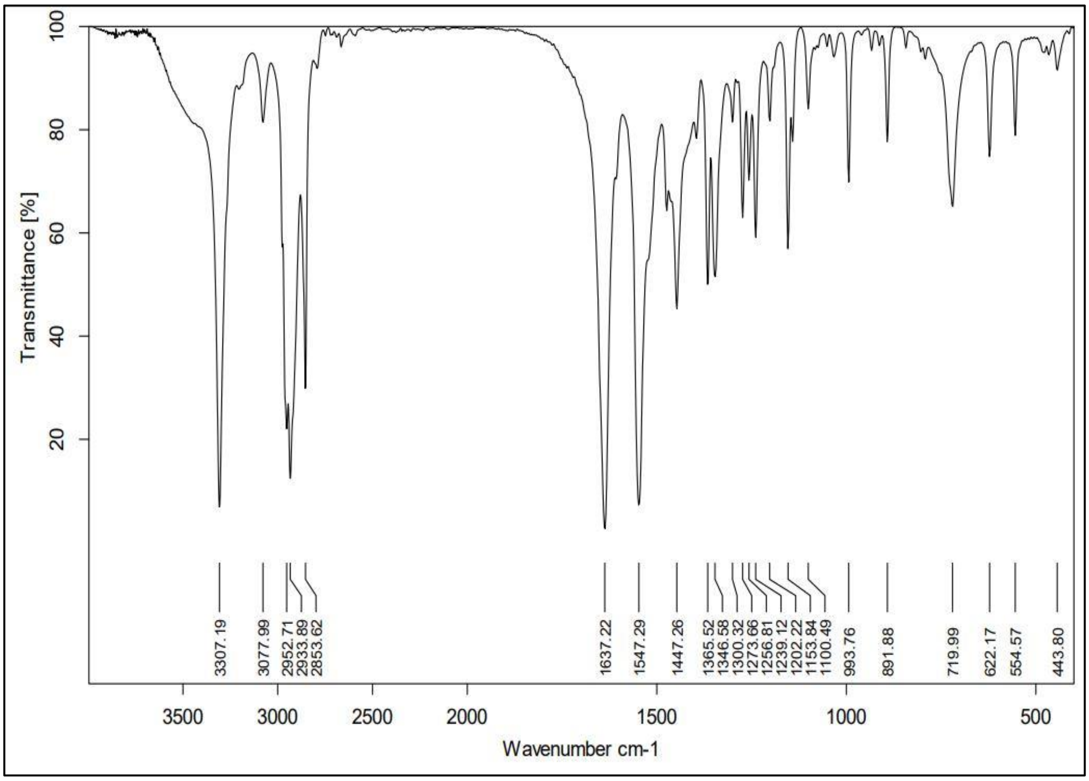
Transmittance [%]
20
40
60
80
100
3307.19
3077.99
2952.71
2933.89
2853.62
1637.22
1547.29
1447.26
1365.52
1346.58
1300.32
1273.66
1256.81
1239.12
1202.22
1153.84
1100.49
993.76
891.88
719.99
622.17
554.57
443.80
3500
3000
2500
2000
1500
1000
500
Wavenumber cm-1

TBA5

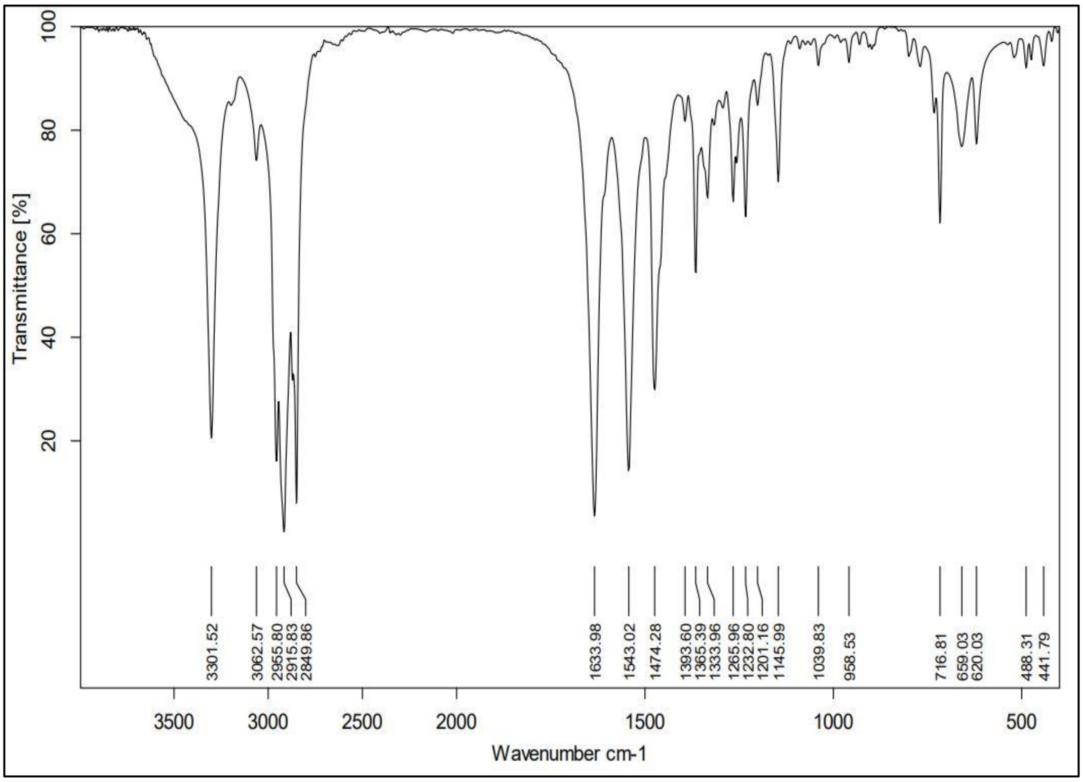
Transmittance [%]
100
80
60
40
20
3301.52
3062.57
2955.80
2915.83
2849.86
1633.98
1543.02
1474.28
1393.60
1365.39
1333.96
1265.96
1232.80
1201.16
1145.99
1039.83
958.53
716.81
659.03
620.03
488.31
441.79
3500
3000
2500
2000
1500
1000
500
Wavenumber cm-1

TBA6

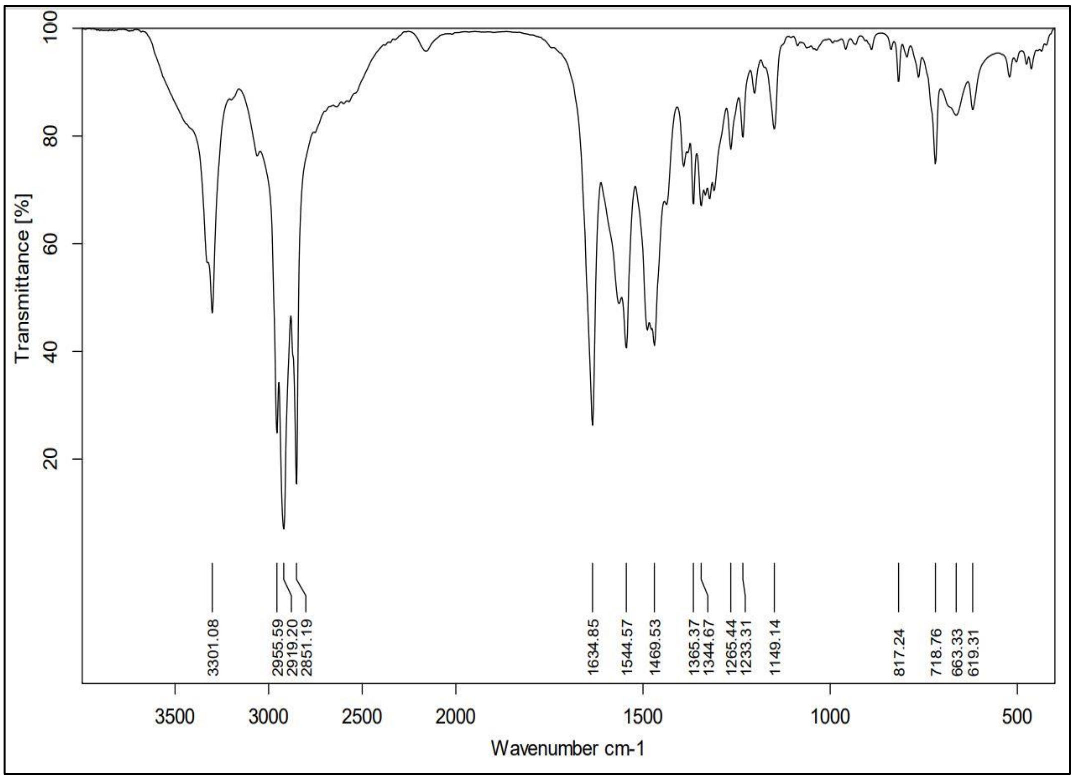
Transmittance [%]
100
80
60
40
20
3301.08
2955.59
2919.20
2851.19
1634.85
1544.57
1469.53
1365.37
1344.67
1265.44
1233.31
1149.14
817.24
718.76
663.33
619.31
3500
3000
2500
2000
1500
1000
500
Wavenumber cm-1

This page intentionally left blank.